LITHOLOGY, GEOCHEMISTRY AND GEOCHRONOLOGY OF THE AILLIK GROUP AND FOLIATED GRANITIC INTRUSIONS: IMPLICATIONS ON THE FORMATION AND EARLY EVOLUTION OF THE AILLIK DOMAIN, MAKKOVIK PROVINCE, LABRADOR

CRYSTAL LaFLAMME

Lithology, geochemistry and geochronology of the Aillik Group and foliated granitic intrusions: implications on the formation and early evolution of the Aillik domain, Makkovik Province, Labrador

By
Crystal LaFlamme (BScH)
Acadia University
Wolfville, Nova Scotia (2007)

A thesis submitted to the School of Graduate Studies in partial fulfillment of the requirements for the degree of

Master of Science

Department of Earth Sciences
Memorial University of Newfoundland
St. John's Newfoundland

January 2011

Abstract

The Makkovik Province of eastern Labrador is part of an accretionary orogenic belt that formed during the Paleoproterozoic Makkovikian orogeny. The Aillik domain represents one of three domains that make up the Makkovik Province and is composed of the Aillik Group, a package of Paleoproterozoic bi-modal volcano-sedimentary rocks, and abundant variably deformed Paleoproterozoic intrusive suites. The Aillik Group has experienced several phases of deformation and has been metamorphosed to lower amphibolite facies during the Makkovikian orogeny. Two areas, Middle Head and Pomaidluk Point, are the focus of this project and are used as case studies to assess and examine the Aillik Group with respect to the objectives as outlined below. Middle Head is dominated by arkosic sandstone, felsic tuff, rhyolite and basalt; whereas, Pomiadluk Point is composed primarily of felsic tuff and polymictic conglomerate with lesser preserved rhyolite and basalt. This study consists of detailed bedrock mapping in conjunction with: *insitu* SHRIMP U-Pb zircon geochronology, *insitu* LA-MC-ICPMS Hf isotopic geochemistry, major and trace element geochemistry, and whole rock Nd isotope geochemistry. These methods are used to: 1) constrain the timing of volcanism within the Aillik Group, 2) determine the source of magmatism, 3) resolve the overall tectonic setting in which the Aillik Group was deposited, and 4) briefly investigate the subsequent evolution of the Aillik domain.

U-Pb SHRIMP zircon geochronology on felsic tuff samples yields magmatic ages that range from ca. 1852 at Middle Head to ca. 1854 - 1862 Ma at Pomiadluk Point. These U-Pb ages indicate that sections of the Aillik Group occurring 27 km from one another were deposited contemporaneously, and that felsic volcanism continued to as late as ca. 1852 Ma. A foliated Paleoproterozoic granite from Middle Head yields an age of 1805 ±4 Ma, which further constrains the timing of deformation within the Aillik Group as continuing past its emplacement. One population of inherited zircons occurs between 1880 and 1920 Ma and is interpreted to be xenocrystic in nature.

Initial εHf_t in zircon from a ca. 1852 Ma felsic tuff and ca. 1805 Ma granite at Middle Head range uniformly from -1.6 to -5.0 with felsic crustal extraction ages of ca. 2.4 to 2.6 Ga. In contrast, two felsic tuff samples at Pomiadluk Point with magmatic ages of ca. 1854 and ca. 1861 Ma have initial εHf_t values in zircon that range from -4.8 to -11.9 in 18 of 20 grains analyzed, giving (felsic) crust formation ages of 2.6 to 3.0 Ga. A third sample from Pomiadluk Point, a ca. 1862 Ma foliated felsic tuff that outcrops between two conglomerate beds, contains magmatic zircons with initial εHf_t that range from +2.1 to -1.6, and crust formation ages of 2.3 to 2.5 Ga. None of the felsic volcanic rocks analyzed from the Aillik Group show Hf-isotope evidence of derivation from the North Atlantic Craton as the model ages are too young. Additionally, none of the samples demonstrate their formation on a truly juvenile, 1.9-2.0 Ga crust with short residence times (<100 Ma), as might be expected for an intra-oceanic island arc origin. Inherited zircon grains (1880 to 1920 Ma) demonstrate a similar Hf isotopic signature and depleted mantle model ages as the magmatic grains.

Trace and REE geochemistry demonstrate that felsic volcanic rocks of the Aillik Group as well as temporally distinct deformed granitic intrusions are 'A-type' in nature. Felsic volcanic rocks and a deformed monzogranite demonstrate a range in Nd isotopic signatures ($\varepsilon Nd_{(T)} = -1.1$ to -5.0), which reflects partial melting of a heterogeneous felsic crust. Based on geochemical signatures, mafic volcanic rocks can be classified into two groups. Group A basalts have geochemical signatures that demonstrate flat rare-earth element pattern, consistent with melting of a depleted mantle source, and are composed of primary plagioclase and clinopyroxene and metamorphic amphibole and biotite. Group B basalts and mafic tuff are chemically more evolved, and composed of primary plagioclase and metamorphic amphibole and magnetite. The two different REE patterns seen in mafic volcanic rocks are interpreted to reflect a variable amount of crustal contamination. Furthermore, Group A basalts demonstrate systematically more elevated $\varepsilon Nd_{(T)}$ signatures (+2.8 to +4.3) than Group B basalts and mafic tuff (-3.5 to +2.2). Based on mixing models, mafic magmas of the Aillik Group are determined to have formed by mixing of the depleted mantle with a small to moderately significant amount (5 to 35%) of the felsic volcanic rocks of the Aillik Group.

The combination of early clastic sedimentation, bimodal volcanism and geochemical signatures of felsic and mafic melts suggests that the ca. 1883 to 1852 Ma Aillik Group formed in a continental back-arc setting, forming from a crust that had an age range of at least 700 Ma, including both Paleoproterozic and Late Archean components. The similar Hf isotopic signatures of the Cross Lake granite, the felsic volcanic rocks of the Aillik Group, and the xenocrysts in the felsic volcanic rocks of the Aillik Group confirms that the Aillik domain was generated from the same basement over 115 million years.

Acknowledgments

This study was made possible by the logistical and financial support of the Geological Survey of Newfoundland and Labrador to the first author, by an NSERC grant to Dr. Paul Sylvester and C.L. and by funding for geochronology analyses provided by Dr. Charlie Jefferson. My co-supervisors were Dr. Alana Hinchey and Dr. Paul Sylvester. Dr. Hinchey is thanked for her excellent guidance and patience both in the field and in St. John's. Dr. Sylvester is thanked for his aid in deciphering geochemistry data and his reviews. Assistance and guidance from Dr. Bill Davis during SHRIMP analyses is greatly appreciated. Dr. Rebecca Lam is thanked for her direction during Hf analyses. Discussions with Bill Davis, Charlie Jefferson and Greg Sparks in the field were very helpful. Wayne Tuttle is thanked for logistic support while in Labrador. Helicopter support was provided by Helicopter Transport Services. Field assistance from Andrea MacFarlane, Chris Furey and Ned Welty is greatly appreciated. Pam King is thanked for her help during the sample preparation process. Neil Stapleton is thanked for digitizing maps in ArcGIS for a Current Research publication which was completed for the Geological Survey of Newfoundland and Labrador in 2009 which included preliminary data collected in the field (ie. description of lithologies).

I'd especially like to thank my parents and brother for their constant encouragement and my friends for being sources of distraction. Finally, and most importantly, I'd like to thank my boyfriend John for listening to me and laughing with me.

Table of Contents

List of Figures

List of Tables

Chapter 1

Introduction and Overview

1.1 INTRODUCTION

Bimodal volcano-sedimentary belts have long been of interest for uranium, base metal and precious metal exploration. The bimodal volcano-sedimentary Aillik Group, located within the Makkovik Province, is a known host to uranium and base metal deposits and lies entirely within the Central Mineral Belt of Labrador (Figure 1.1). Interest in the area has increased over the past decade with the rising of stock market prices and prices of commodities. In 2006, a multiyear, regional-scale (1:50,000) project to map and interpret the bedrock geology of the Aillik domain was undertaken by the Geological Survey of Newfoundland and Labrador. This project facilitated the detailed work reported in this thesis.

Field work during the summer of 2008 consisted of detailed (1:10,000-scale) bedrock mapping and sampling of two stratigraphic sections within the Aillik domain. Laboratory analyses reported include petrological, geochemical, geochronological and isotopic studies. The purpose of this study focuses on two themes: 1) the timing and crust-mantle source of volcanism and 2) the tectonic setting and evolution of the Aillik Group. Two study areas that were examined are named Middle Head and Pomiadluk Point.

1.2 LOCATION, ACCESS AND PHYSIOGRAPHY

Both study areas are adjacent to the coast; they are readily accessible and relatively well exposed. Access to these study areas is possible by boat and by helicopter from the town of Makkovik. The locations of the two study areas are shown in Figure 1.2.

The Middle Head study area is located 14 km southwest from the town of Makkovik and encompasses an area of 12 square kilometers. Bedrock exposure in this region is poor in the heavily wooded areas to the north and in the central area due to bog/swamp and is best on four prominent hills. In the south, about half of the forest cover was destroyed by a fire more than a decade ago; consequently exposure in this area is moderately good. Relief is moderate; elevation ranges from sea level at the coast to 450 m at the top of the highest hill.

Thirteen km to the east of Makkovik is Pomiadluk Point, a peninsula covering an area of 16 square kilometers. In contrast to Middle Head, the coastal region of Pomiadluk Point displays 85-90% exposure with the only hindrance being minor lichen cover. Exposure is best near the coast but outcrop is well exposed inland. Relief at Pomiadluk Point is relatively low with topography gently rising from sea level at the coast to 200 m inland. The peninsula provides a good cross-section through the north-south striking units of the Aillik Group.

1.3 PREVIOUS WORK

Both the Geological Survey of Canada and the Geological Survey of Newfoundland began mapping in what is now known as the Makkovik Province in the late 1930s to 1950s (Kranck, 1939, 1953; Christie et al., 1953; Douglas, 1953). Regional bedrock maps, which encompassed both of the current study areas, were published for the

Makkovik Bay area (Gandhi et al., 1969) and for the Aillik domain, at the scale of 1:100 000, by the Geological Survey of Newfoundland and Labrador (Gower et al., 1982). Regional bedrock studies at the scale of 1:50 000 were published by the Geological Survey of Newfoundland and Labrador (Hinchey, 2007; Hinchey and LaFlamme, 2009). The geochemistry and geochronology of the various intrusive suites have been reported in numerous papers and reports including Kerr (1989), Kerr et al. (1992), Kerr and Fryer (1994), Barr et al. (2001), Ketchum et al. (2001), Ketchum et al. (2002), Sinclair et al. (2002), Barr et al. (2007) and Hinchey and Rayner (2008). Lamprophyres have been investigated by King and McMillan (1975), Hawkins (1976), Foley (1982), Malpas et al. (1986), and Tappe et al. (2006). Both study areas, Pomiadluk Point and Middle Head, were included in a regional-scale Ph.D. study of the Makkovik Bay area by Clark (1973). The Aillik Group at Pomiadluk Point has been part of several metallogenic and stratigraphic studies (Wilton, 1996; Sinclair, 1999). Both study areas have been mapped as part of a regional bedrock study (Hinchey, 2007; Hinchey and LaFlamme, 2009).

1.4 REGIONAL GEOLOGY

The Makkovik Province of Labrador is part of a Paleoproterozoic accretionary orogen wedged between the Nain Province to the north and the Grenville Province to the south (Figure 1.1; Ketchum et al., 2002 and references therein). The Makkovik Province comprises Paleoproterozoic volcano-sedimentary units, variably deformed to undeformed intrusive suites, reworked Archean rocks and abundant mafic dykes (Kerr et al., 1992). The Makkovik Province was affected by several episodes of metamorphism and plutonism from orogenic events, including the Makkovikian orogeny (1900-1710 Ma;

Gower and Ryan, 1986; Ketchum et al., 2002) and to a lesser extent the Labradorian (1710–1620 Ma; Scharer et al., 1986; Scharer and Gower, 1988; Gower, 1990; Kerr et al., 1992) and Grenvillian (1080–985 Ma; Gower and Ryan, 1986) orogenies. The Makkovik Province has been divided into three domains: the Kaipokok domain, the Aillik domain, and the Cape Harrison domain (Figure 1.3; Kerr et al., 1996).

The Kaipokok domain contains amphibolite-facies polydeformed Archean gneiss of the Nain Province and the unconformably overlying, volcano-sedimentary units of the Post Hill Group (previously termed Lower Aillik by Marten, 1977) and Moran Lake Group (Marten, 1977; Ryan, 1984). These two groups are long thin belts of supracrustal strata; they are interpreted to be stratigraphic equivalents of one another (Wardle and Bailey, 1981). Foliated calc-alkaline plutons of the Island Harbour Bay Plutonic Suite (1895-1870 Ma) intrude the Kaipokok domain as well as lesser granitoid plutons of various ages (Barr et al., 2001). The domain is bounded to the northwest by the Kanairiktok shear zone that separates Archean gneiss of the Nain Province from correlative gneiss in the Makkovik Province; the latter gneiss was reworked during the Paleoproteozoic (Ermanovics and Ryan, 1990; Ermanovics, 1993; Ketchum et al., 2002). The southern boundary is marked by a system of transpressive, ductile shear zones termed the Kaipokok Bay shear zone which separates the Kaipokok domain from the Aillik Domain (cf., Kaipokok Bay structural zone of Kerr et al., 1996; Ketchum et al., 1997; Culshaw et al., 2000). The Kaipokok domain is interpreted to be the foreland zone to the Makkovik Province (Kerr et al., 1996).

The Aillik domain comprises: a) the Aillik Group, a sequence of metamorphosed, dominantly felsic and lesser mafic volcano-sedimentary units; b) a slice of

Paleoproterozoic reworked Archean orthogneiss; c) several foliated and non-foliated Paleoproterozoic intrusive suites dated at ca. 1857 Ma, 1800 Ma, 1720 Ma and 1650 Ma; and d) numerous swarms of dominantly mafic dykes (Kerr, 1989; Kerr et al., 1992; Hinchey and Rayner, 2008). The southern boundary of the Aillik domain with the Cape Harrison domain is obscured by abundant younger plutonic rocks.

The Cape Harrison domain is composed primarily of plutonic suites dated at around 1800 Ma, 1720 Ma and dominantly 1650 Ma (Kerr, 1989, 1994; Kerr et al., 1992). Most of the ca. 1800 Ma plutonic suites are foliated and, based on major and trace element geochemistry, are interpreted to have been emplaced during the late stages of the Makkovikian orogeny (Gower and Ryan, 1986; Kerr, 1994). Based on lithology and major and trace element geochemistry, undeformed ca. 1720 Ma and ca. 1650 Ma suites are interpreted to be post-tectonic intrusions, emplaced after the Makkovikian orogeny (Kerr et al., 1992; Kerr, 1994). The Cape Harrison domain also contains ca. 1815 tonalitic orthogneiss (Cape Harrison Metamorphic Suite) composed of juvenile material and minor supracrustal rocks (Kerr and Fryer, 1994; Ketchum et al., 1997, 2002).

Most recently, the Aillik and Cape Harrison domains have been interpreted as a rifted arc to composite arc based on field evidence as well as the composition and chemistry of bimodal volcanic rocks and the abundance of mafic dykes that cut all units (Ketchum et al., 2002). In the model of Ketchum et al. (2002), accretion of the Aillik and Cape Harrison domains marks the initiation of the ca. 1900–1780 Ma Makkovikian orogeny; this event was characterized by a penetrative planar fabric, abundant plutonic intrusions, regional deformation and upper greenschist to lower amphibolite facies metamorphism (Gandhi et al., 1969; Sutton, 1972; Marten, 1977; Clark, 1979; Gower et al., 1982; Kerr, 1994; Kerr et al., 1996; Culshaw et al., 1998; Ketchum et al., 2001, 2002). The Makkovik Province has been tentatively correlated with the Ketilidian mobile belt of Greenland based on: a) reflection seismology, specifically the Lithoprobe Eastern Canada Shield Onshore – Offshore Transect; b) geochronology; and, c) lithological similarities (Hall et al., 1995; Kerr et al., 1997; Wardle et al., 2002, James et al., 2002).

1.5 LOCAL GEOLOGY AND PREVIOUS STUDIES OF AILLIK DOMAIN

Previous work within the Aillik Domain has focused primarily on the Aillik and Kaipokok domains. The Aillik Group is best exposed to the north; whereas, the southern portion of the Aillik domain is partly obscured by plutonic intrusions. This study focuses on the northern part of the Aillik domain known as the Makkovik Bay area (Figure 1.4), and the subsequent section overviews the previous studies in this region. The following gives details regarding the rock types, structure and metamorphism of the Aillik domain and is based on the reports by Gandhi et al. (1969), Clark (1973), Bailey (1981), Culshaw et al. (2000), Ketchum et al. (2002), Hinchey (2007) and Hinchey and LaFlamme (2009a). Previous geochronological work from Schärer et al. (1988), Kerr (1989), Sinclair (1999), Cox et al. (2003), and Hinchey and Rayner (2008) is also included. This provides a tectonic framework and current understanding of the evolution of the Aillik domain.

1.5.1 Aillik Group Lithologies

The Aillik Group is composed of Paleoproterozoic metasedimentary and metavolcanic rocks (Gandhi et al., 1969; Bailey, 1981; Gower et al., 1982, Ketchum et al., 2002). The stratigraphy of the Aillik Group is complicated because most units are not laterally continuous, it has locally complex structures as a result of Makkovikian deformation, and it is further complicated by late brittle faulting (Hinchey 2007; Hinchey and LaFlamme, 2009).

Aillik Group volcanic rocks are bimodal, composed dominantly of felsic units and less abundant mafic units (Clark, 1973; Gower et al., 1982). The felsic volcanic rocks are dominated by rhyolite and felsic tuff whereas the mafic volcanic rocks are dominated by basalt and less abundant mafic tuff units (Kerr, 1989; Hinchey 2007). Abundant tuffites occur which include primarily tuffaceous sandstone (Hinchey, 2007).

Aillik Group sedimentary rocks are composed primarily of interbedded sandstone-siltstone and less abundant polymictic conglomerate. Primary sedimentary structures include graded bedding, cross bedding, ripple marks and load casts (Hinchey, 2007). Conglomerate occurs throughout the Aillik Group; three units in the Makkovik Bay area were described in detail by Hinchey (2007). Each of these units may contain several distinct beds of conglomerate separated by thinner beds of felsic volcanic and sedimentary units. Calc-silicate-rich beds and marble lenses locally occur within the sandstone and conglomerate (Hinchey, 2007).

1.5.2 Intrusive Lithologies

In the Aillik domain there are abundant intrusions of quartz–feldspar porphyritic granite as well as various foliated and non-foliated plutonic suites. The sheet-like bodies of quartz–feldspar porphyritic granite are interpreted to have intruded during formation of the Aillik Group (Hinchey, 2007). In addition to this syn-volcanic granite, there are abundant foliated and non-foliated plutonic suites that occur in the Aillik domain and are interpreted to have formed during the final and post-compressional stages of the Makkovikian orogeny. These plutonic suites have largely been divisible into two age groupings: ca. 1800 Ma which includes both foliated and undeformed suites and ca. 1720 Ma non-foliated suites (Kerr, 1989; Kerr et al., 1992). The youngest plutonic event occurring within the Aillik domain is the ca. 1650–1640 Ma plutonic intrusion, which has been attributed as being a far-field effect of the Labradorian orogeny (Kerr et al., 1996).

ca. 1858 Ma porphyritic granite

In the Makkovik Bay area, the oldest plutonic intrusions are a suite of fine- to medium-grained, foliated, quartz–feldspar-porphyritic granites interpreted to have been intruded during the formation of the Aillik Group at ca. 1858 Ma (Hinchey and Rayner, 2008). This suite of porphyritic granites occurs as sill-like, hypabyssal bodies within the Aillik Group (Hinchey, 2007).

ca. 1800 Ma plutonic suites

Only one plutonic suite with an age of ca. 1800 Ma outcrops in the Makkovik Bay area and has been termed the Kennedy Mountain Intrusive Suite (Kerr, 1994). These granitic plutons contain a single penetrative fabric. They demonstrate A-type granite geochemical signature, and are interpreted to have intruded during the final transpressive phase of Makkovikian orogeny (Kerr, 1994; Ketchum et al., 2002).

ca. 1720 Ma plutonic suites

In the Makkovik Bay area, the ca. 1720 Ma granitoid suites include only the Strawberry Intrusive Suite, which yielded a U-Pb age of 1719 ± 2 Ma (Kerr, 1989; Kerr et al., 1992). Kerr and Fryer (1994) demonstrated these granitic, undeformed plutons have an A-type granite geochemical signature.

ca. 1650–1640 Ma plutonic suites

In the Makkovik Bay area, the ca. 1650-1640 Ma suites include the felsic Monkey Hill Intrusive Suite and the mafic Adlavik Intrusive Suite. Both suites intrude the Aillik Group. The Adlavik Intrusive Suite has been dated at ca. 1640 Ma (Kerr et al., 1992) and the Monkey Hill Intrusive Suite is, based on intrusive relations, interpreted to be younger than the Adlavik Intrusive Suite (Kerr, 1994). These plutons have been interpreted to have formed as a result of far-field effects of the Labradorian orogeny (Kerr, 1989). The October Harbour granite, located at Pomiadluk Point, was originally interpreted to be part of the Strawberry Intrusive Suite (Kerr, 1994); however, new data from Cox et al. (2003; see geochronology below) indicate that it is associated with the younger *ca.* 1650-1640 Ma intrusion.

1.5.3 Dyke Lithologies

Numerous syn- to post-volcanic dykes crosscut the Aillik Group in the Makkovik Bay area (King, 1963; Gandhi et al., 1969; Malpas et al., 1986; Hinchey, 2007). The dykes include at least two swarms of mafic dykes that are deformed and metamorphosed to amphibolite facies. One type is a fine-grained, garnet amphibolite, whereas the other contains recrystallized plagioclase feldspar phenocrysts (Hinchey 2007). Several generations of dykes post date the regional penetrative fabric in the Aillik Group and in some of the ca. 1800 Ma intrusions. Hinchey (2007) identified at least seven types of dykes that crosscut all volcano-sedimentary units of the Aillik Group within the Makkovik Bay area including: diabase dykes, net-veined gabbroic dykes, meter-wide lamprophyric dykes, plagioclase megacrystic diabase dykes, aplitic granitic dykes, pegmatitic granitic dykes and diatreme dykes. Granitic aplite dykes are 2–10 m wide; they cut the amphibolite dykes but predate undeformed mafic dykes (Hinchey, 2007).

Ultramafic lamprophyre dykes from Aillik Bay have been divided into two lithological groups: (i) olivine lamproites with an age of 1374 ± 4 Ma and (ii) aillikites-carbonatites having ages of 590–555 Ma (Tappe et al., 2007). Rare breccia-filled lamprophyre (diatreme) dykes from Ford's Bight were originally dated, based on fossil evidence, at ca. 197–164 Ma (King and McMillan, 1975), but a refined age of ca. 141 Ma, based on the U-Pb geochronology of perovskite, has now been determined (Tappe et al., 2007).

1.5.4 Structural Evolution

Early studies of deformation in the Aillik Group characterized the folds as large, gently plunging, upward facing structures (Clark, 1973, 1979; Gower et al., 1982). Clark (1979) reported that the Aillik Group, in the Makkovik Bay area, has undergone four stages of deformation that produced regional folding, a penetrative fabric and late brittle faulting. Culshaw et al. (2000) indicated that six stages of deformation are required to explain structures in the whole of the Makkovik Province of which only D_3 to D_6 affected the Aillik domain. Culshaw et al. (2000) proposed that the folding and the penetrative fabric are the result of sinistral transpression, regionally a D_3 event, and that shear zones in the Aillik Group were subsequently reactivated during D_4 and $D_{5\text{-}6}$ events.

Hinchey (2007) and Hinchey and Rayner (2008) concluded that in order to explain the patterns of rock units, the structural data, and the range in ages, the deformational history of the Aillik Group must be more complex than previously interpreted. Hinchey (2007) and Hinchey and LaFlamme (2009) reinterpreted the structural history of the Aillik Group as being characterized by regional-scale, closed to tight, moderately plunging, upright to overturned folds (F_1 locally) that were subsequently refolded (F_2 locally). Regional-scale folds (F_3) are isoclinal to open and upright to overturned.

A 1-km-wide, highly strained zone extends southward from Cape Makkovik through Big Island and inland to the south of Ranger Bight. This was previously defined as the Ranger Bight slide by Clark (1979) or straightened zone by Culshaw et al. (2000) and the Big Island Shear zone (BISZ) by Ketchum et al. (2002). Culshaw et al. (2000) suggested that this high-strain zone likely represents one of a series of ductile shear zones that cut parts of the Aillik Group. The vergence of the regional folds changes about this shear zone, from folds that verge to the northwest in the west to folds that verge to the northeast in the east (Hinchey, 2007).

The Aillik Group is further complicated by an abundant amount of brittle faults, likely associated with the Grenvillian orogeny, that dissect the area and redistribute units (Hinchey and LaFlamme, 2009). These faults show both dextral and sinistral motion (Hinchey and LaFlamme, 2009).

1.5.5 Metamorphism

Previous work has indicated that the volcanic and sedimentary rocks of the Aillik Group have undergone upper greenschist to lower amphibolite facies metamorphism during the Makkovikian orogeny (Clark, 1973; Bailey, 1981; Gower et al., 1982; Sinclair, 1999; Hinchey, 2007). The western area of the Aillik Group preserves upper greenschist facies assemblages while central and eastern areas of the Aillik Group preserve lower amphibolites facies assemblages which are locally retrograded to greenschist facies (Hinchey, 2007). Some sections of Aillik Group in Makkovik Bay area are low strain and preserve primary features including cross bedding and ripple marks while other areas are highly strained, most of the primary features being destroyed (Clark, 1973, 1979; Bailey, 1981; Sinclair, 1999; Wilton, 1996; Hinchey, 2007). Geochemistry and field observations indicate that sodic and alkalic alteration is widespread throughout the Aillik Group whereas metavolcanic and sedimentary units to the south of Cape Makkovik are commonly silicified (Gandhi, 1978; Bailey, 1981; Gower and Ryan, 1987; MacDougall, 1988; Sinclair, 1999; Hinchey, 2007).

1.5.6 Geochronology

Relevant U-Pb geochronological data from the Aillik domain are summarized below and the historical data from the Aillik Group are displayed in Figure 1.4. The first U-Pb zircon ages, measured via TIMS analysis, for the Aillik Group were reported by Schärer et al. (1988) as two intercept ages at 1861 +9/-3 Ma and 1856 ± 2 Ma for a rhyolite flow and an ash flow tuff, respectively. Hinchey and Rayner (2008) reported three zircon dates from the Aillik Group using SHRIMP geochronology: a) a felsic tuff from a high strain zone at Aillik Bay yielded an age of 1861 ± 6 Ma; b) a rhyolite from the eastern side of Kaipokok Bay yielded an age of 1883 ± 7 Ma; and 3) a rhyolite from Ford's Bight area yielded an age of 1876 ± 6 Ma. Hinchey and Rayner (1980) also reported a U-Pb SHRIMP date of 1858 ± 6 Ma on Figure 1.4 from the quartz-feldspar-porphyritic granite, interpreted to be syn-volcanic with the Aillik Group. Sinclair et al. (2002) dated a porphyritic granite and reported a discordant intercept TIMS U-Pb date of 1929 +10/-9 Ma. This age is difficult to reconcile with the geological field relationships (see Hinchey, 2007).

Kerr (1989) produced 10 U-Pb TIMS dates for zircon crystallization from abundant post-volcanic, variably foliated to undeformed plutons that occur throughout the Aillik domain. The plutonic rocks relevant to this study include the Kennedy Mountain Intrusive Suite, the Adlavik Intrusive Suite and Monkey Hill Intrusive Suite (Figure 3). The

Kennedy Mountain Intrusive Suite, at Kennedy Mountain, was dated at 1801 ± 2 Ma (Barr et al., 2007). The Adlavik Intrusive Suite yielded an emplacement age of 1649 ± 1 Ma and the Monkey Hill Intrusive Suite yielded a discordia line giving an imprecise lower age limit of ca. 1641 Ma (Kerr et al., 1992). The upper age limit for the Monkey Hill Intrusive Suite is ca. 1649 Ma based on the occurrence of xenoliths interpreted to be Adlavik Intrusive Suite near the margins of the Monkey Hill Intrusive Suite (Kerr et al., 1992; Kerr, 1994).

The October Harbour Granite was originally interpreted as being part of the ca. 1720 Ma Strawberry Intrusive Suite because its compositions of primary and secondary minerals are similar to those in members of the Suite (Gower et al., 1982; Kerr, 1989). Cox et al. (2003) dated a sample of this granite from the study area by LA-ICP-MS (Laser ablation – inductively coupled plasma – mass spectrometer) and determined a zircon U-Pb age of 1657 ± 10 Ma indicating that this intrusion is actually part of the ca. 1650–1640 Ma intrusive suites (see Figure 1.3 for location).

1.5.7 Geochemistry

Regional geochemical studies within the Makkovik Bay area of the Aillik domain have focused mainly on the plutonic suites intruding the Aillik Group. Kerr (1989) and Kerr and Fryer (1994) determined that the ca. 1800 Ma and ca. 1720 Ma plutonic suites have an A-type signature, typical of anorogenic, post-orogenic and rift intrusive rocks. They reported that the ca. 1650-1640 Ma suites have an I-type signature and are likely an effect from the Labradorian orogeny, in the accretion of the Grenville Province. A single detailed geochemical study from a single location, the Ranger Bight area, was reported by Sinclair et al. (2001). Based on the chemical characteristics of the analysed mafic volcanic rocks, Sinclair et al. (2001) interpreted an extensional tectonic setting strongly influenced by a volcanic arc.

1.5.8 Isotopic Geochemistry

Prior isotopic geochemistry has focused solely on whole-rock Sm-Nd analyses of plutonic rocks (Kerr and Fryer, 1994). Based on εNd values for ca. 1800 Ma and *ca.* 1720 Ma plutonic suites, Kerr and Fryer (1994) interpreted a change in the nature and antiquity of the continental crust from the western Aillik domain ($\varepsilon Nd_{(T)}$ = -8) to the eastern Aillik domain ($\varepsilon Nd_{(T)}$ = +4). This change was interpreted to define a boundary between an Archean block and an Early Proterozoic block. Based on $\varepsilon Nd_{(T)}$ values that lie between those expected for a depleted mantle reservoir and those measured for exposed basement rocks, they interpreted the data to reflect mixing between juvenile material with depleted mantle characteristics and older crustal rocks. Based on a two-component mixing model, Kerr and Fryer (1994) interpreted that most of the post-Makkovikian plutons in the western domain are dominated volumetrically by new mantle-derived material suggesting significant crustal growth via late-stage magmatism, and direct interaction of mantle-derived magmas with lower crustal rocks.

The ca. 1650-1640 Ma igneous suites do not mimic the other intrusive suites; rather they lack a clear systematic variation in $\varepsilon Nd_{(T)}$. These plutons have εNd ranging from -5.0 to +0.2; Kerr and Fryer (1994) interpreted the suite as representing crustal growth via later, distal, arc-type magmatism.

Kerr and Fryer (1994) also reported whole-rock $\varepsilon Nd_{(T)}$ data for two ca. 1860 Ma volcanic rocks from the Aillik Group. They found that a rhyolite flow or sill from Ranger Bight has a $\varepsilon Nd_{(T)}$ value of -0.6 and a model age of 2380 Ma; whereas, a weakly foliated ash-flow tuff from the Michelin Ridge area yielded a $\varepsilon Nd_{(T)}$ value of -6.3 and a model age of 2560 Ma. Sinclair et al. (2001) reported the ca. 1929 Ma porphyritic granite (Measles' Point granite) that has a $\varepsilon Nd_{(T)}$ value of +0.87.

1.6 OBJECTIVES

The goal of this thesis is to further characterize the Aillik Group, by determining the timing and nature of volcanism, and investigating the tectonic setting in which it formed. Moreover, this thesis aims to provide insight into the formation of Paleoproterozoic bimodal volcano-sedimentary belts. These objectives are achieved by studying two separate exposures of the Aillik Group by the following procedures:

1. Producing detailed 1:10000 scale maps and tectonostratigraphic columns of the Pomiadluk Point and Middle Head areas.
2. Constraining the timing of felsic volcanism in both areas via U-Pb SHRIMP zircon geochronology.
3. Characterizing the major and trace element geochemical signatures of volcanic, plutonic and sedimentary units within the Aillik domain.
4. Determining the source of mafic and felsic magmatism using Nd and Hf isotope geochemistry.

The methods above provide data to further constrain the timing and evolution of the Aillik domain and provide insight into the formation of Paleoproterozoic bimodal volcano-sedimentary belts.

1.7 METHODOLOGY

This section explains the methodology and theory behind data collection, laboratory analyses and data interpretation used during the completion of this thesis.

1.7.1 Field and Petrographic Studies

During the summer of 2008, detailed bedrock mapping of two stratigraphic sequences, Middle Head and Pomiadluk Point, was completed. Traditional mapping methods were complimented by a handheld computer linked to a GPS. Stations, measurements, and observations were recorded directly to the handheld computer in the field using ArcPad. Two 1:10,000 scale maps were produced and digitized in ArcGIS.

Petrographic analysis included examining 58 polished thin sections from 56 samples. Rock slabs cut for each sample were stained for potassium feldspar following the procedures outlined by Lyons (1971).

1.7.2 Major and Trace Element Geochemistry

All major lithologies in the map areas were sampled for whole-rock geochemistry which included 22 samples from Middle Head and 18 from Pomiadluk Point. All sample preparation was done at Memorial University. Major and selected trace element analyses were completed at the Geological Survey of Newfoundland by ICP-AES and ICP-ES, respectively, following the procedures of Finch (2001). REE and selected trace element analyses were completed at Memorial University by ICP-MS following the procedures of Longerich et al. (1990). To interpret Aillik Group rocks and plutons of the Aillik domain, the software Igpet 2008 was used to plot Harker diagrams, discrimination diagrams and spider diagrams. Immobile elements such as Ta (or Nb), Yb (or Y), Th Zr, and Ti are useful discriminators of tectonic environments. Analytical methods are described in Appendix A.3.

To determine the style affecting the lithologies of the Aillik domain, samples were plotted in the alteration box after Large et al. (2001). The alteration box plot is a graphical representation of two alteration indices: the Ishikawa alteration index (AI) and the chlorite-carbonate-pyrite index (CCPI). These two indices have been developed to measure the intensity of sericite, chlorite, carbonate and pyrite replacement of sodic feldspars and glass.

The AI quantifies the intensity of sericite and chlorite replacement of sodic plagioclase and volcanic glass (Ishikawa et al., 1976). The AI is devised to ratio the principle rock-forming elements gained during chlorite and sericite alteration (K_2O + MgO) over the elements gained and lost (K_2O + MgO + CaO + Na_2O); it is defined by:

$$\mathrm{AI} = \frac{100(\mathrm{K_2O} + \mathrm{MgO})}{(\mathrm{K_2O} + \mathrm{MgO} + \mathrm{Na_2O} + \mathrm{CaO})}$$

The CCPI is designed to measure the chlorite and/or carbonate and/or pyrite replacement of albite, potassium feldspar or sericite (Large et al., 2001, modified after Lentz, 1996; 1999). The CCPI quantifies the increase in MgO and FeO associated with the Mg-Fe chlorite/carbonite/pyrite development leading to the loss of Na_2O and K_2O in sodic plagioclase/potassium feldspar/sericite; it is defined by:

$$\mathrm{CCPI} = \frac{100(\mathrm{MgO} + \mathrm{FeO})}{(\mathrm{MgO} + \mathrm{FeO} + \mathrm{Na_2O} + \mathrm{K_2O})}.$$

The alteration box plots AI on the horizontal axis against CCPI on the vertical axis to distinguish between diagenetic alteration and hydrothermal alteration. Common diagenetic minerals: albite, potassium feldspar, calcite and epidote plot on the left and lower axes, whereas common hydrothermal minerals: sericite, chlorite, pyrite, dolomite and ankerite plot on the right and upper axes. A diagonal line joining epidote to potassium feldspar separates the field of diagenetic alteration (lower left) from hydrothermal alteration (upper right). Common alteration trends are defined by the arrows and described in the figure caption.

1.7.3 Radiogenic Isotopes

1.7.3.1 U-Pb Zircon Geochronology

U-Pb zircon geochronology is reported to constrain the timing of volcanism within the Aillik Group and to determine the age of the Cross Lake granite. Five samples were chosen for U-Pb zircon geochronology including 4 felsic tuff samples (1 from Middle Head and 3 from Pomiadluk Point) and 1 monzogranite (from Middle Head).

The premise of U-Pb geochronology is based on the fact that the U decay system is paired;

$$^{238}U \rightarrow {}^{206}Pb + 8\,\alpha + 6\,\beta^- \text{ (half life: 4468 m.y)}$$

$$^{235}U \rightarrow {}^{207}Pb + 7\,\alpha + 4\,\beta^- \text{ (half life: 704 m.y).}$$

Two age determinations can be made on the same sample using the same two elements (Jaffey et al., 1971; Davis and Krogh, 2003). Because parents ^{235}U and ^{238}U and daughters ^{207}Pb and ^{206}Pb show coherent chemical behavior, age information can be obtained from disturbed systems that often occur in silicate rocks (Dickin, 1995). U-Pb analysis is often completed on the mineral zircon ($ZrSiO_4$) which contains high U concentrations, preserves the original U and accumulated radiogenic Pb contents during metamorphism, and strongly discriminates against Pb during crystallization. Zircon is fairly common in felsic rocks and is relatively easily extracted from samples (Hanchar and Miller, 1993).

In this paper, $^{207}Pb/^{206}Pb$ dates are calculated by weighted mean for each sample from the analyses. A mean-square of weighted deviates (MSWD) and probability of fit (POF) are reported to assess variation about the mean and degree of concordancy.

Previous geochronological studies report multi-domained, complex, small zircon grains from felsic volcanic rocks of the Aillik Group (eg. Scharer et al., 1988; Hinchey and Rayner, 2008). Therefore, *in situ* sensitive high resolution ion microprobe (SHRIMP) U-Pb zircon geochronology is preferred for this study since it samples a select portion of the zircon grain, rather than the more conventional techniques of isotope dilution - thermal ionization mass spectrometry (ID-TIMS) which dissolve the whole zircon grain before analyzing U and Pb concentrations. In utilizing the accuracy of SHRIMP U-Pb geochronology, precision is sacrificed because of a smaller pit size, as well as instrumentation and analytical capabilities. The resulting error varies inversely with the square-root of the number of analyses (Davis and Krogh, 2003). U-Pb geochronology was completed on the SHRIMP-II at the Geological Survey of Canada in Ottawa. Analytical methods are described in Appendix A.1.

For this study, samples were imaged in cathodoluminescence (CL) and in backscattered electron (BSE) before analyses. These images can reveal features such as cores, magmatic and metamorphic overgrowths and areas of recrystallization as well as fractures and inclusions (Corfu et al., 2003; Belousova et al., 2006). U content of each domain can clearly be seen in CL (Hanchar and Miller, 1993; Corfu et al., 2003). Resulting $^{207}Pb/^{206}Pb$ dates are interpreted based on spot location. Anomalously high or low dates may occur because of a spot analysis being located on a fracture, inclusion, area of recrystallization or a core. Pits made by SHRIMP analysis were reimaged in BSE at Memorial University. Each analysis was compared to the BSE images of pits, taken after analyses are completed.

1.7.3.2 Nd Isotopes

Whole-rock Sm-Nd data are reported to characterize the source and isotopic composition of the lithological units within the study areas. Sixteen samples for Sm-Nd analyses were chosen, crushed and prepared in the sample manner for geochemistry at Memorial University (see Appendix A.3). Samples were analysed at Carleton University in the Isotope Geochemistry and Geochronology Research Centre. Analytical methods are described in Appendix A.4.

Samarium (Sm) and Neodymium (Nd) occur in many rock-forming silicate minerals and are used in the dating of terrestrial rocks. ^{147}Sm decays to ^{143}Nd ($T_{1/2}$= 1.06 * 10^{11} yr) by the following equation,

$$^{147}_{62}Sm \rightarrow ^{143}_{60}Nd + ^{4}_{2}He + E\ ,$$

where $^{4}_{2}He$ is an α particle and E is decay energy.

The premise behind the Sm-Nd isotopic system is to determine whether rocks have higher or lower ratios of Sm-Nd than the chondritic uniform reservoir (CHUR; DePaolo and Wasserberg, 1976a; Faure and Mensing, 1986). This is done by comparing the initial $^{143}Nd/^{144}Nd$ of igneous rocks in the Earth's crust with the corresponding $^{143}Nd/^{144}Nd$ of CHUR at the time of crystallization of the rocks. Partial melting of the CHUR gives rise to magmas having lower $^{143}Nd/^{144}Nd$ and Sm/Nd ratios than CHUR (DePaolo and Wasserburg, 1976a). The residual solids that remain behind after withdrawal of the magma have higher $^{143}Nd/^{144}Nd$ and $^{147}Sm/^{144}Nd$ ratios than the chondritic reservoir (Figure 1.5; Depaolo and Wasserburg, 1976a). The following equation after Depaolo and Wasserburg (1976a) and DePaolo (1981) relates the two variables above,

$$\left(\frac{^{143}Nd}{^{144}Nd}\right)^{t}_{CHUR} = \left(\frac{^{143}Nd}{^{144}Nd}\right)^{0}_{CHUR} - \left(\frac{^{147}Sm}{^{144}Nd}\right)^{0}_{CHUR} \left(e^{\lambda t} - 1\right)$$

In this equation $\left(\frac{^{143}Nd}{^{144}Nd}\right)^{0}_{CHUR} = 0.512638$ and $\left(\frac{^{147}Sm}{^{144}Nd}\right)^{0}_{CHUR} = 0.1967$. The decay constant λ for $^{147}Sm = 6.54 * 10^{-12}$ (Lugmair and Marti, 1978). The subscript zero signifies the present time ($t = 0$) and the subscript t signifies at time t. Because the differences in the isotope ratios that are being compared are quite small, an elipson parameter is introduced by DePaolo and Wasserburg (1976a),

$$\varepsilon Nd_{(T)} = \left[\frac{\left(\frac{^{143}Nd}{^{144}Nd}\right)^{t}_{s} - \left(\frac{^{143}Nd}{^{144}Nd}\right)^{t}_{CHUR}}{\left(\frac{^{143}Nd}{^{144}Nd}\right)^{t}_{CHUR}} * 10^{4} \right].$$

Model ages in this study are determined following DePaolo (1988),

$$t = \frac{1}{\lambda} \ln \left[\frac{\left(\frac{^{143}Nd}{^{144}Nd}\right)^{0}_{s} - \left(\frac{^{143}Nd}{^{144}Nd}\right)^{0}_{DM}}{\left(\frac{^{147}Sm}{^{144}Nd}\right)^{0}_{s} - \left(\frac{^{147}Sm}{^{144}Nd}\right)^{0}_{DM}} + 1 \right],$$

where, $\left(\frac{^{143}Nd}{^{144}Nd}\right)^{0}_{DM} = 0.513613$ and $\left(\frac{^{147}Sm}{^{144}Nd}\right)^{0}_{DM} = 0.21370$ (Goldstein et al., 1984). Model ages are meant to be estimates of when Nd in a crustal rock could have separated from the chondritic reservoir and should not be taken as entirely meaningful.

1.7.3.3 Hf Isotopes

Lu-Hf isotope geochemistry was completed on the same five samples that were chosen for geochronology, and 57 spots were analysed. Analyses were completed at Memorial University using LA-MC-ICPMS. Analytical methods are described in Appendix A.2. Lu-Hf isotope geochemical analyses of zircon grains were studied to further characterize the samples. The systematics of Lu-Hf in zircon are similar to Sm-Nd, as both are particularly sensitive to the involvement of a juvenile magmatic component (Kinny and Mass, 2003). The significant difference is that Lu-Hf analyses are *in situ* and completed by LA-MC-ICPMS on the same analytical sites used for the U-Pb SHRIMP geochronology, giving more accurate results with respect to model ages.

Because the initial chondritic Lu/Hf ratio for Earth's mantle has been modified over time by generating basaltic magmas which have depleted the residual mantle in Hf relative to Lu, we can classify magmas as either Lu/Hf_{mantle} or Lu/Hf_{crust}. Lu/Hf_{mantle} and $^{176}Hf/^{177}Hf_{mantle}$ are > chondrites and Lu/Hf_{crust} and $^{176}Hf/^{177}Hf_{crust}$ are < chondrites (Kinny and Maas, 2003). Paleoproterozoic magmatic rocks derived from a source with a recycled Archean crustal component can be distinguished from those with a mantle source using $^{176}Hf/^{177}Hf$ ratios (Figure 1.6). The basic equation relating to the Lu-Hf decay system is as follows,

$$\left(\frac{^{176}Hf}{^{177}Hf}\right)^{t}_{CHUR} = \left(\frac{^{176}Hf}{^{177}Hf}\right)^{0}_{CHUR} - \left(\frac{^{176}Lu}{^{177}Hf}\right)^{0}_{CHUR} \left(e^{\lambda t} - 1\right)$$

where $\left(\frac{^{176}Hf}{^{177}Hf}\right)^{0}_{CHUR} = 0.282785$ and $\left(\frac{^{176}Lu}{^{177}Hf}\right)^{0}_{CHUR} = 0.0336$ (Bouvier et al., 2008). The decay constant λ for $^{176}Lu = 1.867 * 10^{-11}\ yr^{-1}$ (Söderlund et al., 2004). The subscript zero signifies the present time ($t = 0$) and the subscript t signifies at time t. An epsilon parameter is introduced, as in Nd notation, to amplify the small differences in ratios. Initial εHf values at age t are determined by the following equation,

$$\varepsilon Hf_{(T)} = \left[\frac{\left(\frac{^{176}Hf}{^{177}Hf}\right)_s^t - \left(\frac{^{176}Hf}{^{177}Hf}\right)_{CHUR}^t}{\left(\frac{^{176}Hf}{^{177}Hf}\right)_{CHUR}^t} * 10^4 \right],$$

using *in situ* SHRIMP $^{207}Pb/^{206}Pb$ ages from each spot analysis.

Model ages are determined using the following equation,

$$t = \frac{1}{\lambda} \ln \left[\frac{\left(\frac{^{176}Hf}{^{177}Hf}\right)_{DM}^0 - \left(\frac{^{176}Hf}{^{177}Hf}\right)_s^t}{\left(\frac{^{176}Lu}{^{177}Hf}\right)_{Crust}^0 - \left(\frac{^{176}Lu}{^{177}Hf}\right)_{DM}^0} + 1 \right]$$

where $\left(\frac{^{176}Hf}{^{177}Hf}\right)_{DM}^0 = 0.28325$ and $\left(\frac{^{176}Lu}{^{177}Hf}\right)_{DM}^0$ = of 0.0388 (Griffin et al. 2000; updated by Andersen et al. 2009). $\left(\frac{^{176}Lu}{^{177}Hf}\right)_{Crust}^0 = 0.022$ for mafic crust and $\left(\frac{^{176}Lu}{^{177}Hf}\right)_{Crust}^0 = 0.01$ for felsic crust (Pietranik et al., 2008).

1.7.4 Mixing

Magmatic rocks are differentiated by various processes including crystal fractionation in magma chambers (fractional crystallization), contamination of magma by an assimilating wall rock (assimilation), and mixing of magma components (simple mixing). To differentiate between processes the FC-AFC-FCA spreadsheet program by

Ersoy and Helvaci (2009), used to graphically model mixing and fractional crystallization, is introduced. The program requires the compositions of starting liquid and contaminant, as well as the amount of contaminant added in the form of a ratio 'r'. The program also requires an input of 'F' which represents the incremental amount of melt remaining and r is the ratio of fractionating material to assimilated materials in the model. For a given liquid composition, the program calculates compositions and proportions of liquidus phases and equilibrium temperatures. In each step, the type and amount of each mineral, and the equilibrium temperature are calculated.

The mixing process is graphically represented by the concentration of an element in a magma resulted from the simple mixing of two different magmas (eg. Lassen et al., 2004). The process is expressed by:

$$C_m = X(C_a - C_b) + C_b$$

where C_a, C_b and C_m are the concentration of an element in magma *a*, magma *b*, and in the mixed magma resulting from the mixing of magma *a* and *b*, respectively. *X* is the degree of mixing.

Fractional crystallization processes are generally combined with the assimilation of wall rocks surrounding the magma chamber (DePaolo, 1981). A relationship between the amount of material assimilated and the amount of material crystallized during magma cooling is expressed in the following equation:

$$C^{AFC} = C_0 = \left[F^{-z} + \left(\frac{r}{r-1}\right)\frac{C_a}{zC_0}(1 - F^{-z})\right]$$

where C^{AFC} is the concentration of the element in the resulting magma, C_0 is the concentration of the element in the parent magma, and C_a is the concentration of the element in the assimilating material. The F and the r values are panels in which the user controls during modeling. The z value is expressed by

$$z = \frac{r + D - 1}{r - 1}$$

where D is the bulk partition coefficient of elements for fractionating mineral phases.

1.8 STRUCTURE OF THE THESIS

The following section gives a brief introduction to the four chapters that comprise this thesis.

1.8.1 Introduction

This thesis is divided into 4 chapters, of which Chapter 2 and Chapter 3 are intended to be publishable papers. The first chapter is an introductory chapter aimed to provide the reader with the regional geological overview and historical studies of the Aillik domain. It also provides the overall scope and goals of the research, and outlines and explains the methods used to undertake said objectives. Chapter 2 and Chapter 3 are stand-alone manuscripts. There is a certain amount of unavoidable repetition (e.g., regional geology, description of lithologies). Chapter 4 is a brief conclusion which summarizes the objectives and results obtained in Chapter 2 and Chapter 3. It also seeks to unify the material for the purpose of this thesis. The following is a brief outline of Chapter 2 and Chapter 3.

1.8.2 Chapter Two – "*In situ* U-Pb zircon geochronology and Hf-isotope zircon data from two Paleoproterozoic bimodal volcanic segments of the Aillik Group, Makkovik Province, Labrador" (C. LaFlamme, A. Hinchey, P. Sylvester, and W. Davis)

This paper addresses the timing of volcanism and the nature of the magma source in forming the Aillik Group. Methods used include description of the lithologies and tectonostratigraphy of two study areas as well as U-Pb zircon geochronology and Hf isotope geochemistry from four felsic volcanic samples and one foliated intrusion. The data is used to further constrain the timing of volcanism across the Aillik domain and to demonstrate the type of crust involved in the formation of the Aillik Group.

1.8.3 Chapter Three – "Geochemical and Nd isotopic data from the Aillik Group and implications on the formation and evolution of the Aillik domain" (C. LaFlamme, A. Hinchey, and P. Sylvester).

This paper focuses on the tectonic setting in which the Aillik Group formed and the subsequent evolution of the Aillik domain during the Makkovikian orogeny. This paper presents the major and trace element geochemical analyses, Nd isotope geochemistry and petrographic analyses from both study areas. These data are used to characterize the Aillik Group and foliated granitic plutons in terms of petrogenesis and geodynamic evolution.

1.8.4 Summary

Chapter 4 summarizes and unifies the findings in Chapters 2 and 3. It also gives direction for further study.

1.9 CO-AUTHORSHIP CONTRIBUTIONS

These manuscripts contain 3 co-authors. My supervisor, Dr. Alana Hinchey, aided in field mapping interpretation, in choosing methods appropriate for analyses, interpreting resulting data, and reporting in a clear, concise manner. My other supervisor, Dr. Paul

Sylvester, aided in discussions related to geochemical analyses and provided insight to the meaning of results attained in Hf and Nd isotope geochemistry. Dr. Bill Davis was present during SHRIMP analyses at the Geological Survey of Canada. Dr. Davis was responsible for insuring that the raw data was within acceptable accuracies and for interpreting the age of the rocks.

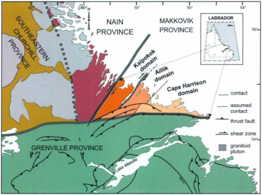

Figure 1.1: Simplified tectonic framework of south-central Labrador after Wardle et al. (1997), showing the Kaipokok, Aillik and Cape Harrison domains of the Makkovik Province.

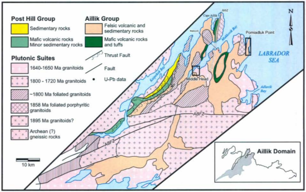

Figure 1.2: The simplified geology of the Aillik domain modified after Kerr et al. (1996) and Hinchey (2007). Location of the Middle Head area and Pomiadluk Point study areas are outlined in black.

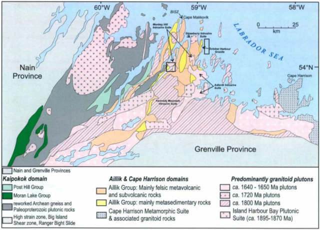

Figure 1.3: Simplified geology of the Makkovik Province after Ketchum et al. (2002). Figure highlights volcano-sedimentary packages as well as plutonic and metamorphic suites mentioned in text. Locations of study areas enclosed

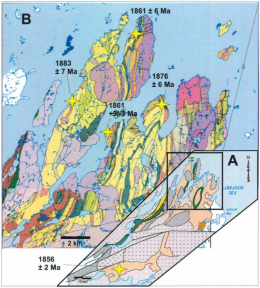

Figure 1.4: Summary of U-Pb geochronology from the Aillik Group. A) Geological map of the Aillik domain is after Kerr et al. (1996). B) Enlarged geological map of the Makkovik Bay area is from Hinchey (2007) and Hinchey and LaFlamme (2009). Age data are from Schärer et al. (1988) and Hinchey and Rayner (2008).

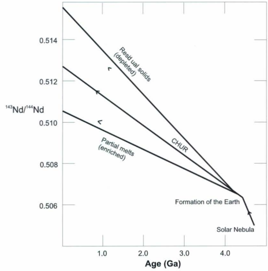

Figure 1.5: Evolution of $^{143}Nd/^{144}Nd$ within the crust over time after Faure (1986). CHUR - Chondritic uniform reservoir.

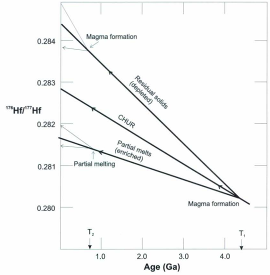

Figure 1.6: Evolution of $^{176}Hf/^{177}Hf$ within the crust over time after Faure (1986). CHUR - Chondritic uniform reservoir.

Chapter 2

GEOLOGY AND *IN SITU* ZIRCON U-PB AND LU-HF ISOTOPE SYSTEMATICS FROM PALEOPROTEROZOIC MAGMATIC ROCKS OF THE AILLIK DOMAIN, MAKKOVIK PROVINCE, LABRADOR

ABSTRACT

The Makkovik Province of eastern Labrador is part of an accretionary orogenic belt that formed prior to and during the Paleoproterozoic Makkovikian orogeny. The Aillik domain of the Makkovik Province is largely composed of: a) the Aillik Group, a package of Paleoproterozoic, polydeformed, bi-modal volcano-sedimentary rocks, and b) abundant undeformed to variably deformed Paleoproterozoic intrusive suites that intrude the Aillik Group. Basement rocks to the Aillik domain are not observed in the field. Extensive alteration and metamorphism of the Aillik Group has limited previous whole rock geochemical and geochronological studies that aimed to characterize the nature and timing of magma generation. This paper presents new data to constrain the timing and characterize the nature of Paleoproterozoic magmatic events of the Aillik domain, by presenting lithological observations from two distinct study areas, new in situ zircon U-Pb SHRIMP geochronology and new Lu-Hf LA-MC-ICPMS isotopic data from felsic volcanic rocks of the Aillik Group and a foliated intrusion.

The two study areas within the Aillik domain are: a) Middle Head, which is dominated by arkosic sandstone, felsic tuff, rhyolite and basalt; and b) Pomiadluk Point, which is composed primarily of felsic tuff and polymictic conglomerate with lesser preserved rhyolite and basalt. The Middle Head area is intruded by a deformed Cross Lake granite, the undeformed Monkey Hill granite and variably deformed dykes. The

Pomiadluk Point area is intruded by a deformed quartz-feldspar porphyritic granite, the undeformed October Harbour granite and numerous generations of variably deformed mafic and felsic dykes. The Aillik Group in both areas preserved lower amphibolite facies metamorphism which has been locally retrograded to greenschist facies. U-Pb SHRIMP zircon geochronology from a felsic tuff sample at Middle Head yields a magmatic $^{207}Pb/^{206}Pb$ *date of 1852 ± 7 Ma. Three felsic tuff samples at Pomiadluk Point yield magmatic* $^{207}Pb/^{206}Pb$ *dates of 1854 ± 7 Ma, 1862 ± 7 Ma, 1861 ± 7 Ma which are statistically indistinguishable. These U-Pb ages indicate that sections of the Aillik Group occurring 14 km from one another were deposited contemporaneously, and that felsic volcanism continued to as late as ca. 1852 Ma. Most inherited grains range in age from 1880 to 1920 Ma and are thought to be inherited from the source material. A foliated syn-deformational Paleoproterozoic monzogranite from Middle Head, known as the Cross Lake granite, yields a* $^{207}Pb/^{206}Pb$ *date of 1805 ± 6 Ma; which indicates that the development of the pervasive planar fabric continued after this time.*

Initial εHf_s^i *in zircon from a ca. 1852 Ma felsic tuff and ca. 1805 Ma monzogranite at Middle Head, range uniformly from -1.6 to -5.0 with crust formation ages of ca 2.4 to 2.6 Ga for their felsic crustal sources. In contrast, two felsic tuff samples at Pomiadluk Point with magmatic ages of ca. 1854 and 1861 Ma have initial* εHf_s^i *values in zircon that range from -4.8 to -11.9 in 18 of 20 grains analyzed, corresponding to (felsic) crust formation ages of 2.6 to 3.0 Ga. A third sample from Pomiadluk Point, a ca. 1862 Ma foliated felsic tuff that outcrops between two conglomerate beds, contains magmatic zircons with initial* εHf_s^i *that range from +2.1 to*

-1.6, and crust formation ages of 2.3 to 2.5 Ga. The main population of inherited zircon grains yield εHf_t^i *that range from -4.8 to +4.3, corresponding to model ages that vary between 2200 to 2660 Ga.*

The new Hf-isotope data suggest that the Aillik Group was deposited on a heterogeneous crust that had an age range of at least 700 Ma and included both Paleoproterozic and Archean components. The similar Hf isotopic signatures of the inherited zircon from xenocrysts in felsic tuff, the magmatic zircon in felsic volcanic rocks of the Aillik Group and magmatic zircon in the Cross Lake granite demonstrate that magma was derived from the same crust over a period of at least 115 million years.

2.1 INTRODUCTION

The tectonic environment in which Paleoproterozoic magmatic belts form is commonly obscured by polyorogenic events including: alteration, overprinting fabrics, folding, thrusting and lithologic discontinuities. Within the past 10 years, *in situ* analytical techniques, specifically sensitive high resolution ion microprobe (SHRIMP) U-Pb zircon geochronology coupled with laser ablation-multicollector-inductively coupled plasma-mass spectrometry (LA-MC-ICPMS) Lu-Hf isotope geochemistry have been developed and improved to offer a means of studying the timing of volcanism as well as the magma source characteristics of complex Paleoproterozoic terranes (e.g.,Vervoort and Blichert-Toft, 1999; Kosler and Sylvester, 2003; Condie et al., 2005; Hawkesworth and Kemp, 2006). The application of *in situ* U-Pb zircon geochronology can determine and constrain both the timing of magmatism (determined from magmatic zircon grains) and the ages of magmatic source rocks (determined from inherited zircon grains). *In situ* Lu-Hf isotopic analysis of magmatic zircon grains can provide information about the relative roles of juvenile crustal accretion or reworking of older continental crust (Flowerdew et al., 2006; Hawkesworth and Kemp, 2006). Recent studies including Flowerdew et al. (2009) and Matteini et al. (2009) have combined these two methods to provide insight into the crustal evolution and petrogenesis of Proterozoic magmatic belts.

Zircon grains are highly robust and contain U-Pb and Lu-Hf ratios that are largely resistant to weathering, deformation and alteration, all of which can disturb other radiogenic isotope systems in whole rocks (eg. Sm-Nd; Kinny and Mass, 2003). Zircon grains, existing as refractory relics in felsic magmas, carry radiogenic isotopic information about their deep crustal sources, which may be otherwise inaccessible (Hawkesworth and Kemp, 2006). The low intra-crystalline diffusion rate of Hf in zircon and the high closure temperature of the Lu–Hf isotope system suggest that Hf isotope compositions remain largely unaffected by post-crystallization thermal events (Cherniak and Watson, 2000). By analysing zircon grains, it is possible to target specific areas of a complex grain such as a core, rim or area of recrystallization, which represent an array of formation processes such as inheritance from source rocks, magmatic crystallization, and metamorphism. Hence, ε_{Hf} values and Hf T_{DM} model ages obtained for zircon compliment geologic field mapping of surface exposures by offering a means of characterizing the nature of the magmatic source (Kinny and Mass, 2003; Hawkesworth and Kemp, 2006; Matteini et al., 2010). These methods are especially useful in the Aillik domain where source terrains are not preserved.

The Aillik domain is one of three domains that make up the Makkovik Province of Labrador (Ryan et al., 1983; Gower and Ryan, 1986; Kerr et al., 1996). It comprises the Aillik Group, a sequence of Paleoproterozoic metasedimentary and metavolcanic rocks that has been intruded by numerous suites of variably deformed Proterozoic intrusions, as well as by numerous suites of mafic and felsic dykes (Kerr, 1989; Ketchum et al., 2002; Hinchey, 2007). Basement rocks to the Aillik Group and subsequent syn-deformational granitic intrusions have yet to be identified in the field and their age is presently highly speculative (Kerr and Fryer, 1994; Sinclair et al., 2001; Ketchum et al., 2002; Hinchey and Rayner, 2008). New data from preserved zircon grains characterizes the nature of basement involved in the formation of the Aillik Group and subsequent syn-deformational granitic intrusions.

Previous studies investigating the nature of the Aillik domain have focussed on TIMS U-Pb zircon geochronology as well as whole rock Sm-Nd isotopic studies of foliated intrusions. The results from these studies are the basis for several tectonic models for the formation of the evolution of the Aillik domain; however, little data have been reported specifically from the Aillik Group. Based on Nd isotopic signatures, Kerr and Fryer (1994) suggested that the western Aillik domain formed on older reworked Archean rocks to the west known as the Kaipokok domain, and that the eastern Aillik domain formed on a juvenile crust. Based on TIMS U-Pb geochronology of a ca. 1929 Ma porphyritic granite, Sinclair et al. (2002) interpreted this granite as being the basement to the Aillik Group. Ketchum et al. (2002) acknowledged that there is limited evidence to support the formation of the Aillik Group on the accreted Kaipokok domain and recognize that the present-day basement to the Aillik Group may differ from its depositional basement because of lateral transport over significant distances, as defined by Culshaw et al. (2000). Ketchum et al. (2002) proposed that the Aillik Group formed on a juvenile(?) island arc complex following its collision with the North Atlantic Craton. No study has yet focused on the volcanic rocks of the Aillik Group, making this area an ideal location for the application of a paired, *in situ* U-Pb geochronological and Lu-Hf isotopic study of zircon. These *in situ* techniques are useful when studying the origin of the Aillik Group of the Makkovik Province because of the lack of exposed basement rocks, discontinuous stratigraphic sections and pervasive alteration.

This paper focuses on two geographically distinct areas of the northeastern Aillik domain, Middle Head and Pomiadluk Point, which preserve sections of Aillik Group and syn-deformational plutonic intrusions (Figure 2.2). In this study we present results based on field mapping, petrography, U-Pb SHRIMP zircon geochronology and Lu-Hf LA-MC-ICPMS isotope zircon geochemistry to further constrain the timing of formation of the Aillik Group and characterize the source rocks involved. Furthering our understanding of the timing and source of magma generation will facilitate the evaluation of tectonic models for the formation of the Aillik Group, and subsequently of the entire Makkovik Province.

2.2 REGIONAL GEOLOGY

The Makkovik Province of Labrador is part of a Paleoproterozoic accretionary orogen wedged between the Nain Province to the north and the Grenville Province to the south (Figure 2.1; Ketchum et al., 2002 and references therein) and comprises Paleoproterozoic volcano-sedimentary units, variably deformed intrusive suites, reworked Archean rocks and abundant mafic dykes (Kerr et al., 1992). The Makkovik Province has been affected by several episodes of deformation, metamorphism and plutonism from orogenic events, including the Makkovikian orogeny (1900-1710 Ma; Ketchum et al., 2002) and to a lesser extent the Labradorian (1710–1655 Ma; Scharer et al., 1986; Scharer and Gower, 1988; Gower 1990; Kerr, 1989) and Grenvillian (1080–985 Ma; Gower and Ryan, 1986) orogenies. The Makkovik Province is divided into three domains, from northwest to southeast: the Kaipokok domain, the Aillik domain, and the Cape Harrison domain (Figure 2.2; Kerr et al., 1996). The Ketilidian orogen in southern Greenland is interpreted to be an extension of the Makkovik orogen, based on: a) reflection seismology, specifically the Lithoprobe Eastern Canada Shield Onshore – Offshore Transect; b) geochronology; and, c) lithological similarities (Hall et al., 1995; Kerr et al., 1997; Wardle et al., 2002).

Based on field evidence, lithological composition and chemistry, the Kaipokok domain is interpreted to be the foreland zone (Kerr et al., 1996), while the Aillik and Cape Harrison domains have been interpreted to be a rifted arc to composite arc that accreted to the Nain Province (Ketchum et al., 2002). The accretion of the Aillik and Cape Harrison domains marks the initiation of the 1900 – 1710 Ma Makkovikian orogeny, characterized by a penetrative planar fabric, abundant plutonic intrusions, regional deformation and upper greenschist to lower amphibolite facies metamorphism

(Gower et al., 1982; Kerr, 1994; Kerr et al., 1996; Culshaw et al., 1998; Ketchum et al., 2001, 2002).

The Aillik domain is composed of the Aillik Group, a metamorphosed Paleoproterozoic volcano-sedimentary package, numerous Proterozoic variably deformed intrusive suites, and an abundance of deformed and undeformed mafic dykes. The Aillik Group consists of volcanic and sedimentary units metamorphosed to upper greenschist to lower amphibolites facies (Gandhi et al., 1969; Bailey, 1981; Gower et al., 1982, Ketchum et al., 2002; Hinchey, 2007). Volcanic rocks of the Aillik Group are bimodal in composition, composed dominantly of felsic units and lesser preserved mafic units (Clark, 1973; Gower et al., 1982; Hinchey, 2007).

The Aillik Group was deformed and metamorphosed following its deposition. Early studies of deformation described folds as large, gently plunging, upward facing structures (Clark, 1973, 1979; Gower et al., 1982). More recently, Hinchey (2007) and Hinchey and LaFlamme (2009) reinterpreted the structural history as being characterized by regional-scale, closed to tight, moderately plunging, upright to overturned folds (F_1 locally) that were subsequently refolded (F_2 locally). Regional-scale folds (F_3) are isoclinal to open and upright to overturned. Culshaw et al. (2000) indicated that six stages of deformation are required to explain structures in the whole of the Makkovik Province of which only D_3 to D_6 affected the Aillik domain. Culshaw et al. (2000) proposed that the folding and the penetrative fabric are the result of sinistral transpression, regionally a D_3 event, and that shear zones in the Aillik Group were subsequently reactivated during D_4 and D_{5-6} events. The D_3 event described by Culshaw et al. (2000) reflects northwest transport of the Aillik Group onto the North Atlantic Craton and is defined by a penetrative fabric, mineral lineations and the development of shear zones.

Areas of high strain are recognized in the Aillik domain (Clark, 1979; Culshaw et al., 2000; Ketchum et al., 2002; Hinchey, 2007). A 1-km-wide, highly strained zone extends southward from Cape Makkovik through Big Island and inland to the south of Ranger Bight. This has been most recently named the Big Island Shear Zone (BISZ; Ketchum et al., 2002). Hinchey (2007) suggested that this high-strain zone likely represents one of a series of ductile shear zones that excise parts of the Aillik Group. These ductile shear zones (D_3; Culshaw et al., 2000) are unique to the Aillik domain. Units of the Aillik Group have complex stratigraphy due to the fact that units are not laterally continuous, it has a complicated deformational history, and units are further truncated by brittle faulting (Hinchey 2007; Hinchey and LaFlamme, 2009). Lithologic and stratigraphic characteristics of the Aillik Group suggest deposition in a shallow marine to subaerial environment (Wardle and Bailey, 1981; Gower et al., 1982; Hinchey 2007).

Previous U-Pb geochronology studies of zircon from the felsic volcanic rocks of the Aillik Group are presented in Figure 2.3 and include two analyses by thermal ionization mass spectrometry (TIMS) with upper intercept ages of 1861 +9/-3 Ma and 1856 ± 2 Ma (Schärer et al., 1988) and three ages via SHRIMP analysis: 1883 ± 7 Ma, 1876 ± 6 Ma, and 1861 ± 6 Ma (Hinchey and Rayner, 2008). The recent SHRIMP zircon geochronology extends volcanism to a minimum of 18 million years (Hinchey and Rayner, 2008). Recent geochronological data coupled with 1:50,000 scale mapping, has improved the understanding of the structurally modified stratigraphy in the Aillik Group (Hinchey, 2007; Hinchey and Rayner, 2008; Hinchey and LaFlamme; 2009).

The age of basement to the Aillik domain was investigated by Kerr and Fryer (1994). Based on a variation in Nd isotope signatures of foliated plutons, Kerr and Fryer (1994) interpreted that Makkovikian magmatism in the Aillik domain is a product of variable proportions of mixing between the mantle and Archean crust (North Atlantic Craton). Ketchum et al. (2002) determined that there is not enough evidence to preclude that the magmatism of the Aillik domain formed from the Archean gneisses of the North Atlantic Craton. Instead Ketchum et al. (2002) used the geochronology of Kerr (1989) and Ketchum et al. (2001) as well as structural data from Culshaw et al. (2000) to conclude that the Aillik domain was deposited on an island arc terrane with an undefined age.

The Measles Point granite, a high-level quartz-feldspar porphyritic granite within the Aillik domain, was dated by Sinclair et al. (2002) using TIMS U-Pb zircon analysis to yield an upper intercept age of 1929 +10/-9 Ma, interpreted to be the age of crystallization, and a meaningless lower intercept age of 956 Ma. Sinclair et al. (2002) suggested that this intrusion may represent basement to the Aillik Group; however, Hinchey and Rayner (2008) argued that this interpretation is not consistent with geological relationships. Hinchey (2010) interpreted the ca. 1929 Ma date as resulting from mixing between complex areas of the zircon grains in the dissolutions used for TIMS analysis. In particular, Hinchey (2007) reported that the Measles Point granite intrudes the Aillik Group and is geochemically indistinguishable from Aillik Group rhyolites. A similarintrusion of quartz porphyritic granite in the Aillik domain yielded a U-Pb SHRIMP zircon age of 1857 ± 6 Ma (Hinchey and Rayner, 2008).

2.3 METHODS

The following section gives details on the methods used to analyze the lithologies at Middle Head and Pomiadluk Point. This includes field mapping, U-Pb SHRIMP zircon geochronology and Lu-Hf isotopic geochemistry. Further details can be found in Chapter 1 as well as in Appendix A.1 and A.2.

2.3.1 Mapping

Detailed 1:10,000 scale mapping was completed using both traditional and modern mapping techniques;lithological and structural observations were manually plotted using enlarged air-photographs as well as digitized directly in the field using a hand-held device connected to a GPS. These qualitative and quantitative data were then uploaded to ArcGIS and plotted manually on a map daily.

2.3.2 U-Pb SHRIMP zircon geochronology

U-Pb geochronology was completed using the SHRIMP-II at the Geological Survey of Canada (GSC) in Ottawa. Three felsic tuff samples (one from Middle Head and three from Pomiadluk Point) and one monzogranite sample (Cross Lake granite from Middle Head) were analysed. Zircon grains of were separated and concentrated from the samples using conventional Wilfley water table, heavy liquid and Frantz magnetic separation techniques. This work was completed in the Earth Science Department at Memorial University. Clear, inclusion-free grains were selected by hand-picking under an optical microscope, mounted in epoxy resin, and imaged with backscattered electron (BSE) and cathodoluminescence (CL) detectors on the scanning electron microscope (SEM) at the GSC prior being analyzed.. Analytical procedures for work completed at the GSC followed those described by Stern (1997), with standards and U-Pb calibration methods of Stern and Amelin (2003). Analytical procedures are discussed in more detail in Appendix A.1. After analysis, the analytic sites of the SHRIMP in the zircon were imaged by BSE on the SEM at Memorial University.

2.3.3 Lu-Hf isotope geochemistry

In situ measurements of Lu-Hf isotopes were carried out using a GeoLas ArF gas (193 nm) laser ablation system coupled to a Thermo Finnigan Neptune Multicollector ICPMS at Memorial University. Analytical procedures are described in Appendix A.2. Data reduction calculations were carried out using an in-house, Excel-based spreadsheet "MCTool-Hf_laser_RL_150f.xlt" (modified by R. Lam, after Košler et al., 2008) on selected zircons previously analysed by SHRIMP geochronology in the five samples described above. The systematics of Lu-Hf isotopic geochemistry are described in Chapter 1.

2.4 RESULTS

Results including geology and tectonostratigraphy, deformational history, geochronology and Lu-Hf isotope geochemistry pertaining to the two geographically distinct study areas, Middle Head and Pomiadluk Point, are presented below. The locations of the study areas are presented in Figure 2.3. Figure 2.4 displays the detailed

(1:10,000 scale) map of the Middle Head area; whereas, Figure 2.5 shows the detailed (1:10,000 scale) map of the Pomiadluk Point area.

2.4.1 Lithologiesat Middle Head

Volcanic units at Middle Head are bimodal in composition and are dominated by basalt with less abundant rhyolite and felsic tuff. Sedimentary units include arkosic sandstone, tuffaceous sandstone, calcsilicate rock and volcaniclastic breccia. The Aillik Group at Middle Head is intruded by the foliated Cross Lake granite, which is in turn intruded by the non-foliated Monkey Hill granite. Deformed dykes cut all units minus the Monkey Hill granite and undeformed mafic (to intermediate) dykes and undeformed granitic pegmatite cut all lithologies at Middle Head. Volcanic, sedimentary and plutonic lithologies are presented below.

2.4.1.1 Aillik Group

The Aillik Group at Middle Head is north-northeasterly trending and units dip to the east. This is in agreement with Aillik Group lithologies west of the Big Island Shear Zone (Hinchey, 2007). The supracrustal lithologies at Middle Head are intruded by cross-cutting foliated granite, unfoliated granite and numerous dykes. The tectonostratigraphy at Middle Head contains mafic and felsic volcanic rocks as well as sedimentary rocks metamorphosed to lower amphibolite facies. The western map area is dominated by volcanic rocks, including rhyolite, crystal to crystal-lithic felsic tuff, and basalt as well as lesser sedimentary units including arkosic sandstone interbedded with lesser tuffaceous sandstone and minor calcsilicate rock. The eastern map area is dominated by arkosic sandstone interbedded with lesser siltstone, calcsilicate rock and tuffaceous sandstone with lesser volcaniclastic breccia and basalt.

The units at Middle Head are strongly foliated, moderately lineated and flattened. Foliation and lineation are defined by biotite laths in sandstone and tuffaceous sandstone, hornblende laths in basalt, and lithic and crystal fragments in felsic tuff. Depositional features and way up indicators were not observed in the field; however, primary volcanic textures including porphyries in rhyolite and brecciated volcanic fragments in the volcaniclastic breccia unit are preserved. The preserved stratigraphy at Middle Head is complex due to the deformation, laterally discontinuous and repeating lithologies, and late faulting. A columnar cross section of A and B is presented in Figure 2.6.

Rhyolite (unit 7) forms north to northeast trending flows within the western outcrop area of the Aillik Group. The flows are approximately 35 m wide and are locally porphyritic. In porphyritic rhyolite, phenocrysts are feldspathic and range in length from 1 to 3 mm. The rhyolite flows are moderately foliated, prominently laminated and recrystallized. Although contacts between mafic and felsic volcanic units are transposed, small fragments (<4 cm) of basalt are found in rhyolite demonstrating that mafic volcanism is, at least in part, older than felsic volcanism (Figure 2.7a). Felsic tuff (unit 8), occurring in the western outcrop area, comprises both lithic and crystal-lithic varieties (Figure 2.7b). Lithic fragments include elongated fragments of coarser grained tuff and tuffaceous sandstone that are up to 2 cm long. Crystals are elongated and up to 1 mm in length. Minor, thin layers of tuffaceous sandstone are interbedded with the tuff. The felsic tuff has been recrystallized and contains a foliation defined by elongated phenocrysts and aligned minor mafic minerals in the matrix.

Fine-grained basalt (unit 4) occurs in both the eastern and western sections of the Aillik Group at Middle Head. Basalt occurs as flows that are up to 60 m thick. Small relict pillows are seen within various parts of the basalt pile. Pillows that are up to 15 cm long and 10 cm wide, weather preferentially and, in places, are defined by epidote-altered selvages (Figure 2.7c). Pillows are flattened due to regional deformation, eradicating facing directions. The basalt is strongly foliated, defined by aligned biotite and hornblende grains. Basalt contains an abundance of epidote and quartz veins, as well as epidote nodules (Figure 2.7d). Rare, two-meter wide beds of dark, recrystallized quartzite (possibly relict chert) layers occur within the basalt pile.

Arkosic sandstone (unit 1) occurs as a thick (300 m wide) north- to northeast-striking unit in the eastern outcrop area and as several thin (less than 20 m wide) layers in the western outcrop area. In the western area the sandstone is composed of feldspar, quartz and biotite and is interbedded with less abundant siltstone. The arkosic sandstone becomes increasingly enriched in diopside until it grades into calcsilicate rock to the east and west of the succession. In the western area, arkosic sandstone is interlayered with lesser tuffaceous sandstone and contains fewer mafic minerals than in the eastern area.

Calcsilicate rock (unit 2) occurs to the east and west of the arkosic sandstone and also occurs as a thin layers (<10 m wide) within the volcanic pile in the western area. The presence of abundant diopside lends a mafic appearance to the rock in hand sample (Figure 2.7e). Veinlettes (< 1 cm wide) of calcite cut the calcsilicate rock unit.

Tuffaceous sandstone (unit 4) occurs in the far eastern part of the map area. The unit is fine-grained and composed of quartz, feldspar and flakes of biotite. A weak foliation is defined by biotite laths in the matrix. Volcaniclastic breccia (unit 3) occurs as a 50 m-wide layer in the eastern outcrop area. The unit contains fragments of felsic and mafic volcanic rocks supported by an epidote-altered matrix. The volcanic clasts are subangular to angular and range in length from 1 to 7 cm (Figure 2.7f). A foliation is developed in the unit by aligned brecciated fragments.

2.4.1.2 Intrusions

Two granitic intrusions occur at Middle Head. The oldest is a foliated hornblende-biotite (hbl-bt) monzogranite (unit 9) which intrudes the supracrustal rocks of the Aillik Group and the youngest is an undeformed biotite-hornblende monzogranite. The hbl-bt monzogranite is foliated and lineated, coarse grained and locally potassium feldspar porphyritic (Figure 2.8a). Based on its lithology, it is interpreted to be part of the nearby Cross Lake granite. Mafic minerals in the Cross Lake granite make up to 6% of its composition and define a moderate foliation and lineation.

The bt-hbl monzogranite (unit 10) intrudes the Cross Lake granite in the northern extent of the map area. The unit is non-foliated, medium grained, leucrocratic and slightly plagioclase porphyritic (Figure 2.8b). Locally developed plagioclase phenocrysts are typically up to 1 cm long. Based on its lithology, the monzogranite is interpreted to be a member of the Monkey Hill Intrusive Suite. Mafic minerals include primary biotite and hornblende, accounting for 5% of its composition. Accessory chlorite, fluorite and magnetite occur throughout the unit.

2.4.1.3 Dykes

Variably deformed dykes cut most of the lithologies at Middle Head. These dykes include a suite of deformed amphibolite dykes, a suite of undeformed appinitic diorite and granodioritic dykes and a suite of granitic pegmatite dykes. The amphibolite dykes are deformed and observed as folded within the Aillik Group and do not cut the Monkey Hill granite. These dykes are foliated, recrystallized and up to 1 m wide. Undeformed appinitic diorite/granodiorite dykes (unit 9) are 5 to 15 m wide, linear, and intrude both the Aillik Group and the Cross Lake granite (Figure 2.8c). Granitic pegmatite (unit 12) dykes cut the Aillik Group and Cross Lake granite and are composed of large blocky crystals of quartz, plagioclase, potassium feldspar, biotite and fluorite (Figure 2.8d).

2.4.2 Lithologies at Pomiadluk Point

Volcanic units at Pomiadluk Point are bimodal in composition and dominated by felsic tuff and rhyolite with less abundant basalt and mafic tuff. Sedimentary units include a thick succession of polymictic conglomerate with siltstone. The Aillik Group at Pomiadluk Point is intruded by a weakly foliated quartz-feldspar porphyritic granite, the non-foliated October Harbour granite and a non-foliated sill of the Adlavik Intrusive Suite. Deformed dykes cut all units except the October Harbour granie and undeformed mafic and felsic dykes cut all other lithologies at Pomiadluk Point. Volcanic, sedimentary and plutonic lithologies are presented below.

2.4.2.1 Aillik Group

The Aillik Group at Pomiadluk Point contains mafic and felsic volcanic rocks as well as sedimentary rocks metamorphosed to lower amphibolite facies that are locally retrograded to chlorite grade. At Pomiadluk Point the Aillik Group is dominantly comprised of metamorphosed conglomerate and felsic tuff. Less abundant metavolcanic rocks include rhyolite, basalt and mafic tuff and less abundant metasedimentary rocks include siltstone.

The volcano-sedimentary units at Pomiadluk Point are foliated and lineated, trending at 10 degrees and dipping to the east, this is consistent with the overall the penetrative planar fabric affecting the Aillik domain described by Hinchey (2007). Overall units are weakly deformed but localized areas are highly strained, occurring in 3 to 80 m wide shear zones. In areas not affected by shear, graded bedding and cross bedding are commonly preserved in conglomerate and felsic tuff and indicate way up direction. Preserved primary volcanic features include porphyries, lapilli, flow banding and rare flattened pillows. Even though units are only weakly deformed, the stratigraphy at Pomiadluk Point is complex due to the repetition of units and local shear zones. A columnar cross section of C is presented in Figure 2.9.

Crystal-lithic felsic tuff (unit 1) occurs on the west and east coasts of Pomiadluk Point and is finely bedded parallel to foliation and fine-grained. The crystal-lithic tuff contains up to 4% fragments of volcanic material, and up to 2% calcsilicate-rich pods. Lithic fragments which, for the most part, are composed of coarser grained felsic tuff, are elongated in the direction of the foliation and are less than 1 cm in length. Crystals are feldspathic and less than 1 mm in diameter. Crystal felsic tuff (unit 3) occurs near the eastern coast of Pomiadluk Point and is 20 m wide. Crystals in this unit are feldspathic, account for 4% volume and are up to 3 mm across. Bedding within crystal and crystal-lithic felsic tuff is defined by grain size variations in the matrix. A moderate foliation is defined by slightly flattened crystals and/or lithic fragments. Shear zones that are up to 80 m wide occur within the felsic tuff on the west coast, producing well defined cleavages subparallel to the foliation (Figure 2.10a). Calcite-rich veins up to 10 cm wide cut the crystal-lithic felsic tuff (Figure 2.10b).

Polymictic conglomerate forms,unit 5, and is locally interrupted by thin, discontinuous layers of siltstone, tuffaceous sandstone, mafic tuff and rhyolite. In the west the conglomerate contains subangular to subrounded pebble to boulder-sized clasts of granite (40%), granodiorite (30%), felsic tuff (20%), mafic tuff (10%), rhyolite (5%) and arkosic sandstone (5%) as well as minor quartzite, basalt and jasperoid supported by a felsic matrix (Figure 2.10c). Moving towards the east there is an increase in volcanic clasts (less than 10% granite clasts occur) and clast size decreases. Calcite and epidote veining are also more common. Shear zones up to 50 m wide cut the conglomerate.. The wider shear zones are restricted to the eastern side of Pomiadluk Point. Intense zones of shearing produced proto-mylonitic textures in conglomerate by flattening and stretching out competent mafic and felsic volcanic clasts (Figure 2.10d). Most of the shear zones are less than 5 m wide.

Rhyolite (unit 4) occurs on the east and west coasts of Pomiadluk Point as several distinct flows which are 30 to 40 m in width and laterally discontinuous. It is locally flow banded and varies from porphyritic to non porphyritic. Flow banding is defined by darker coloured layers in outcrop (Figure 2.11a). Where phenocrysts occur they are feldspathic, subrounded and up to 2 mm across. The rhyolite is recrystallized and a weak foliation is developed, defined by elongate phenocrysts in porphyritic rhyolite.. At least one shear zone cuts the rhyolite on the west coast producing proto-mylonitic textures (Figure 2.11b).

Basalt (unit 2) occurs as two 30 m wide outcrops near Papa's Cove and the adjacent islands. It is likely the same unit repeated by folding. Locally, pillows are preserved and identifiable by their epidote-altered selvages (Figure 2.11c). Mafic minerals hornblende and biotite align to define a pronounced foliation. Basalt contains epidote nodules as well as quartz and epidote veins. Hinchey (2007) reported that the basalt is cut by numerous thin calcite-epidote-titanite-diopside veins and contains galena-covellite-molybdenite vugs and nodules. Mafic tuff (unit 6) outcrops in two, 8 m wide, laterally discontinuous horizons. Mafic tuff is fine-grained and has a sugary texture in hand sample (Figure 2.11d). The unit is recrystallized and a foliation is developed parallel to bedding and defined by aligned hornblende and biotite grains.

A thin layer of laminated siltstone (unit 7) occurs at Pomiadluk Point. The siltstone-sandstone beds are about 10 m thick and composed of laminated to thinly bedded, grey siltstone and beige, thin- and parallel-bedded sandstone. Cross bedding and graded bedding are preserved in the sandstone on the western side of Pomiadluk Point, and indicate 'younging' to the west. The unit is foliated parallel to planar bedding, likely due to the rotation of units in the direction of the planar fabric.

2.4.2.2 Intrusions

A deformed syn-volcanic quartz-feldspar porphyritic granite (unit 8) occurs on the west coast of Pomiadluk Point. Phenocrysts, up to 3 mm across, are composed of quartz and feldspar and occur in a medium-grained groundmass (Figure 2.12a). Locally, this unit contains ellipsoidal mafic-oxide pods of biotite, magnetite and amphibole that are typically 2 to 8 cm long, 1 to 4 cm thick, and account for less than 2% modal abundance of the rock. Accessory magnetite occurs throughout the unit. Flattened and aligned phenocrysts define a weak foliated. This granite is part of the ca. 1858 Ma suite of granites which have been interpreted as sheet- or sill-like bodies that intruded synchronous with formation of the volcanic sequence (Hinchey, 2007).

An undeformed pluton, termed the October Harbour granite (unit 9), outcrops on the east coast of Pomiadluk Point between Papa's Cove and Frank's Point. The unit is a potassium-feldspar-porphyritic, biotite-fluorite monzogranite. Phenocrysts of potassium feldspar are 8 mm long and set in a coarse grained and equigranular groundmass. Secondary minerals account for 6% of the unit. A date of 1657 ±10 Ma was obtained for this unit by Cox et al. (2003) using U-Pb LA-ICPMS zircon geochronology. Contacts between the October Harbour granite and the Aillik Group rocks at Pomiadluk Point are sharp. Near the margins of the granite-rhyolite contact in the southernmost portion of the map area the OHG contains xenoliths of amphibolite dykes and rhyolite (Figure 2.12b).

*2.4.2.3 Dykes*A single flat-lying sheet of hornblende gabbro (unit 10) occurs in the center of the map area, 1200 m southwest of October Harbour. It has a thickness of less than 10 m and has intruded the polymictic conglomerate, displaying chilled margins along its edges. The sill is undeformed, medium grained, net veined and contains 3 mm long euhedral hornblende crystals (Figure 2.12c). The dyke is tentatively interpreted as being part of the Adlavik Intrusive Suite, based on its similarity and proximity to the latter, more extensive plutonic rocks, which outcrop to the south of the current study area (see Hinchey, 2007 and Hinchey and LaFlamme, 2009).

Several generations of mafic and felsic dykes cut the Aillik Group at Pomiadluk Point. Two generations of dykes are deformed. The earliest generation forms a series of dark green, amphibolite dykes that have been folded, boudinaged and metamorphosed. Amphibolite dykes are up to 2 m wide and pinch out over tens of meters. The next oldest generation is a series of deformed diabase dykes (unit 11) that are linear and strike north-northeast. These dykes are plagioclase-porphyritic with elongated, epidote altered phenocrysts that are up to 5 cm. Diabase dykes are schistose, with schistosity defined by metamorphic amphibole (Figure 2.12d).

Two groups of undeformed dykes are also exposed in the study area. The oldest swarm includes a number of feldspar-phyric granitic dykes (unit 12). The orientation of the dykes is controlled by jointing in host rocks. Felsic dykes cut all units except for gabbro dykes and sills at Pomiadluk Point. Based on lithology, granitic dykes are likely associated with the October Harbour granite. The width of the felsic dykes increases towards the east of Pomiadluk Point, indicating that the central source of the OHG may occur off the eastern coast. Xenoliths of Aillik Group rocks occur within the felsic dykes and are 1 to 2 cm wide (Figure 2.12e). The youngest suite forms non-foliated plagioclase porphyritic gabbro dykes (unit 13) that strike to the northeast. This suite is composed of megacrystic phenocrysts of plagioclase set in a groundmass of medium grained plagioclase biotite and hornblende (Figure 2.12f). Phenocrysts of plagioclase are up to 15 cm in length, euhedral, and demonstrate simple twinning in hand sample.

2.4.3 Local deformational history

Evidence for more than one phase of deformation is displayed in Aillik Group rocks at Middle Head and Pomiadluk Point. The earliest period of folding (F_1) is preserved locally by small-scale, re-oriented isoclinal folds of a pre-existing fabric (S_1) in sandstone at Middle Head and felsic tuff at Pomiadluk Point (Figure 2.13a, b). The fold axial traces of F_1 are parallel to the pervasive planar fabric (S_2) in the area, which strike north to northeast. Outcrop-scale folds are interpreted to be F_2. These folds are most readily observed in amphibolite dykes at Middle Head and Pomiadluk Point and are rarely observed in felsic tuff at Pomiadluk Point (Figure 2.13c, d). The regional folding pattern as inferred by Culshaw et al. (2000), Hinchey (2007) and Hinchey and LaFlamme (2009) is observed in both study areas and defined by reversals in 'younging' directions and a change in the degree of the dip of S_2 from steep to shallow.

Moving from east to west at Pomiadluk Point way up indicators demonstrate reversals in 'younging' directions. Cross bedding in a felsic tuff preserved on the eastern section as well as in a felsic tuff to the west of Papa's Cove indicates 'younging' to the west. However, between these units the graded-bedding within the conglomerate indicates younging towards the east. A baked contact of felsic tuff against a basalt flow on an island to the east of Papa's Cove indicates that the succession on the island is younger to the east. These reversals in 'younging' directions and fabric measurements support at least one overturned regional anticline and one overturned regional syncline in the Pomiadluk Point area. Units at Middle Head and Pomiadluk Point dip to the east, varying from shallow (~40°) to steep (>85°). Lineation directions trend to the northeast.

Many discrete shear zones cut the Aillik Group felsic tuff, conglomerate, basalt and rhyolite lithologies at Pomiadluk Point. These shear zones are 3 to 80 m wide and trend N-S. Culshaw et al. (2002) demonstrated that based on amphibole and mica $^{40}Ar/^{39}Ar$ cooling ages these shear zones were periodically reactivated well after the deposition of the Aillik Group and emplacement of deformed amphibolite dykes. Several intense shear zones up to 3 m wide that are cutting the conglomerate and rhyolite units form proto-mylonitic textures. Shear zones at Pomiadluk Point coincide with the D_3 event, reflecting northwest transport of Aillik Group rocks onto the North Atlantic Craton, described by Culshaw et al. (2000).

2.4.4 U-Pb zircon geochronology

Location of each dated sample is shown in Figure 2.4 and 2.5 and is depicted in an outcrop scale photograph, along with its representative photomictographs under crossed polars in Figure 2.13 (Middle Head) and Figure 2.14 (Pomiadluk Point). Isotopic results are displayed in Table 2.1 and representative images of zircon grains are shown in Figure 2.16 (Middle Head) and Figure 2.17 (Pomiadluk Point). Ages in Table 2.1 are weighted mean $^{207}Pb/^{206}Pb$ age and errors are quoted at 1σ. $^{207}Pb/^{206}Pb$ ratios and ages reported in the Table 2.1 are corrected for mass fractionation. Weighted mean (Figures 2.18-2.22) diagrams are plotted at the 2σ uncertainty level and weighted mean ages are reported at 2σ level.

2.4.4.1 08CL198A-03

Sample 08CL198A-03 is a recrystallized, foliated, lithic felsic tuff occurring in the western map area adjacent to the Cross Lake granite (Figure 2.5). The outcrop selected for sampling is a well exposed ridge devoid of veining and xenoliths (Figure 2.14a). The felsic tuff contains elongated lithic fragments that account for 8% of the sample, are up 0.5 cm across, and are composed of quartz, plagioclase, potassium feldspar and biotite (Figure 2.14b). The matrix is composed of quartz, plagioclase and potassium feldspar. Petrographic evidence for recrystallization includes granoblastic textures.

The zircon population is light brown to transparent and grains range in length from 40 to 250 μm. Grains are both equant and prismatic, subhedral and have aspect ratios ranging from 1:1 to 3:1. Representative grains are shown in Figure 2.16a. CL images show oscillatory and concentric zoning in most grains. This zoning is similar to that displayed by zircons generated by magmatic crystallization (Belousova et al., 2006). A total of 21 analyses yielded a single age population that has a weighted mean $^{207}Pb/^{206}Pb$ date of 1852 ± 7 Ma (Figure 2.18) with a mean square weighted deviation (MSWD) of 0.83 and a probability of fit (POF) of 0.68. This date is interpreted as the igneous crystallization age based on the magmatic character of the zircon..

One analysis, 39.1 in Table 2.1, was excluded from the calculation as it yielded a statistically older age of 1873 ± 14 Ma (2σ). This analysis comes from a subhedral and heavily fractures grain. This age is interpreted to reflect either an entirely inherited grain or to reflect overlap of the SHRIMP spot an older component and the ca. 1852 Ma zircon.

2.4.4.2 08CL199A-03

Sample 08CL199A-03 is a coarse grained, equigranular to potassium feldspar porphyritic, hornblende-biotite monzogranite (Figure 2.14c), termed the Cross Lake granite. It intrudes the Aillik Group at Middle Head and is located in the central map area (Figure 2.4). The outcrop selected for geochronological sampling is a well exposed ridge (Figure 2.14d). Accessory phase minerals; hornblende (3%), biotite (1 to 2%), and magnetite (0.5 to 1%), define a strong foliation and moderate lineation.

Zircon grains are brown to transparent in colour, have a 2:1 to 3:1 aspect ratio and are 100 to 300 μm in length. In CL grains display euhedral zoning, typical of zoning displayed by zircons generated by magmatic crystallization (Belousova et al., 2006). Grains selected for geochronological analyses are prismatic and are subhedral to euhedral. Representative images of grains are shown in Figure 2.16b. A total of 23 analyses on 22 grains yielded an age population with a weighted mean $^{207}Pb/^{206}Pb$ date of 1805 ± 6 Ma (MSWD = 0.92; POF= 0.52; Figure 2.19). This date is interpreted as the igneous crystallization age of the monzogranite based on the magmatic character of the zircon grains.

In addition, two analyses, 10.1 and 17.1 in Table 2.1, yielded statistically younger $^{207}Pb/^{206}Pb$ ages of 1767 ± 12 Ma and 1781 ± 9 Ma (2σ) (see grain 17 in Figure 2.16b). Both of these analyses are located in dark areas of the zircon grains which lack zoning in CL and are interpreted as being recrystallized, possibly being related to metamorphism or deformational events. One additional analysis (26.1 in Table 2.1) yielded an older age of 1887 ± 15 Ma. This analysis is from a grain that is subrounded and anhedral and is interpreted a being inherited, likely from the Aillik Group, which is intruded by this granite.

2.4.4.3 08CL452A-03

Sample 08CL452A-03 is a foliated, bedded, fine-grained felsic crystal-lithic tuff (Figure 2.15a). The unit outcrops as a 10 m wide bed within conglomerate on the north coast of Pomiadluk Point and pinches out 50 m to the south. The outcrop selected for geochronological sampling is well exposed along the coastline (Figure 2.15b). Crystals occurring within the felsic tuff account for <2% by volume, are angular, 2 mm wide and occur as lapilli. Lithic fragments account for <5% by volume and are composed of quartz + plagioclase + potassium feldspar + biotite ± calcite, are up to 3 cm across and subrounded. The felsic tuff has a matrix composed of plagioclase, quartz, potassium feldspar and flakes of biotite. Weak bedding is defined by grain size fining within the matrix. A strong foliation is parallel to bedding and defined by the biotite grains in matrix.

The zircon population is characterized by transparent, equant sized grains with 2:1 aspect ratios. The grains are anhedral to subhedral prismatic, contain oscillatory zoning in CL and are 40—150 μm in length. Zoning is similar to that displayed by zircons generated by magmatic crystallization (Belousova et al., 2006). Representative images of grains are shown in Figure 2.17a. Forty-four zircon analyses gave a mixed population of ages, the majority of which fall into 2 age domains. Seventeen analyses completed on 16 grains yielded a weighted mean a $^{207}Pb/^{206}Pb$ date of 1862 ± 7 Ma (MSWD = 0.58; Fit = 0.90; Figure 2.20). This is interpreted to be the magmatic crystallization age of the felsic tuff based on the magmatic signature of analyzed zircon grains.

This sample contains a significant population of older grains. Sixteen analyses from 15 grains yielded $^{207}Pb/^{206}Pb$ dates ranging from 1883 ± 8 Ma to 1921 ± 6 Ma. These analyses do not fall into a statistically defined single age population and are interpreted as inherited grains. This interpretation is supported by the fact that these older zircon grains are anhedral and contain reworked edges. In addition, four analyses (52.1, 56.1, 56.2 and 43.1 in Table 2.1) yielded even older $^{207}Pb/^{206}Pb$ dates at 2085 ± 12 Ma, 2160 ± 7 Ma, 2161 ± 6 Ma and 2743 ± 15 Ma (see grains 43 and 56 in Figure 2.17a). These grains are interpreted as being inherited, supported by their subrounded and reworked appearace. The oldest zircon grain has distinct U-Pb zonation patterns in CL (see grain 43.1 in Figure 2.17a). One analysis from a bright, structureless rim yielded a significantly younger age of 1813 ± 19 Ma, which is interpreted to be recrystallized possibly during regional metamorphism.

2.4.4.4 08CL453A-03

Sample 08CL453A-03 is a very fine- to fine-grained crystal felsic tuff (Plate 2.15c). The outcrop selected for geochronological sampling occurs on the eastern coast, near Papa's Cove and is homogeneous and well exposed (Plate 2.15d). Crystals of quartz, potassium feldspar and albite make up 10% volume of the unit and are angular and about 2 mm wide. Crystals occur in a matrix made up of the same minerals. Weak bedding is defined by interlayered finer and coarser grains within the matrix. A strong foliation is parallel to bedding and defined by flattened crystals of quartz, potassium feldspar and albite. Evidence for recrystallization includes granoblastic textures in the matrix.

Zircon grains are transparent and are typically 30—90 μm in size. The grains are equant to prismatic with flat terminations; few grains contain fractures and inclusions. In CL, oscillatory zoning is observed in most grains. Zoning is similar to that displayed by zircons generated by magmatic crystallization (Belousova et al., 2006). Representative images of grains are shown in Figure 2.17b. A total of 22 analyses yielded a weighted mean $^{207}Pb/^{206}Pb$ age of 1861 ± 7 Ma (MSWD = 1.13; Fit = 0.31; Figure 2.22). This is interpreted as the igneous crystallization date for the felsic tuff based on the magmatic character of the zircon grains.

Additional complexities in the zircon population include one statistically younger analysis (7.1 from Table 2.1), which yielded an age 1837 ± 10 Ma from a rim which is dark and structureless in CL. This age is interpreted as indicating recrystallization, likely related to the regional metamorphic event. One analysis, 56.1 in Table 2.1, yielded an older age of 1906 ± 29 Ma (see grain 56 in Figure 2.17b). The grain is interpreted as being inherited, based on its subrounded nature and nebulous CL zoning.

2.4.4.5 08CL458A-03

Sample 08CL458A-03 is a foliated, fine-grained felsic crystal-lithic tuff (Figure 2.15e) from the northwestern coast of Pomiadluk Point. The outcrop is well exposed and homogeneous (Figure 2.15f). Crystals account for <2% volume, are composed of quartz and albite, are subrounded, up to 1 mm wide and flattened in the plane of the foliation. Lithic fragments are up to across 2 cm, account for < 6% volume, and are composed of quartz + potassium feldspar + plagioclase + biotite + hornblende. Lithic fragments and crystals occur in a heterogeneous, matrix of quartz, potassium feldspar and plagioclase.

Evidence for recrystallization includes undulatory extinction in quartz and granoblastic textures.

The zircon population is transparent and ranges in size from 40 – 150 µm. Grains are of prismatic and typically show oscillatory zoning in CL typical of igneous zircon (Belousova et al., 2006). Representative images of grains are shown in Figure 2.17c. A total of 28 analyses yielded a weighted mean $^{207}Pb/^{206}Pb$ age of 1854 ± 7 Ma (MSWD = 0.88; POF = 0.65; Figure 2.22). This is date is interpreted as the timing of crystallization of the felsic tuff based on the igneous features of the analyzed zircon grains.

Additional analyses which are not part of the mean igneous population include an age of 1806 ± 17 Ma from the rim of a ca. 1854 Ma grain which displays nebulous zoning in CL indicative of recrystallization (see grain 33 in Figure 2.17c). This recrystallization is likely attributed to the regional metamorphic event. Two additional analysis (15.1 and 48.1 in Table 2.1) from dark, unzoned in CL rims are interpreted as mixed between these metamorphic and igneous ages, yielding ages of ca. 1818 ± 12 Ma and 1822 ± 15 Ma. Two grains (5.1 and 35.1 in Table 2.1) yielded older ages of 1883 ± 12 Ma and 1882 ± 13 Ma from cores that are interpreted as inherited.

2.4.5 Hf isotope geochemistry

Lu-Hf isotope compositions of zircon grains were studied in order to distinguish units with juvenile sources from those with sources which resided in the crust for a significant amount of time before magma genesis. ^{176}Lu decays to ^{176}Hf and the primitive, chondritic Lu/Hf ratio of Earth's upper mantle has increased over time due to partial melting and the generation mantle derived melts, which are enriched in Hf relative to Lu

(Kinny and Maas, 2003).. Therefore, the Lu/Hf and $^{176}Hf/^{177}Hf$ of the mantle are greater than chondrites, whereas, Lu/Hf and $^{176}Hf/^{177}Hf$ of the crust are less than chondrites. Zircon has a much greater crystal-chemical affinity for Hf over Lu, and thus the present-day, measured $^{176}Hf/^{177}Hf$ ratio in zircon requires only small corrections for in growth of ^{176}Hf from ^{176}Lu since the time of zircon crystallization (Faure and Mensing, 2005). For that reason, the radioactive decay of ^{176}Lu does not significantly change the Hf isotope composition of zircon over time.

The systematics of Lu-Hf in zircon are comparable to whole-rock Sm-Nd as both are particularly sensitive to the involvement of a juvenile magmatic component (Kinny and Mass, 2003). The two advantages of the zircon Lu-Hf approach to source tracing compared to the whole rock Sm-Nd approach are that (1) the ingrowth correction for ^{176}Hf in zircon is much smaller than for ^{143}Nd in whole rocks and (2) metamorphism and/or secondary alteration is less likely to have disturbed the magmatic Lu-Hf compositions of zircon than the magmatic Sm-Nd compositions of whole rocks. Zircon is a refractory mineral and Lu and Hf are bound in its crystal lattice, whereas whole rocks, particularly metamorphosed and/or altered units, carry Sm and Nd in a variety of both low and high temperature phases (Hawkesworth and Kemp, 2006).

When calculating crust formation model ages using Lu-Hf, it is necessary to take into account the type of crust involved in magma generation. Although new crust extracted from the mantle is generally of basaltic composition, intracrustal melting and differentiation of mafic crust produces felsic crust that will evolve along $^{176}Hf/^{177}Hf$ growth curves that differ from those of mafic crust (Wedepohl, 1995; Hawkesworth and

Kemp, 2006; Pietranik et al., 2008). Therefore different Lu/Hf ratios must be assumed for calculating crust formation model ages, depending on the composition of the source material. In this study a Lu/Hf ratio of 0.022 is used for mafic source rock and a Lu/Hf ratio of 0.01 is used for felsic source rock (Wedepohl, 1995; Pietranik et al., 2008).

Results for Aillik Group samples are presented in Table 2.2 showing the analyzed values for $^{176}Hf/^{177}Hf$ and $^{176}Lu/^{177}Hf$, initial εHf values as well as the calculated model ages for both mafic and felsic crustal sources. Calculation of uncertainties is based on 2σ of the mean. $^{176}Hf/^{177}Hf_{(t)}$ is plotted against $^{176}Lu/^{177}Hf$ plot for each grain in each sample from Middle Head in Figure 2.23 and from Pomiadluk Point in Figures 2.24 and 2.25. εHf_t^i is plotted for each zircon against its respective *in situ* SHRIMP $^{207}Pb/^{206}Pb$ date for each grain in Figure 2.26 (Middle Head) and Figures 2.27 and 2.28 (Pomiadluk Point). Hf-evolution lines for hypothetical crustal sources of the Aillik Group magmatism are shown in Figures 2.26 to 2.28, and are discussed below.

2.4.5.1 Magmatic Grains

Only zircon grains that were interpreted to be of magmatic origin, based on U-Pb zircon geochronology and CL imaging, are included in this discussion. Analyses from a ca. 1852 Ma lithic felsic tuff (08CL198A-03) occurring at Middle Head yield well constrained measured $^{176}Hf/^{177}Hf$ ratios that range from 0.281511 to 0.281584, corresponding to an initial εHf_t^i of -4.9 to -2.0. Analyses from the ca. 1805 Ma Cross Lake granite (08CL199A-03) yield well constrained measured $^{176}Hf/^{177}Hf$ ratios that range from 0.281550 to 0.281615, corresponding to an initial εHf_t^i of -5.0 to -1.6.

From Pomiadluk Point, the ca. 1862 Ma crystal-lithic felsic tuff (08CL452A-03) yield well constrained measured $^{176}Hf/^{177}Hf$ ratios that range from 0.281583 to 0.281714, corresponding to an initial εHf_t^i of -1.9 to +2.1. Analyses from the ca. 1861 Ma crystal felsic tuff (08CL453A-03) and the ca. 1854 Ma crystal-lithic felsic tuff have a broader range in measured $^{176}Hf/^{177}Hf$ and calculated εHf_t^i . Sample 08CL453A-03 yields measured $^{176}Hf/^{177}Hf$ that range from 0.281362 to 0.281741, corresponding to an initial εHf_t^i of -11.9 to +3.6; whereas, sample 08CL458A-03 yields measured $^{176}Hf/^{177}Hf$ that range from 0.281405 to 0.281505, corresponding to an initial εHf_t^i of -9.8 to -4.8.

Calculated crust formation ages for the lithic felsic tuff occurring at Middle Head (08CL198A-03) range from 2480 to 2610 Ma for felsic crustal sources and from 2910 to 3160 Ma for mafic crustal sources. The calculated crust formation ages for the Cross Lake granite range from 2420 to 2590 Ma for felsic crustal sources and 2840 and 3140 Ma for mafic crustal sources. The crust formation ages for the lithic felsic tuff overlap those from the monzogranite, which is about 60 m.y. younger than the tuff. The calculated crust formation ages in 18 of 20 grains for the crystal and crystal-lithic felsic tuffs occurring on the eastern and western coasts of Pomiadluk Point (08CL453A-03 and 08CL458A-03) range from 2630 to 2960 Ma for felsic crustal sources and from 3170 to 3750 Ma if a mafic crustal source is used. The remaining crystal-lithic felsic tuff, occurring on the northern coast of Pomiadluk Point, yields crust formation ages ranging from 2260 to 2480 Ma for felsic crustal sources and ranging from 2550 to 2910 Ma for a mafic crustal source.

2.4.5.2 *Inherited Grains*

Five inherited zircon grains within the dominant age population of 1880 to 1920 Ma in crystal-lithic felsic tuff sample 08CL452A-03 yield measured $^{176}Hf/^{177}Hf$ ratios ranging from 0.281561 to 0.281725, corresponding to initial εHf_t^i values ranging from 2.0 and +3.7 (see Table 2.2). The three oldest grains from this sample (see grains 43.1, 52.1 and 56.1 in Table 2.2) yield measured $^{176}Hf/^{177}Hf$ ratios of 0.281097, 0.281729 and 0.281477, corresponding to initial εHf_t^i values of of +1.2, +7.8 and +1.2, respectively. One inherited grain from crystal felsic tuff sample 08CL453A-03 was analyzed, and the ca. 1899 Ma zircon yields a measured $^{176}Hf/^{177}Hf$ ratio of 0.281463, corresponding to a εHf_t^i value of -4.8 (see grain 56.1 in Table 2.2).

Calculated model ages for six grains from the dominant population of inherited zircon grains model ages of 2200 to 2660 Ma for a felsic crustal source and 2410 to 3190 Ma for a mafic crustal source. Two older grains (ca. 2085 Ma and 2160 Ma) yield crustal formation ages of 2150 and 2550 Ma for a felsic crustal source and 2190 and 2830 Ma for a mafic crustal source. The remaining grain, having an Archean age of ca. 2743 Ma, gives a model age of 3030 Ma for a felsic crustal source and a model age of 3230 Ma for a mafic crustal source. The calculated model age of one inherited grain from crystal felsic tuff sample 08CL453A-03 is equal to 2660 Ma for a felsic crustal source and 3190 Ma for a mafic crustal source.

2.5 INTERPRETATION AND DISCUSSION

2.5.1 Timing and duration of Aillik Group volcanism

Previous U-Pb zircon geochronology of felsic volcanic rocks from the Aillik Group include two dates from Schärer *et al.* (1988): 1861 +9/-3 Ma and 1856 ± 2 Ma, and three dates from Hinchey and Rayner (2008): 1883 ± 7 Ma, 1876 ± 6 Ma and 1861 ± 6 Ma. The results presented in this study include a lithic felsic tuff from Middle Head that yields the youngest volcanic $^{207}Pb/^{206}Pb$ date yet reported from the Aillik Group, 1852 ± 7 Ma, as well as three crystal to crystal-lithic felsic tuff units from Pomiadluk Point that yield $^{207}Pb/^{206}Pb$ dates within error of one another: 1862 ± 7 Ma, 1861 ± 7 Ma and 1854 ± 7 Ma. When the age of the crystal felsic tuff from Middle Head is combined with the oldest known age of the Aillik Group (1883 ± 7 Ma; Hinchey and Rayner, 2008), the duration of volcanism within the Aillik Group is extended to 31 million years.

No systematic pattern of ages across the map area is apparent in Figure 2.3. The rhyolite with an age of 1876 ± 6 Ma occurs between the two study areas and the rhyolite with an age of 1883 ± 7 Ma occurs 3 km to the west of Middle Head. The scattered distribution of older and younger $^{207}Pb/^{206}Pb$ ages across the Aillik Group, reported in this study and in previous studies, is interpreted to be a product of tectonic interleaving of volcanic packages that occurred during D_3 of Culshaw et al. (2000), rather than a representation of original stratigraphy.

2.5.2 Timing of deformation of the Aillik Group

The Cross Lake granite at Middle Head has a crystallization age of 1805 ± 6 Ma, which is within error of the known age of the Kennedy Mountain intrusive suite (1800.6

± 2.3 Ma; Barr et al. 2007). The Cross Lake granite had been interpreted by Kerr (1989) to be part of this suite and results obtained in this study confirm this interpretation. The Cross Lake granite contains a foliation that is neither as well formed nor as pronounced as in Aillik Group rocks. The nature of deformation preserved in the Cross Lake granite may occur either due to its rigidity or because it intruded during the waning stages of the development of S_2, coinciding with D_3 of Culshaw et al., 2000, in Aillik Group rocks. Therefore, based on the new date for the body, deformation must have commenced at a time after to 1805 Ma. The maximum age of D_3 can now be constrained to occur after *ca.* 1852 Ma, the youngest known age of volcanism within the Aillik Group.

2.5.3 Nature and age of basement rocks to the Aillik Group

The nature and age of the basement rocks upon which the supracrustal rocks of the Aillik Group formed has remained unresolved because these basement rocks are not known to be exposed (Kerr, 1989; Hinchey, 2007). As a result, the assessment of the balance between recycled versus juvenile components in the source regions of magmas of the Aillik Group has relied almost exclusively on whole rock Sm-Nd isotope data (e.g., Kerr, 1989; Kerr and Fryer, 1994; Sinclair, 1999; Sinclair et al., 2001; Ketchum et al., 2002), which has been debated extensively.

Based on Sm-Nd isotope analyses from foliated intrusions, Kerr and Fryer (1994) interpreted the western portion of the Aillik domain (εNd ≈. -8) to have formed via mixing of mantle-derived magmas with Archean rocks of the North Atlantic Craton, now present as reworked Archean rocks of the Kaipokok domain. In contrast, the eastern portion (εNd ≈ about +4) was proposed to have formed by mixing between mantle-derived magmas and a juvenile component of the crust. According to Kerr and Fryer (1994), because of mixing between the crust and mantle, a specific age for the basement to the Aillik domain cannot be determined.

Ketchum et al. (2002) argued that there is little evidence available to conclude that the Aillik Group formed from Archean rocks of the North Atlantic Craton. Based on the geochronology from Kerr (1989) and Ketchum et al. (2001) and structural interpretations from Culshaw et al. (2000), Ketchum et al. (2002) suggested that the Aillik Group was deposited on a (now unexposed) island arc complex with an unknown age, and did not require Archean sources in its genesis. Because of the ongoing debate regarding the age and nature of the basement to the Aillik Group, a unified tectonic model for the Aillik Group and evolution of the Makkovik Province is lacking. The *in situ* Lu-Hf isotope geochemistry and U-Pb geochronology of zircons reported here offer new insights into the nature and age of the magmatic source to the Aillik Group.

2.5.3.1 Evidence for a felsic source for Aillik Group magmatism

For interpreting the Hf isotope zircon data of felsic volcanic rocks from the Aillik Group, it is assumed that their source rocks were composed of felsic crust rather than mafic crust for the following reasons. If the felsic magmas were produced by the fractionation of mafic magmas, with or without crustal assimilation, we would expect a spectrum of volcanic rocks including intermediate and felsic lithologies (Brewer et al., 2004; Reagan et al., 2003; Arculus, 1994), yet andesitic magmas have not been identified either within the volcanic rocks of the Aillik Group or as clasts within associated conglomerates (Hinchey, 2007; Hinchey and LaFlamme, 2009). Secondly, because fractional crystallization of mafic magmas produces subordinate volumes of felsic magmas (Bowen 1928), it would be expected that a greater abundance of mafic volcanic units over felsic volcanic units would exist in the Aillik Group, but in fact the reverse is observed (Hinchey, 2007; Hinchey and LaFlamme, 2009). And thirdly, if the felsic magmas were produced by the partial melting of mafic crust, sodium-rich, tonalitic to trondhjemitic compositions would be expected (Rapp et al., 1991); however, the compositions of the magmatic rocks of the Aillik Group are potassium-rich and monzogranitic (Sinclair et al., 2002). Therefore, we interpret the Aillik Group to have formed largely from a felsic crustal source.

2.5.3.2 Hf-isotope heterogeneity of the magmatic zircons

The variability in Hf isotope compositions of magmatic zircon occurring in an individual whole-rock sample reflects the scale of isotopic homogeneity present in the parent magma during crystallization. The degree to which Hf-isotopic homogeneity is achieved in felsic magmas is related to the extent of Hf-isotopic variation in the crustal protolith(s) and the efficiency of mixing partial melts of the protolith(s) in the parent magma. Most studies of Hf-isotopes in magmatic zircons from felsic magmatic rocks have found significant Hf-isotope heterogeneities, with variations of 5 to 10 epsilon units typical from the zircons in a single sample (e.g., Flowerdew et al., 2006; Kurhila et al., 2010). By examining the range in εHf_t^i of magmatic zircon grains within a single sample, it is possible to determine the degree of melt homogeneity and the degree of mixing from isotopically distinct sources.

At Middle Head, a lithic felsic tuff (08CL198A-02) and the Cross Lake granite (08CL199A-02) demonstrate Hf-isotope homogeneity with εHf_i^t that range from -5.0 to -2.1 and -5.1 to -1.7, respectively. Calculated model ages range from 2480 to 2610 Ma for the lithic felsic tuff and 2420 to 2590 Ma for the Cross Lake granite. The εHf_i^t and model ages of both samples overlap even though the Cross Lake granite is 60 m.y. younger than the felsic tuff, demonstrating that they were likely formed from a similar source that existed beneath the Aillik Group for this time interval. At Pomiadluk Point the easternmost and westernmost crystal and crystal-lithic felsic tuff units yield more negative εHf_i^t values than the lithic felsic tuff from Middle Head; εHf_i^t in sample 08CL453A-02 ranges from -7.0 to -11.9 (with the exception of two grains) and εHf_i^t in sample 08CL458A-02 ranges from -4.8 to -9.8. These data correspond to calculated model ages ranging from 2740 to 2970 Ma and 2630 to 2810 Ma, respectively. The thin unit of crystal-lithic felsic tuff on the northern coast of Pomiadluk Point (08CL452A-02) presents εHf_i^t that range from -1.9 to +2.1. Crust formation ages for this sample ranges from 2260 to 2480 Ma. The rather small εHf_i^t variation of 3 to 5 epsilon units found in each of the five samples of this study (compared to studies of other felsic rocks reported in the literature) demonstrates that within each sample, isotopic heterogeneity of the protolith(s) was limited. The heterogeneity that is present is explained by heterogeneity in the age of the magmatic source (about 200 m.y), this is reflected in the range of the calculated crust formation ages.

There tends to be a greater Hf-isotopic heterogeneity between the magmatic zircons of different felsic samples of the Aillik Group than there is within the magmatic zircons of each sample. Excluding the two zircons with anomalously high $^{176}Hf/^{177}Hf_{(t)}$ ratios in sample 08CL453A-03, the magmatic zircons of the five samples analyzed have εHf_{t}^{t} values that vary from -11.8 to +2.2, a range of some 14 epsilon units. This is likely the result of even a larger range in the ages of crustal protoliths between the samples of the Aillik Group. The range of crust formation ages for all of the analyzed magmatic zircons spans from 2260 to 2970 Ma, or some 700 m.y.

An alternative interpretation would be that the Hf-heterogeneity found between samples is due to mixing of partial melts from crustal protoliths with mantle-derived mafic melts, in variable proportions, similar to the model proposed by Kerr and Fryer (1994) for foliated granitic intrusions of the Aillik domain based on Sm-Nd isotope analyses. In order to test the mixing hypothesis, initial $^{176}Hf/^{177}Hf_{(t)}$ is plotted against 1/Hf in Figure 2.29 for each zircon analysed. If the zircons are related by two-component mixing, their compositions would fall along a line connecting the composition of the felsic, crustal source at one end and the mafic, mantle source on the other end. In fact, one can see from the least squares regression of the compositions that the data are not well fit by a line in that the correlation coefficient is very poor (r^2=0.14). Additionally, when the $^{176}Hf/^{177}Hf$ compositions (calculated at 1860 Ma) of the two likely end-members in the mixing model, the depleted mantle and the Archean continental crust, are plotted on the diagram, it is apparent that the mafic component in the samples would vary from only a few percent to more than 50%. In fact all of the felsic rocks analyzed are extremely silicic (70—78 wt.% SiO_2), which precludes their origin as mixtures of melts containing large amounts of a mafic component.

The Hf-isotope zircon geochemistry of analyzed felsic rocks indicates that the Aillik Group formed from crustal protoliths ranging in age from 2260 Ma (Paleoproterozoic) to 2970 Ma (Neoarchean). The rather limited Hf-isotope range occurring within each sample demonstrates that each sample was formed from sources with an age range of 200 m.y. In contrast, the more extensive heterogeneity in the Hf isotopic data occurring over the range of samples is likely the result of formation of the felsic magmatic rocks of the Aillik Group via the partial melting of crustal sources with an age range of 700 m.y. The Hf data provide no evidence that the Aillik Group was derived from a truly juvenile, 1900—2000 Ma crust with short residence times (<100 m.y.), as suggested by Ketchum et al. (2002).

2.5.3.3 Significance of inherited zircon grains

Inherited zircon grains occur in all analyzed felsic volcanic samples from the Aillik Group. Inherited zircon grains; however, are most prevalent in crystal-lithic felsic tuff sample 08CL452A-03, from the northern coast of Pomiadluk Point, which occurs between two conglomerate units. With the exception of three older grains occurring in sample 08CL452A-03, inherited zircon grains for the felsic volcanic samples yield $^{207}Pb/^{206}Pb$ dates that range from 1880 ± 8 Ma to 1920 ± 6 Ma. There are two possibilities for the source of these inherited grains. They could either be 1) derived from the deep-seated, basement rocks that were partially melted to produce the felsic volcanic rocks of the Aillik Group or 2) incorporated into the volcanic rocks as xenocrysts derived from near-surface country rocks during eruption and deposition of the Aillik Group. The latter interpretation is favoured in this case because the $^{207}Pb/^{206}Pb$ ages of the inherited zircon grains are much younger than the model Hf ages calculated for the source rocks of the felsic volcanic rocks of the Aillik Group.

Of the 1880—1920 Ma group of inherited zircon grains, five are from crystal-lithic felsic tuff sample 08CL452A-03 with $^{207}Pb/^{206}Pb$ ages of ca. 1888 to 1916 Ma yield $\varepsilon Hf_t'$ that range from +7.8 to -2.0 with crust formation ages of 2210 to 2520 Ma. One inherited zircon from crystal felsic tuff sample 08CL453A-03 with a $^{207}Pb/^{206}Pb$ age of ca. 1906 Ma yields $\varepsilon Hf_t'$ equal to -4.8 and a crust formation age of 2660 Ma. For the three anomalously older grains from sample 08CL452A-03, they have $^{207}Pb/^{206}Pb$ ages of ca. 2085 Ma, ca. 2160 Ma and ca. 2743 Ma and $\varepsilon Hf_t'$ of +7.8, +1.2 and +1.2, corresponding to crust formation ages of 2150 Ma, 2560 Ma and 3030 Ma, respectively. With the exception of the one Archean zircon, the similarity in Hf isotope crust formation ages for the magmatic and inherited zircon of each sample is interpreted to indicate that the inherited zircon formed from the same basement sources as the Aillik Group and the later foliated granitic intrusions. The indication is that magma in the Aillik domain was generated from the same basement sources over a period of at least 115 million years, from 1920 to 1880 Ma (represented by the majority of the inherited zircon grains in the felsic volcanics of the Aillik Group), through 1883 to 1852 Ma (represented by the magmatic zircons in the felsic volcanics of the Aillik Group), and up until 1805 Ma (represented by the magmatic zircons of the Cross Lake Granite).

2.6 SUMMARY OF CONCLUSIONS

(1) Middle Head preserves a thick succession of basalt with lesser felsic tuff and rhyolite; whereas, Pomiadluk Point preserves predominantly felsic volcanic rocks with lesser basalt and mafic tuff, but overall, the Aillik Group is dominated by felsic volcanic rocks.

(2) *In situ*, SHRIMP U-Pb zircon geochronology of a crystal felsic tuff from Middle Head yields the youngest reported volcanic $^{207}Pb/^{206}Pb$ date yet found within the Aillik Group: 1852 ± 7 Ma. When combined with previous geochronology, the duration of volcanism within the Aillik Group is extended to 31 million years.

(3) Multiple stages of deformation are identifiable at Middle Head and Pomiadluk Point. The original volcanic stratigraphy is not preserved. Shear zones preserved at Pomiadluk Point are related to the D_3 event described by Culshaw et al. (2000), reflecting the northwest transport of Aillik Group rocks. A foliated monzogranite from the Cross Lake granite at Middle Head yields a $^{207}Pb/^{206}Pb$ age of 1805 ± 6 Ma, confirming that this intrusion is part of the Kennedy Mountain Intrusive Suite. Deformation and the formation of a pervasive planar fabric that may represent a regional D_3, postdated the intrusion of the granite at ca. 1805 Ma.

(4) A small component of inherited zircon grains occur within the dated samples of felsic volcanic rocks of the Aillik Group and range in age from 1880 to 1920 Ma. It is likely that these grains were incorporated as xenocrysts from the supracrustal rocks on which the Aillik Group was deposited.

(5) εHf_t^i in magmatic zircons range from approximately -5 to -2 in a felsic tuff and monzogranite at Middle Head. Two felsic tuff samples on the easternmost and westernmost coasts of Pomiadluk Point have εHf_t^i of magmatic zircons that range from about -12 to -5. One sample of felsic tuff on the northern coast of Pomiadluk Point yields εHf_t^i varying between approximately -2 and +2.

(6) Crust formation Hf model ages for the Aillik group, assuming felsic sources, range from 2.5—2.6 Ga at Middle Head and 2.3 to 3.0 Ga at Pomiadluk Point. This range in ages indicates that the Aillik Group likely formed from a crust that had an age range of at least 700 Ma and included both Paleoproterozic and Neoarchean components. These results reflect significant age heterogeneity of the hidden crystalline basement rather than variable proportions of magma mixing during Aillik Group magmatism.

(7) The Aillik domain likely continued to generate from an attached basement source for a period of at least 115 million years, from 1920 Ma to 1805 Ma.

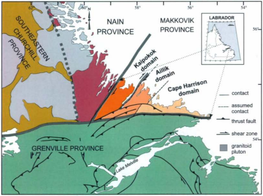

Figure 2.1: Simplified tectonic framework of south-central Labrador after Wardle et al. (1997), showing the Kaipokok, Aillik and Cape Harrison domains of the Makkovik Province.

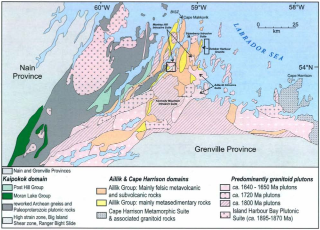

Figure 2.2: Simplified geology of the Makkovik Province after Ketchum et al. (2002). Figure highlights volcano-sedimentary packages as well as plutonic and metamorphic suites mentioned in text. Locations of study areas enclosed

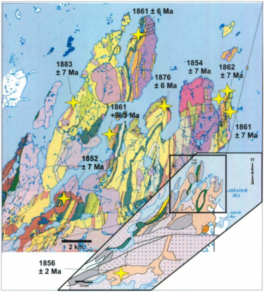

Figure 2.3: Summary of U-Pb geochronology from volcanic units in the Aillik domain. Data are from Schärer et al. (1988), Hinchey and Rayner (2008) and this paper.

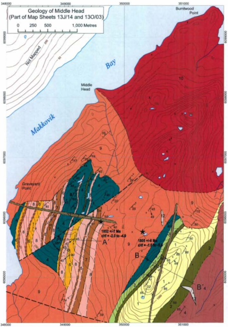

Figure 2.4: Geological map of the Middle Head area showing locations of samples analysed for U-Pb zircon geochronology by SHRIMP and Hf isotope zircon geochemistry by LA-MC-ICPMS. Location of the area is shown in Figure 2.2.

Intrusive Rocks

Dykes (Age Unknown)

- 12 Granitic pegmatite dykes
- 11 Hornblende diorite dykes

Non-foliated Intrusive Unit *ca.* 1640 Ma

- 10 Medium-grained, leucocratic, undeformed bt-hbl monzogranite *(Monkey Hill Granite, part of Monkey Hill Intrusive Suite)*

Foliated Intrusive Unit 1805 ± 6 Ma

- 9 Coarse-grained, foliated hbl-bt monzogranite *(Cross Lake granite)*

Volcanic and Sedimentary Rocks

Aillik Group *ca.* 1883 - 1852 Ma (tectonostratigraphy, no stratigraphic order implied)

- 8 Crystal and crystal-lithic felsic tuff
- 7 Porphyritic to equigranular rhyolite
- 6 Arkosic sandstone interbedded with minor tuffaceous sandstone, containing <4% mafic minerals
- 5 Basalt
- 4 Tuffaceous sandstone
- 3 Volcaniclastic breccia having subangular felsic and mafic volcanic clasts
- 2 Calc-silicate rock
- 1 Arkosic sandstone, containing 7% mafic minerals

Symbols

- ★ Geochronology (zircon U-Pb age and eHf data)
- Station
- Lineation (generation unknown)
- Fold Axis (generation unknown)
- Bedding (tops known, tops unknown)
- Flow Contact (generation unknown)
- Foliation or Cleavage (generation unknown)
- Contact (defined, approximate, assumed)
- Fault (assumed)

Legend for Figure 2.3

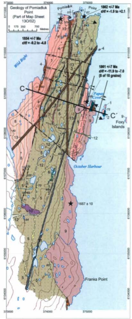

Figure 2.5: Geological map of the Pomiadluk Point area showing locations of samples analysed for U-Pb zircon geochronology by SHRIMP and Hf isotope zircon geochemistry by LA-MC-ICPMS. Area is shown in Figure 2.2.

Intrusive Rocks

Dykes (Age Unknown)

13 Undeformed plagioclase porphyritic gabbro dykes

12 Undeformed potassium feldspar porphyritic felsic dykes

11 Schistose plagioclase porphyritic diabase dyke

Non-foliated Intrusive Unit *ca.* 1650 Ma

10 Medium-grained, undeformed bt-hbl gabbro *(Adlavik Intrusive Suite)*

9 Coarse-grained, undeformed bt-fl monzogranite *(October Harbour Granite 1657 ± 10 Ma (Cox et al. 2003))*

Foliated Intrusive Unit *ca.* 1857 Ma

8 Medium-grained quartz feldspar - porphyritic granite

Volcanic and Sedimentary Rocks

Aillik Group *ca.* 1883 - 1852 Ma (tectonostratigraphy, no stratigraphic order implied)

7 Laminated siltstone

6 Mafic tuff

5 Polymictic conglomerate having subrounded, poorly sorted clasts of granite, granodiorite, mafic tuff, felsic tuff, rhyolite and sandstone. Variations in degree of strain.

4 Porphyritic to equigranular, locally flow banded rhyolite

3 Crystal felsic tuff

2 Crystal-lithic felsic tuff

1 Basalt

Symbols

★ Geochronology (zircon U-Pb age and eHf data)

Station

Fold Axial Plane (generation unknown)

Linear Fabric (generation unknown)

Fold Axis (generation unknown)

Bedding (tops unknown)

Foliation or Cleavage (generation unknown)

Contact (defined, approximate, assumed)

Limit of mapping

Anticlinal Axis (defined)

Synclinal Axis (defined)

Strike-slip Fault (approximate, sinistral, dextral)

Legend for Figure 2.4

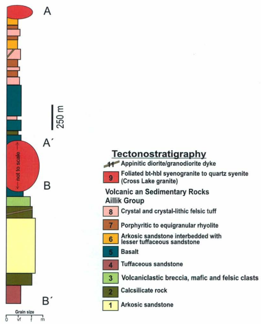

Figure 2.6: Columnar cross sections at A and B shown in Figure 2.4 depicting tectonostratigraphy at Middle Head.

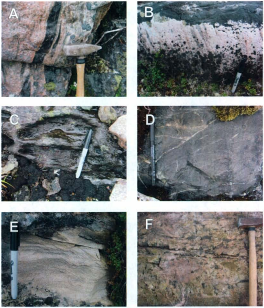

Figure 2.7: Representative photographs of supracrustal lithologies of the Aillik Group at Middle Head: a) basalt fragment within rhyolite; b) crystal-lithic felsic tuff; c) weathered basalt pillows, d) epidote and quartz veins and epidote nodules in basalt; e) calcsilicate rock with abundant diopside; and f) volcanic clasts of both felsic and mafic compositions occurring in a volcaniclastic breccia.

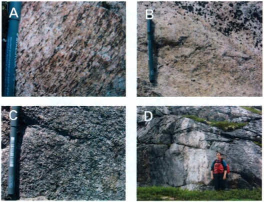

Figure 2.8: Representative photographs of intrusive lithologies at Middle Head: a) foliated hornblende-biotite syenogranite (Cross Lake granite); b) non-foliated biotite-hornblende monzogranite (Monkey Hill granite); c) undeformed appinitic granodiorite dyke; and d) granitic pegmatite cutting sandstone.

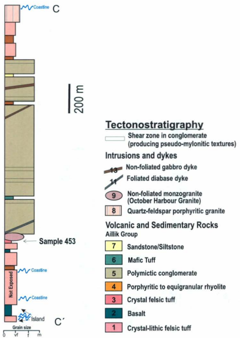

Figure 2.9: Columnar cross section at C shown in Figure 2.8 depicting tectonostratigraphy at Middle Head.

Figure 2.10: Representative photographs of supracrustal lithologies in the Aillik Group at Pomiadluk Point: a) cleavage subparallel to bedding within felsic tuff; b) calcite-epidote-diopsode vein occurring in felsic tuff; c) polymictic conglomerate with clasts of granite, granodiorite, felsic tuff, mafic tuff and rhyolite; and d) flattened volcanic clasts as layers and elongated competent granitic clasts in polymictic conglomerate.

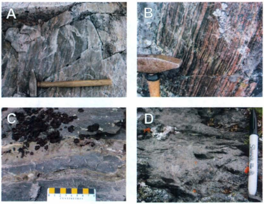

Figure 2.11: Representative photographs of supracrustal lithologies in the Aillik Group at Pomiadluk Point: a) flow banding in rhyolite; b) shear zone cutting rhyolite; c) pillows defined by epidote altered selvages; and d) mafic tuff.

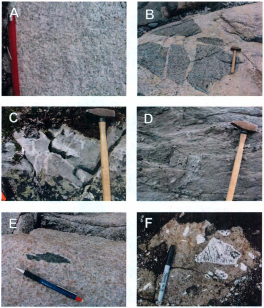

Figure 2.12: Representative photographs of intrusive lithologies at Pomiadluk Point: a) deformed quartz-feldspar porphyritic granite; b) xenoliths of amphibolite dykes in the October Harbour granite; c) net veined sill of hbl-gabbro; d) schistocity in diabase dykes; e) basalt fragment occurring in undeformed granitic dyke; and f) megacrystic plagioclase in a gabbroic dyke.

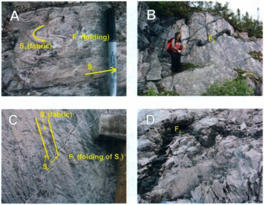

Figure 2.13: Representative photographs of deformation features within the Aillik Group: a) S_1, F_1, S_2 in sandstone at Middle Head; b) F_2 folded mafic dyke that cuts a sandstone at Middle Head; c) S_1, F_1, S_2 in felsic tuff at Pomiadluk Point; and d) F_2 folded mafic dyke that intrudes a felsic tuff at Pomiadluk Point.

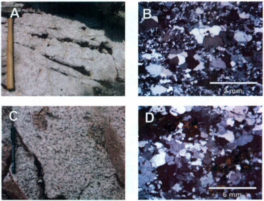

Figure 2.14: Representative outcrop photographs (A and C) and photomicrographs under crossed polars (B and D) of samples collected from Middle Head for geochronology and Hf isotopic geochemistry: a) and b) lithic felsic tuff (08CL198A-03) and, c) and d) hbl-bt monzogranite (Cross Lake granite;

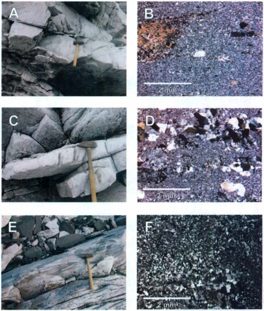

Figure 2.15: Representative outcrop photographs (A, C and E) and photomicrographs under crossed polars (B, D and F) of samples collected from Pomiadluk Point for U-Pb zircon geochronology and Hf isotope zircon geochemistry: a) and b) crystal-lithic felsic tuff (08CL452A-03), c) and d) crystal felsic tuff (08CL453A-03) and, e) and f) crystal-lithic felsic tuff (08CL458A-03).

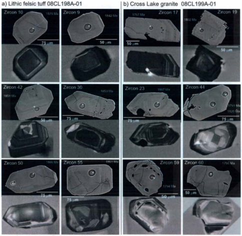

Figure 2.16: Representative zircon grains in both backscatter electon (BSE) and cathodoluminescence (CL) images for two samples from Middle Head: a) foliated crystal-lithic felsic tuff 08CL198A-03; and b) foliated Cross Lake granite 08CL199A-03. Analytical SHRIMP spots can be seen in the grains.

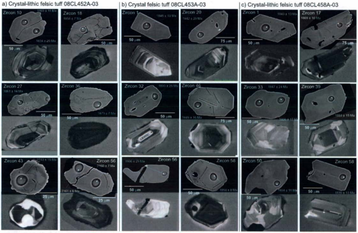

Figure 2.17: Representative zircon grains in both backscatter electon (BSE) and cathodoluminescence (CL) images for three samples from Pomiadluk Point: a) foliated crystal-lithic felsic tuff 08CL452A-03; b) foliated felsic crystal tuff 08CL453A-03; and c) foliated felsic tuff 08CL458A-03. Analytical SHRIMP spots can be seen in the grains.

Lithic felsic tuff 08CL198A-03

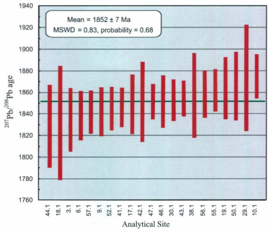

Figure 2.18: Weighted mean $^{207}Pb/^{206}Pb$ SHRIMP dates for sample 08CL198A-03 a foliated lithic felsic tuff. Errors are incorporated at the 2σ level.

Cross Lake granite 08CL199A-03

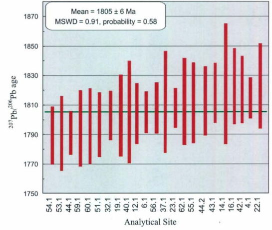

Figure 2.19: Weighted mean $^{207}Pb/^{206}Pb$ SHRIMP dates for sample 08CL199A-03 a foliated Cross Lake granite. Errors are incorporated at the 2σ level.

Crystal-lithic felsic tuff 08CL452A-03

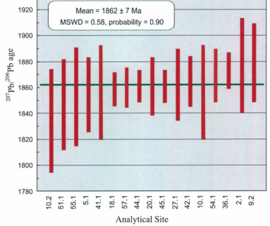

Figure 2.20: Weighted mean $^{207}Pb/^{206}Pb$ SHRIMP dates for sample 08CL452A-03 a foliated crystal-lithic felsic tuff. Errors are incorporated at the 2σ level.

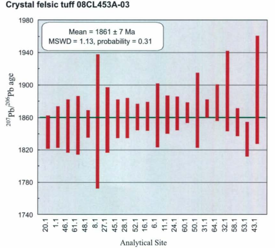

Figure 2.21: Weighted mean $^{207}Pb/^{206}Pb$ SHRIMP dates for sample 08CL453A-03 a foliated crystal felsic tuff. Errors are incorporated at the 2σ level.

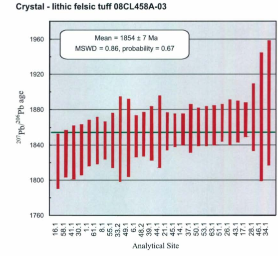

Figure 2.22: Weighted mean $^{207}Pb/^{206}Pb$ SHRIMP dates for sample 08CL458A-03 a foliated crystal-lithic felsic tuff. Errors are incorporated at the 2σ level.

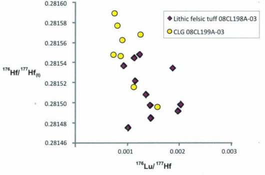

Figure 2.23: Plot of measured $^{176}Lu/^{177}Hf$ vs. $^{176}Hf/^{177}Hf_{(t)}$ for lithic felsic tuff sample 08CL198A-03 and Cross Lake granite sample 08CL199A-03 from Middle Head. $^{176}Hf/^{177}Hf_{(t)}$ is calculated using a ^{176}Lu decay constant of $1.867 * 10^{-11}$/yr from Söderlund et al. (2004) here and in Figure 2.24 and Figure 2.25. Error bars are incorporated into symbols.

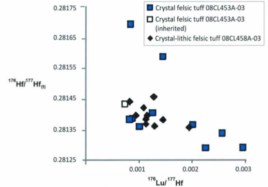

Figure 2.24: Plot of measured $^{176}Lu/^{177}Hf$ vs. $^{176}Hf/^{177}Hf_{(t)}$ for crystal felsic tuff sample 08CL453A-03 and crystal-lithic felsic tuff sample 08CL458A-03 from Pomiadluk Point. Error bars are incorporated into symbols.

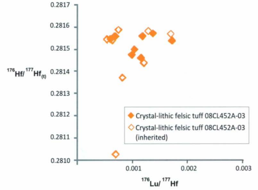

Figure 2.25: Plot of measured $^{176}Lu/^{177}Hf$ vs. $^{176}Hf/^{177}Hf_{(t)}$ for crystal-lithic felsic tuff sample 08CL452A-03 from Pomiadluk Point. Error bars are incorporated into symbols.

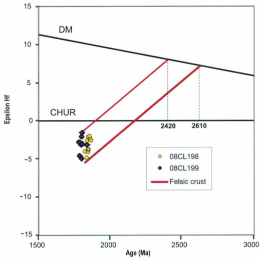

Figure 2.26: Plot of εHf against U-Pb SHRIMP zircon crystallization age for lithic felsic tuff sample 08CL198A-03 and Cross Lake granite sample 08CL199A-03 from Middle Head. Data was calculated using the following parameters: ^{176}Lu decay constant (1.867 * 10^{-11}/yr) of Söderlund et al. (2004), chondritic values of $^{176}Hf/^{177}Hf$ = 0.0336 and $^{176}Lu/^{177}Hf$ = 0.282785 (Bouvier et al., 2008), model depleted mantle with present day $^{176}Hf/^{177}Hf$ ratio of 0.28325 and $^{176}Lu/^{177}Hf$ ratio of 0.0388 (Griffin et al., 2000; updated by Andersen et al., 2009), $^{176}Lu/^{177}Hf$ ratios of mafic and felsic crust from Pietranik et al. (2008) are presented in Appendix B. Red lines are Hf-isotope evolution lines for felsic crust. DM Depleted Mantle, CHUR chondrite uniform reservoir.

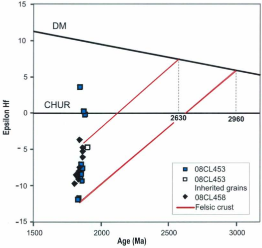

Figure 2.27: Plot of εHf against U-Pb SHRIMP zircon crystallization age for crystal felsic tuff sample 08CL453A-03 and crystal-lithic felsic tuff sample 08CL458A-03 from Pomiadluk Point. Data was calculated using the parameters defined in Figure 2.26.

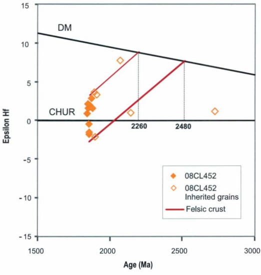

Figure 2.28: Plot of εHf against U-Pb SHRIMP zircon crystallization age for crystal-lithic felsic tuff sample 08CL452A-03 from Pomiadluk Point. Data was calculated using the parameters defined in Figure 2.26.

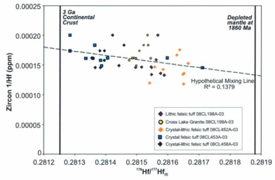

Figure 2.29: Binary plot of $^{177}Hf/^{176}Hf_{(t)}$ vs. 1/Hf of felsic samples from this study, fit by a hypothetical mixing line between a mafic magma derived from depleted mantle at 1860 Ma and 3 Ga continental crust.

Table 2.1: U-Pb SHRIMP geochronology from five samples: a) lithic felsic tuff 08CL198A-03, b) Cross Lake granite 08CL199A-03, c) crystal-lithic felsic tuff 08CL452A-03, d) crystal felsic tuff 08CL453A-03, and e) crystal-lithic felsic tuff 08CL458A-03.

Spot Name	U (ppm)	Th (ppm)	Th/U	Pb* (ppm)	^{204}Pb (ppb)	^{204}Pb/^{206}Pb	±^{204}Pb/^{206}Pb	^{207*}Pb/^{235}U	±^{207}Pb/^{235}U	^{206*}Pb/^{238}U	±^{206}Pb/^{238}U	^{207*}Pb/^{206*}Pb	±^{207}Pb/^{206}Pb	^{206}Pb/^{238}U	±^{206}Pb/^{238}U	^{207}Pb/^{206}Pb	±^{207}Pb/^{206}Pb	Disc (%)
Sample 08CL198A-03 (z=9713): foliated crystal felsic tuff at Middle Head (UTM 349589.37E, 6095957.71N)																		
Weighted mean igneous ^{207}Pb/^{206}Pb age 1852 ± 7 Ma																		
9713-44.1	122	64	0.524	69	7	0.000190	0.000060	5.110	0.099	0.3329	0.0054	0.1118	0.0012	1852	26	1829	19	-2.0
9713-18.1	166	81	0.489	91	5	0.000099	0.000053	5.149	0.111	0.3349	0.0053	0.1120	0.0016	1862	26	1832	26	-2.4
9713-3.1	187	98	0.526	113	6	0.000103	0.000045	5.273	0.093	0.3424	0.0054	0.1121	0.0009	1898	26	1835	15	-4.5
9713-6.1	191	90	0.472	114	2	0.000045	0.000016	5.150	0.087	0.3338	0.0053	0.1124	0.0007	1857	25	1838	11	-1.6
9713-57.1	251	94	0.374	148	4	0.000054	0.000015	5.167	0.085	0.3343	0.0052	0.1126	0.0006	1859	25	1842	10	-1.6
9713-9.1	188	88	0.465	112	1	0.000022	0.000017	5.167	0.088	0.3342	0.0053	0.1126	0.0007	1859	25	1842	11	-1.5
9713-52.1	147	61	0.415	86	2	0.000041	0.000010	5.102	0.085	0.3295	0.0052	0.1128	0.0006	1836	25	1845	10	0.1
9713-41.1	283	127	0.450	168	0	0.000000	0.000000	5.130	0.084	0.3310	0.0051	0.1129	0.0006	1843	25	1846	9	-0.3
9713-17.1	168	80	0.473	97	5	0.000095	0.000031	5.103	0.090	0.3288	0.0052	0.1130	0.0009	1833	25	1849	14	0.5
9713-42.1	328	145	0.443	185	4	0.000041	0.000016	5.201	0.096	0.3347	0.0052	0.1132	0.0011	1861	25	1851	18	-1.1
9713-47.1	325	101	0.311	195	1	0.000015	0.000009	5.270	0.085	0.3391	0.0052	0.1132	0.0005	1882	25	1851	8	-2.4
9713-46.1	122	43	0.357	69	1	0.000039	0.000011	5.089	0.088	0.3275	0.0052	0.1132	0.0008	1826	25	1851	12	1.1
9713-30.1	379	173	0.458	230	3	0.000023	0.000009	5.259	0.093	0.3381	0.0057	0.1133	0.0006	1878	27	1853	10	-2.0
9713-43.1	390	164	0.421	231	4	0.000034	0.000023	5.144	0.082	0.3305	0.0051	0.1134	0.0005	1841	25	1851	8	0.4
9713-38.1	86	37	0.433	48	4	0.000169	0.000049	5.180	0.103	0.3323	0.0056	0.1135	0.0012	1849	27	1857	19	0.0
9713-56.1	245	101	0.413	145	1	0.000016	0.000024	5.211	0.098	0.3341	0.0060	0.1136	0.0007	1858	29	1858	11	-0.5
9713-55.1	212	74	0.351	122	4	0.000063	0.000022	5.125	0.084	0.3279	0.0051	0.1138	0.0006	1828	25	1861	10	1.6
9713-19.1	149	71	0.477	85	4	0.000106	0.000035	5.141	0.092	0.3286	0.0053	0.1140	0.0009	1831	25	1864	14	1.5
9713-50.1	93	45	0.489	54	2	0.000063	0.000022	5.168	0.097	0.3299	0.0055	0.1141	0.0010	1838	26	1866	16	1.2
9713-29.1	108	43	0.401	59	1	0.000044	0.000094	5.273	0.112	0.3353	0.0055	0.1146	0.0015	1864	27	1873	24	0.1
9713-10.1	229	101	0.441	136	2	0.000027	0.000007	5.236	0.087	0.3326	0.0052	0.1147	0.0006	1851	25	1875	10	1.0
Inherited																		
9713-39.1	402	223	0.554	246	4	0.000034	0.000011	5.264	0.089	0.3333	0.0055	0.1150	0.0004	1854	27	1880	7	1.1
Sample 08CL199A-03 (z=9714): foliated bt-hbl syenogranite at Middle Head (UTM 350305.30E, 6095439.52N)																		
Weighted mean igneous ^{207}Pb/^{206}Pb age 1805 ± 6 Ma																		
9714-62.1	127	58	0.456	64	1	0.000041	0.000015	4.499	0.073	0.2960	0.0042	0.1107	0.0009	1671	21	1811	15	8.3
9714-60.1	146	83	0.567	83	3	0.000081	0.000028	4.853	0.074	0.3220	0.0044	0.1098	0.0008	1800	21	1796	13	-0.8
9714-59.1	220	125	0.567	124	2	0.000025	0.000005	4.817	0.072	0.3199	0.0042	0.1097	0.0008	1789	21	1794	13	-0.2
9714-56.1	253	74	0.292	141	2	0.000027	0.000014	4.852	0.068	0.3199	0.0042	0.1105	0.0005	1789	21	1807	9	0.6
9714-55.1	119	44	0.372	64	2	0.000072	0.000026	4.811	0.075	0.3166	0.0043	0.1107	0.0008	1773	21	1811	14	1.9
9714-54.1	231	138	0.596	133	4	0.000059	0.000019	4.781	0.068	0.3184	0.0042	0.1094	0.0006	1782	21	1789	10	-0.1
9714-53.1	135	83	0.615	77	3	0.000089	0.000028	4.813	0.073	0.3203	0.0043	0.1095	0.0007	1791	21	1790	13	-0.5

Table 2.1 cont

Spot Name	U (ppm)	Th (ppm)	Th/U	Pb* (ppm)	^{204}Pb (ppb)	^{204}Pb/^{206}Pb	±^{204}Pb/^{206}Pb	^{207*}Pb/^{235}U	±^{207}Pb/^{235}U	^{206*}Pb/^{238}U	±^{206}Pb/^{238}U	^{207*}Pb/^{206*}Pb	±^{207}Pb/^{206}Pb	^{206}Pb/^{238}U	±^{206}Pb/^{238}U	^{207}Pb/^{206}Pb	±^{207}Pb/^{206}Pb	Disc (%)
9714-51.1	150	80	0.532	85	2	0.000044	0.000013	4.799	0.075	0.3183	0.0046	0.1098	0.0007	1782	22	1796	11	0.5
9714-44.1	385	142	0.369	216	5	0.000044	0.000014	4.758	0.066	0.3166	0.0042	0.1095	0.0004	1773	20	1791	7	0.6
9714-44.2	180	99	0.550	98	4	0.000083	0.000024	4.682	0.069	0.3065	0.0041	0.1113	0.0007	1724	20	1820	11	5.6
9714-43.1	173	99	0.570	98	4	0.000084	0.000027	4.829	0.072	0.3175	0.0043	0.1108	0.0007	1777	21	1812	12	1.7
9714-42.1	164	66	0.404	91	2	0.000041	0.000010	4.802	0.070	0.3149	0.0042	0.1111	0.0006	1765	21	1817	10	2.9
9714-37.1	125	75	0.598	71	1	0.000020	0.000039	4.850	0.087	0.3171	0.0051	0.1114	0.0009	1776	25	1822	14	2.4
9714-40.1	129	64	0.495	69	4	0.000105	0.000057	4.799	0.080	0.3168	0.0043	0.1103	0.0010	1774	21	1805	17	1.5
9714-32.1	333	129	0.388	186	6	0.000064	0.000017	4.762	0.066	0.3148	0.0041	0.1102	0.0005	1765	20	1802	8	1.9
9714-23.1	398	191	0.480	230	2	0.000017	0.000006	4.840	0.066	0.3191	0.0042	0.1105	0.0004	1786	20	1807	7	0.9
9714-22.1	92	31	0.339	48	4	0.000144	0.000046	4.789	0.081	0.3150	0.0044	0.1107	0.0010	1765	22	1812	17	2.4
9714-19.1	197	83	0.421	103	4	0.000072	0.000044	4.597	0.074	0.3039	0.0043	0.1102	0.0008	1711	21	1802	14	5.3
9714-14.1	131	41	0.314	66	2	0.000062	0.000026	4.780	0.084	0.3123	0.0043	0.1115	0.0012	1752	21	1824	20	4.0
9714-16.1	154	92	0.598	87	1	0.000014	0.000008	4.829	0.073	0.3158	0.0042	0.1114	0.0008	1769	21	1822	13	2.9
9714-12.1	184	104	0.565	106	3	0.000060	0.000017	4.850	0.070	0.3204	0.0043	0.1103	0.0006	1791	21	1804	10	0.3
9714-6.1	859	258	0.300	487	5	0.000021	0.000006	4.889	0.066	0.3228	0.0042	0.1103	0.0004	1803	20	1804	7	-0.4
9714-4.1	340	156	0.460	196	1	0.000009	0.000004	4.846	0.066	0.3183	0.0042	0.1109	0.0004	1781	20	1815	7	1.6
Inherited																		
9714-26.1	120	161	1.347	78	0	0.000014	0.000050	5.284	0.085	0.3333	0.0046	0.1155	0.0010	1854	22	1887	15	1.5
Metamorphic																		
9714-17.1	302	126	0.417	172	6	0.000076	0.000019	4.775	0.072	0.3193	0.0046	0.1089	0.0005	1787	22	1781	9	-0.8
9714-10.1	176	106	0.601	100	5	0.000106	0.000026	4.706	0.074	0.3173	0.0045	0.1081	0.0007	1776	22	1767	12	-1.1
Sample 08CL452A-03 (z=9715): foliated crystal felsic tuff at Pomiadluk Point (UTM 374899.39E, 6110895.52N)																		
Weighted mean igneous ^{207}Pb/^{206}Pb age 1862 ± 7 Ma																		
9715-51.1	446	118	0.266	239	3	0.000022	0.000017	5.144	0.084	0.3320	0.0043	0.1129	0.0011	1848	21	1846	17	-0.6
9715-55.1	47	24	0.511	26	1	0.000099	0.000023	4.973	0.090	0.3198	0.0047	0.1133	0.0012	1789	23	1852	19	3.5
9715-57.1	296	67	0.225	171	4	0.000046	0.000015	5.211	0.072	0.3338	0.0044	0.1137	0.0005	1857	21	1859	8	-0.3
9715-27.1	222	79	0.354	104	4	0.000079	0.000026	4.303	0.067	0.2753	0.0037	0.1138	0.0009	1568	19	1861	14	17.4
9715-42.1	280	84	0.299	160	7	0.000087	0.000026	5.185	0.073	0.3310	0.0044	0.1141	0.0006	1843	21	1865	9	0.9
9715-10.1	132	56	0.421	75	2	0.000053	0.000013	5.112	0.076	0.3258	0.0044	0.1143	0.0007	1818	21	1869	11	2.6
9715-2.1	86	41	0.475	48	3	0.000111	0.000058	5.270	0.091	0.3344	0.0047	0.1148	0.0012	1860	23	1877	18	0.6
9715-10.2	182	84	0.464	92	1	0.000031	0.000014	4.634	0.089	0.3010	0.0048	0.1121	0.0012	1696	24	1834	20	8.1
9715-18.1	517	292	0.565	323	3	0.000021	0.000004	5.274	0.083	0.3381	0.0052	0.1136	0.0004	1878	25	1858	7	-1.7
9715-20.1	249	89	0.358	143	6	0.000083	0.000028	5.143	0.086	0.3293	0.0051	0.1138	0.0007	1835	25	1861	11	1.1

Table 2.1 cont

Spot Name	U (ppm)	Th (ppm)	Th/U	Pb* (ppm)	^{204}Pb (ppb)	^{204}Pb/^{206}Pb	±^{204}Pb/^{206}Pb	^{207*}Pb/^{235}U	±^{207}Pb/^{235}U	^{206*}Pb/^{238}U	±^{206}Pb/^{238}U	^{207*}Pb/^{206*}Pb	±^{207}Pb/^{206}Pb	^{206}Pb/^{238}U	±^{206}Pb/^{238}U	^{207}Pb/^{206}Pb	±^{207}Pb/^{206}Pb	Disc (%)
9715-36.1	442	134	0.303	268	2	0.000018	0.000008	5.405	0.085	0.3437	0.0053	0.1146	0.0004	1904	25	1873	7	-2.4
9715-41.1	356	270	0.760	208	1	0.000010	0.000013	5.129	0.094	0.3292	0.0051	0.1135	0.0011	1834	25	1856	18	0.9
9715-44.1	575	345	0.600	348	2	0.000012	0.000005	5.092	0.079	0.3262	0.0050	0.1137	0.0004	1820	24	1860	6	2.0
9715-45.1	523	222	0.424	313	4	0.000025	0.000006	5.170	0.081	0.3308	0.0050	0.1138	0.0004	1842	24	1861	6	0.7
9715-5.1	183	82	0.449	105	6	0.000110	0.000041	5.140	0.091	0.3302	0.0052	0.1134	0.0009	1839	25	1854	14	0.5
9715-54.1	177	54	0.306	105	1	0.000010	0.000009	5.348	0.094	0.3408	0.0057	0.1143	0.0007	1891	27	1869	10	-1.8
9715-9.2	145	31	0.213	77	7	0.000172	0.000045	5.043	0.091	0.3196	0.0051	0.1149	0.0010	1788	25	1879	15	5.1
Inherited																		
9715-53.1	324	103	0.320	185	4	0.000043	0.000019	5.149	0.071	0.3256	0.0043	0.1152	0.0005	1817	21	1883	8	3.5
9715-15.1	489	271	0.554	290	9	0.000065	0.000014	5.133	0.069	0.3240	0.0042	0.1154	0.0004	1809	21	1886	6	4.2
9715-49.1	64	36	0.553	37	1	0.000069	0.000018	5.264	0.086	0.3319	0.0047	0.1155	0.0009	1848	23	1888	15	2.0
9715-25.1	183	60	0.329	104	1	0.000027	0.000027	5.220	0.076	0.3289	0.0044	0.1156	0.0007	1833	21	1889	11	2.9
9715-24.1	281	132	0.469	171	2	0.000030	0.000007	5.365	0.073	0.3371	0.0044	0.1159	0.0005	1873	21	1894	7	0.8
9715-7.1	703	625	0.888	453	7	0.000036	0.000015	5.340	0.071	0.3349	0.0043	0.1161	0.0004	1862	21	1898	6	1.7
9715-47.1	246	96	0.391	145	1	0.000012	0.000011	5.317	0.074	0.3331	0.0044	0.1163	0.0005	1853	21	1916	8	2.4
9715-11.1	192	111	0.576	114	6	0.000101	0.000024	5.250	0.077	0.3288	0.0044	0.1163	0.0007	1833	21	1900	11	3.6
9715-4.1	243	96	0.394	145	2	0.000030	0.000012	5.387	0.075	0.3360	0.0044	0.1168	0.0005	1868	21	1907	8	2.0
9715-50.1	528	202	0.382	308	5	0.000030	0.000009	5.253	0.071	0.3274	0.0043	0.1164	0.0004	1826	21	1909	7	4.6
9715-58.1	284	41	0.144	163	4	0.000051	0.000028	5.435	0.077	0.3386	0.0045	0.1169	0.0006	1880	21	1910	9	1.3
9715-21.1	41	14	0.347	20	2	0.000127	0.000162	5.506	0.145	0.3427	0.0052	0.1170	0.0025	1900	25	1911	39	0.3
9715-13.1	232	69	0.298	136	0	-0.000007	-0.00001	5.394	0.075	0.3349	0.0044	0.1173	0.0005	1862	21	1916	8	2.8
9715-40.1	426	144	0.338	256	3	0.000023	0.000009	5.446	0.073	0.3371	0.0044	0.1177	0.0004	1873	21	1921	6	2.4
9715-52.1	161	102	0.635	106	2	0.000035	0.000044	6.552	0.098	0.3697	0.0050	0.1291	0.0009	2028	23	2085	12	2.8
9715-56.1	208	115	0.554	149	4	0.000062	0.000012	7.287	0.101	0.3940	0.0052	0.1347	0.0006	2142	24	2160	7	0.6
9715-52.2	300	69	0.229	172	7	0.000077	0.000022	5.242	0.085	0.3312	0.0051	0.1153	0.0006	1844	25	1884	9	2.0
9715-59.1	474	198	0.418	299	3	0.000018	0.000004	5.593	0.088	0.3494	0.0053	0.1166	0.0004	1932	26	1905	7	-2.1
9715-56.2	308	168	0.545	230	3	0.000025	0.000007	7.521	0.118	0.4064	0.0062	0.1348	0.0005	2198	29	2161	6	-2.4
9715-43.1	300	150	0.501	245	1	0.000009	0.000007	12.39	0.233	0.4749	0.0077	0.1901	0.0018	2505	34	2743	15	10.2
Metamorphic																		
9715-37.1	107	31	0.291	57	8	0.000249	0.000054	4.959	0.097	0.3260	0.0054	0.1108	0.0012	1819	26	1813	19	-0.9
9715-46.1	412	101	0.245	201	67	0.000638	0.000062	4.314	0.078	0.2937	0.0045	0.1065	0.0010	1660	23	1741	17	4.3

Table 2.1 cont

Spot Name	U (ppm)	Th (ppm)	Th/U	Pb* (ppm)	^{204}Pb (ppb)	^{204}Pb/^{206}Pb	±^{204}Pb/^{206}Pb	^{207*}Pb/^{235}U	±^{207}Pb/^{235}U	^{206*}Pb/^{238}U	±^{206}Pb/^{238}U	^{207*}Pb/^{206*}Pb	±^{207}Pb/^{206}Pb	^{206}Pb/^{238}U	±^{206}Pb/^{238}U	^{207}Pb/^{206}Pb	±^{207}Pb/^{206}Pb	Disc (%)
Sample 08CL453A-03 (z=9716): Crystal-lithic felsic tuff at Pomiadluk Point (UTM 375033.18E, 6108819.05N)																		
Weighted mean igneous ^{207}Pb/^{206}Pb age 1861 ± 7 Ma																		
9716-20.1	180	144	0.797	109	3	0.000062	0.000023	5.059	0.074	0.3272	0.0044	0.1126	0.0006	1825	21	1842	10	0.6
9716-1.1	103	54	0.523	58	1	0.000053	0.000013	4.926	0.077	0.3174	0.0044	0.1130	0.0008	1777	22	1848	13	3.9
9716-46.1	89	44	0.493	50	2	0.000086	0.000049	5.112	0.085	0.3293	0.0046	0.1131	0.0010	1835	22	1849	16	0.4
9716-61.1	128	34	0.264	67	1	0.000027	0.000010	4.982	0.084	0.3208	0.0044	0.1131	0.0011	1793	21	1850	18	3.1
9716-48.1	376	206	0.547	222	5	0.000045	0.000013	5.043	0.075	0.3243	0.0046	0.1132	0.0005	1811	22	1852	8	2.1
9716-8.1	31	12	0.393	14	3	0.000296	0.000161	5.062	0.142	0.3250	0.0053	0.1134	0.0026	1814	26	1855	41	2.1
9716-27.1	97	38	0.390	52	1	0.000023	0.000046	5.132	0.091	0.3292	0.0046	0.1135	0.0013	1835	22	1857	20	0.9
9716-45.1	113	36	0.322	63	2	0.000063	0.000018	5.060	0.077	0.3244	0.0045	0.1136	0.0007	1811	22	1858	12	2.5
9716-28.1	108	43	0.400	60	3	0.000105	0.000018	5.042	0.078	0.3230	0.0045	0.1137	0.0008	1804	22	1859	12	2.9
9716-52.1	285	167	0.584	167	5	0.000061	0.000016	5.023	0.070	0.3216	0.0042	0.1138	0.0005	1797	21	1860	8	3.4
9716-16.1	202	78	0.384	115	2	0.000034	0.000011	5.017	0.071	0.3210	0.0043	0.1138	0.0005	1795	21	1862	9	3.7
9716-6.1	104	68	0.647	58	2	0.000069	0.000072	5.038	0.089	0.3221	0.0045	0.1139	0.0012	1800	22	1863	19	3.4
9716-11.1	111	34	0.311	62	1	0.000045	0.000017	5.111	0.078	0.3266	0.0045	0.1140	0.0007	1822	22	1864	12	2.1
9716-24.1	192	107	0.559	112	1	0.000026	0.000015	5.091	0.074	0.3251	0.0044	0.1141	0.0006	1815	21	1865	10	2.6
9716-60.1	390	142	0.365	227	4	0.000037	0.000010	5.102	0.069	0.3256	0.0043	0.1141	0.0004	1817	21	1866	6	2.6
9716-50.1	36	11	0.298	19	0	-0.000022	-0.00006	5.155	0.103	0.3285	0.0051	0.1143	0.0014	1831	25	1869	23	1.9
9716-31.1	451	118	0.262	266	2	0.000018	0.000006	5.256	0.074	0.3346	0.0046	0.1144	0.0003	1861	22	1871	5	0.2
9716-64.1	161	41	0.251	89	1	0.000026	0.000030	5.126	0.076	0.3250	0.0044	0.1149	0.0007	1814	21	1878	11	3.5
9716-32.1	82	29	0.351	42	1	0.000026	0.000100	5.144	0.101	0.3235	0.0046	0.1158	0.0016	1807	22	1893	25	4.7
9716-58.1	290	189	0.651	171	4	0.000050	0.000010	4.963	0.080	0.3188	0.0049	0.1134	0.0005	1784	24	1854	8	3.9
9716-53.1	233	65	0.278	133	3	0.000050	0.000010	5.082	0.085	0.3303	0.0052	0.1121	0.0006	1840	25	1833	10	-0.9
9716-43.1	35	11	0.316	18	2	0.000196	0.000073	5.272	0.141	0.3313	0.0064	0.1159	0.0021	1845	31	1894	33	2.5
Inherited																		
9716-56.1	41	12	0.301	20	3	0.000263	0.000069	4.954	0.124	0.3092	0.0059	0.1167	0.0019	1737	29	1906	29	9.7
Metamorphic																		
9716-7.1	204	77	0.380	115	4	0.000063	0.000021	4.986	0.072	0.3234	0.0043	0.1123	0.0006	1806	21	1837	10	1.5
Sample 08CL458A-03 (z=9717) Foliated crystal felsic tuff at Pomiadluk Point (UTM 374338.34E, 6110829.47N)																		
Weighted mean igneous ^{207}Pb/^{206}Pb age 1854 ± 7 Ma																		
9717-16.1	111	34	0.305	62	4	0.000139	0.000044	5.065	0.092	0.3313	0.0053	0.1114	0.0010	1845	26	1822	16	-1.9
9717-58.1	143	77	0.537	86	3	0.000067	0.000038	5.205	0.091	0.3388	0.0054	0.1119	0.0008	1881	26	1830	13	-3.7
9717-41.1	109	34	0.309	62	5	0.000148	0.000044	5.191	0.093	0.3376	0.0054	0.1120	0.0009	1875	26	1832	15	-3.2
9717-30.1	165	61	0.370	96	9	0.000182	0.000037	5.156	0.100	0.3348	0.0060	0.1122	0.0009	1862	29	1835	14	-2.2

Table 2.1 cont

Spot Name	U (ppm)	Th (ppm)	Th/U	Pb* (ppm)	^{204}Pb (ppb)	$^{204}Pb/^{206}Pb$	$\pm^{204}Pb/^{206}Pb$	$^{207*}Pb/^{235}U$	$\pm^{207}Pb/^{235}U$	$^{206*}Pb/^{238}U$	$\pm^{206}Pb/^{238}U$	$^{207*}Pb/^{206*}Pb$	$\pm^{207}Pb/^{206}Pb$	$^{206}Pb/^{238}U$	$\pm^{206}Pb/^{238}U$	$^{207}Pb/^{206}Pb$	$\pm^{207}Pb/^{206}Pb$	Disc (%)
9717-1.1	136	53	0.391	76	4	0.000107	0.000029	4.926	0.086	0.3185	0.0051	0.1126	0.0008	1783	25	1843	13	3.3
9717-61.1	134	52	0.390	78	2	0.000049	0.000017	5.195	0.092	0.3354	0.0054	0.1128	0.0008	1864	26	1845	13	-1.7
9717-8.1	192	79	0.414	113	5	0.000090	0.000025	5.199	0.086	0.3356	0.0052	0.1128	0.0007	1866	25	1845	11	-1.8
9717-55.1	291	149	0.513	171	2	0.000018	0.000008	5.190	0.094	0.3350	0.0053	0.1128	0.0010	1863	26	1846	15	-1.6
9717-33.2	124	54	0.435	67	3	0.000085	0.000089	4.993	0.118	0.3221	0.0063	0.1129	0.0015	1800	31	1847	24	2.4
9717-49.1	299	140	0.468	170	7	0.000076	0.000092	5.317	0.105	0.3427	0.0053	0.1130	0.0014	1900	26	1848	22	-3.7
9717-6.1	127	55	0.434	74	-2	-0.00005	-0.00002	5.172	0.089	0.3331	0.0053	0.1131	0.0007	1853	25	1850	12	-0.2
9717-48.2	171	68	0.397	100	3	0.000057	0.000020	5.197	0.090	0.3342	0.0053	0.1133	0.0008	1859	26	1852	12	-0.9
9717-39.1	129	51	0.398	73	6	0.000165	0.000048	5.121	0.093	0.3292	0.0053	0.1133	0.0010	1835	26	1853	15	0.7
9717-44.1	131	43	0.326	72	7	0.000192	0.000059	5.173	0.102	0.3322	0.0054	0.1134	0.0013	1849	26	1855	20	-0.1
9717-21.1	154	59	0.385	91	4	0.000098	0.000015	5.231	0.089	0.3358	0.0054	0.1135	0.0007	1866	26	1856	11	-1.1
9717-45.1	161	68	0.421	98	1	0.000023	0.000008	5.287	0.087	0.3392	0.0053	0.1135	0.0006	1883	25	1857	9	-2.1
9717-14.1	205	90	0.440	123	1	0.000016	0.000011	5.238	0.085	0.3359	0.0052	0.1136	0.0005	1867	25	1858	9	-1.0
9717-37.1	78	23	0.288	44	1	0.000044	0.000003	5.194	0.093	0.3329	0.0054	0.1137	0.0009	1852	26	1859	14	-0.1
9717-50.1	144	61	0.427	84	3	0.000073	0.000013	5.141	0.086	0.3291	0.0052	0.1138	0.0007	1834	25	1861	11	1.2
9717-53.1	194	87	0.448	115	2	0.000039	0.000019	5.223	0.088	0.3342	0.0053	0.1138	0.0007	1859	25	1861	11	-0.3
9717-62.1	148	55	0.369	88	3	0.000080	0.000026	5.300	0.089	0.3390	0.0053	0.1139	0.0007	1882	26	1862	11	-1.7
9717-51.1	149	55	0.373	86	2	0.000035	0.000011	5.184	0.087	0.3310	0.0052	0.1141	0.0006	1843	25	1865	10	0.9
9717-26.1	103	32	0.305	60	1	0.000024	0.000026	5.250	0.091	0.3352	0.0053	0.1141	0.0008	1864	26	1865	13	-0.4
9717-43.1	134	44	0.329	77	3	0.000074	0.000022	5.175	0.088	0.3302	0.0052	0.1142	0.0007	1839	25	1867	12	1.2
9717-17.1	264	129	0.489	159	3	0.000040	0.000027	5.240	0.085	0.3339	0.0051	0.1143	0.0006	1857	25	1869	10	0.2
9717-28.1	133	45	0.336	74	5	0.000120	0.000072	5.183	0.098	0.3298	0.0052	0.1145	0.0012	1837	25	1871	19	1.6
9717-46.1	133	53	0.394	66	4	0.000109	0.000157	5.203	0.135	0.3310	0.0054	0.1145	0.0023	1843	26	1872	36	1.3
9717-34.1	42	11	0.260	21	0	0.000029	0.000069	5.185	0.136	0.3269	0.0057	0.1155	0.0022	1823	28	1888	35	3.5
Inherited																		
9717-5.1	100	30	0.295	57	0	0.000000	0.000000	5.182	0.090	0.3277	0.0053	0.1152	0.0008	1827	25	1883	12	2.9
9717-35.1	151	78	0.519	90	1	0.000012	0.000038	5.292	0.091	0.3347	0.0053	0.1152	0.0008	1861	25	1882	13	0.8
Metamorphic																		
9717-33.1	101	31	0.309	57	5	0.000165	0.000051	5.079	0.102	0.3350	0.0059	0.1104	0.0010	1863	29	1806	17	-4.1
9717-15.1	119	49	0.411	70	5	0.000133	0.000018	5.149	0.089	0.3376	0.0054	0.1111	0.0007	1875	26	1818	12	-4.1
9717-48.1	141	45	0.316	80	9	0.000224	0.000048	5.116	0.091	0.3346	0.0053	0.1114	0.0009	1861	25	1822	15	-3.0

Spot name follows the convention x-y.z; where x = sample number, y = grain number and z = spot number.

Uncertainties reported at 1s (absolute) and are calculated by numerical propagation of all known sources of error

* refers to radiogenic Pb (corrected for common Pb)

Discordance relative to origin = 100 * ((207/206 age -206/238 age)/(207Pb/206Pb age))

Calibration standard 6266; U = 910 ppm; Age = 559 Ma; 206Pb/238U = 0.09059

Error in 206Pb/238U calibration 1.28% (9713,9714, 9715, 9716), 1.50% (9715, 9716, 9717) Samples with each are separated by black line   Th/U calibration: F = 0.03900*UO + 0.856

Table 2.2: LA-MC-ICPMS zircon isotopic Hf data. Analyses completed on the same samples as U-Pb SHRIMP geochronology

Spot	Age (Ma)	±2s	Hf[1] (ppm)	$^{176}Hf/^{177}Hf$	±2SE	$^{176}Lu/^{177}Hf$	±2SE	$^{176}Hf/^{177}Hf_{(t)}$	$\varepsilon Hf_{(T)}$	±2SE	T_{DM}[2] (Ga)	T_{DM}[3] (Ga)
Sample 08CL198A-03: Foliated lithic felsic tuff												
Middle Head (UTM 349589.37E, 6095957.71N)												
29.1	1873	24	5448	0.281562	4.0E-05	0.001148	5.5E-05	0.281522	-2.40	0.15	2.97	2.52
38.1	1857	19	6192	0.281548	3.2E-05	0.001437	4.1E-05	0.281497	-3.63	0.14	3.07	2.57
42.1	1851	18	6170	0.281561	3.0E-05	0.001967	2.1E-06	0.281492	-3.96	0.04	3.09	2.58
43.1	1851	8	6709	0.281569	4.1E-05	0.002022	7.3E-05	0.281498	-3.74	0.15	3.07	2.57
44.1	1829	19	5744	0.281555	3.5E-05	0.001354	4.3E-05	0.281508	-3.90	0.17	3.07	2.56
47.1	1851	8	6861	0.281591	3.4E-05	0.001236	1.3E-05	0.281548	-1.97	0.03	2.92	2.48
50.1	1866	16	4988	0.281600	3.1E-05	0.001869	6.9E-05	0.281534	-2.12	0.10	2.94	2.50
52.1	1845	10	5448	0.281569	3.4E-05	0.000928	1.9E-06	0.281536	-2.52	0.02	2.96	2.50
55.1	1861	10	6192	0.281584	3.4E-05	0.001131	2.8E-05	0.281544	-1.86	0.06	2.91	2.48
56.1	1858	11	6170	0.281536	4.5E-05	0.001446	3.1E-05	0.281485	-4.06	0.11	3.10	2.59
57.1	1842	10	6328	0.281511	3.3E-05	0.001014	5.1E-05	0.281475	-4.77	0.26	3.16	2.61
Sample 08CL199A-03: Foliated bt-hbl syenogranite												
Middle Head (UTM 350305.30E, 6095439.52N)												
23.1	1807	7	6861	0.281550	3.5E-05	0.001575	5.8E-05	0.281496	-4.84	0.20	3.14	2.59
40.1	1805	17	7467	0.281572	3.2E-05	0.000737	1.3E-05	0.281547	-3.06	0.08	2.98	2.49
54.1	1789	10	4988	0.281610	3.4E-05	0.001253	6.4E-05	0.281568	-2.70	0.15	2.94	2.46
55.1	1811	14	7535	0.281615	3.2E-05	0.000754	1.3E-05	0.281589	-1.46	0.04	2.84	2.42
56.1	1807	9	7357	0.281605	2.9E-05	0.000808	2.0E-05	0.281577	-1.96	0.06	2.89	2.44
59.1	1794	13	6826	0.281554	3.5E-05	0.001128	5.1E-05	0.281515	-4.45	0.23	3.10	2.56
60.1	1796	13	6302	0.281593	3.5E-05	0.000903	2.6E-05	0.281562	-2.74	0.10	2.95	2.47
62.1	1811	15	6814	0.281576	3.4E-05	0.000874	5.1E-05	0.281546	-2.96	0.20	2.98	2.49
Sample 08CL452A-03: Foliated crystal felsic tuff												
Pomiadluk Point (UTM 374899.39E, 6110895.52N)												
5.1	1854	14	6536	0.281714	5.3E-05	0.001414	5.3E-05	0.281664	2.24	0.10	2.55	2.26
10.1	1869	11	7350	0.281695	5.1E-05	0.001228	6.0E-05	0.281651	2.10	0.11	2.57	2.28
20.1	1861	11	6803	0.281593	5.5E-05	0.001037	3.2E-05	0.281557	-1.44	0.05	2.88	2.46
27.1	1861	14	5989	0.281690	5.1E-05	0.001758	8.7E-05	0.281628	1.11	0.06	2.65	2.32
36.1	1873	7	8337	0.281583	5.4E-05	0.001204	1.8E-04	0.281540	-1.74	0.27	2.91	2.48
44.1	1860	6	7437	0.281674	4.2E-05	0.000723	1.7E-05	0.281648	1.78	0.05	2.59	2.29
45.1	1861	6	7011	0.281622	2.7E-05	0.001082	5.6E-05	0.281584	-0.46	0.03	2.79	2.41
55.1	1852	19	5686	0.281660	4.0E-05	0.000653	1.1E-05	0.281637	1.22	0.03	2.64	2.31
57.1	1859	8	8457	0.281676	3.6E-05	0.000744	1.2E-05	0.281650	1.84	0.04	2.59	2.28

Table 2.2 cont

Spot	Age (Ma)	±2s	Hf[1] (ppm)	$^{176}Hf/^{177}Hf$	±2SE	$^{176}Lu/^{177}Hf$	±2SE	$^{176}Hf/^{177}Hf_{(t)}$	$\varepsilon Hf_{(T)}$	±2SE	T_{DM}[2] (Ga)	T_{DM}[3] (Ga)
Inherited												
13.1	1916	8	6709	0.281725	6.8E-05	0.001741	2.3E-04	0.281661	3.55	0.49	2.47	2.24
25.1	1889	11	7413	0.281656	6.4E-05	0.000592	2.9E-05	0.281634	1.97	0.11	2.60	2.30
43.1	2743	15	9477	0.281097	3.0E-05	0.000754	8.3E-05	0.281058	1.37	0.16	3.23	3.03
47.1	1916	8	7526	0.281711	3.8E-05	0.000799	6.7E-05	0.281682	4.27	0.38	2.41	2.20
49.1	1888	15	5739	0.281655	4.5E-05	0.000690	7.2E-06	0.281630	1.81	0.03	2.61	2.31
52.1	2085	12	7271	0.281729	7.5E-05	0.001336	1.4E-04	0.281676	7.99	0.87	2.19	2.15
56.1	2160	7	7610	0.281477	7.1E-05	0.000872	1.2E-04	0.281441	1.37	0.20	2.83	2.55
58.1	1910	9	9609	0.281561	3.8E-05	0.001259	2.8E-05	0.281515	-1.79	0.05	2.94	2.51
Sample 08CL453A-03: Foliated crystal-lithic felsic tuff												
Pomiadluk Point (UTM 375033.18E, 6108819.05N)												
8.1	1855	41	6192	0.281394	3.5E-05	0.001015	2.9E-05	0.281358	-8.62	0.44	3.50	2.82
16.1	1862	9	5448	0.281434	5.2E-05	0.001997	8.6E-05	0.281364	-8.27	0.40	3.48	2.81
20.1	1842	10	5744	0.281386	3.7E-05	0.002919	2.0E-04	0.281284	-11.5	0.87	3.75	2.96
27.1	1857	20	6709	0.281417	2.9E-05	0.000885	2.1E-05	0.281386	-7.59	0.26	3.41	2.77
45.1	1858	12	6170	0.281450	3.3E-05	0.001257	6.7E-05	0.281405	-6.87	0.41	3.35	2.73
50.1	1869	23	6328	0.281412	5.2E-05	0.000830	6.7E-05	0.281383	-7.43	0.69	3.41	2.77
53.1	1833	10	4988	0.281362	4.2E-05	0.002236	9.2E-05	0.281284	-11.8	0.55	3.76	2.96
60.1	1866	6	6192	0.281425	9.2E-05	0.002542	3.2E-04	0.281335	-9.19	1.17	3.56	2.86
61.1	1850	16	6861	0.281741	3.4E-05	0.000850	1.7E-05	0.281711	3.80	0.11	2.41	2.18
64.1	1878	11	6170	0.281650	7.9E-05	0.001449	8.5E-05	0.281598	0.43	0.03	2.72	2.37
Inherited												
56.1	1906	29	5448	0.281463	8.9E-05	0.000741	9.3E-05	0.281436	-4.68	0.66	3.19	2.66
Sample 08CL458A-03:Foliated crystal felsic tuff												
Pomiadluk Point (UTM 374338.34E, 6110829.47N)												
6.1	1850	12	5744	0.281432	3.8E-05	0.001453	5.9E-05	0.281381	-7.95	0.38	3.44	2.78
16.1	1822	16	6861	0.281422	3.0E-05	0.001136	2.9E-05	0.281382	-8.52	0.29	3.47	2.79
28.1	1871	19	6709	0.281472	3.5E-05	0.000839	3.5E-05	0.281443	-5.24	0.27	3.22	2.66
37.1	1859	14	6861	0.281406	2.8E-05	0.001139	9.8E-05	0.281366	-8.26	0.77	3.47	2.81
39.1	1853	15	6328	0.281436	4.2E-05	0.001160	4.5E-05	0.281395	-7.35	0.35	3.39	2.76
43.1	1867	12	4988	0.281461	3.3E-05	0.001098	2.1E-05	0.281422	-6.09	0.16	3.29	2.70
46.1	1872	36	5448	0.281505	4.5E-05	0.001284	1.3E-04	0.281459	-4.65	0.57	3.17	2.63
48.2	1852	12	5744	0.281429	2.9E-05	0.000953	1.9E-05	0.281395	-7.36	0.19	3.39	2.75
61.1	1845	13	6170	0.281422	4.7E-05	0.001936	1.4E-04	0.281354	-8.98	0.69	3.53	2.83
62.1	1862	20	6192	0.281405	3.3E-05	0.001296	5.5E-05	0.281359	-8.43	0.45	3.49	2.82

Lu-Hf isotope measurements by LA-MC-ICPMS

^{176}Lu decay constant (1.867×10^{-11}/yr) of Söderlund et al. (2004)

Chondritic values of $^{176}Lu/^{177}Hf$=0.0336 and $^{176}Hf/^{177}Hf$=0.282785 (Bouvier et al., 2008)

Model depleted mantle with present day $^{176}Hf/^{177}Hf$ ratio of 0.28325 and $^{176}Lu/^{177}Hf$ ratio of 0.0388
(Griffin et al., 2000; updated by Andersen et al., 2009)

[1] Hf concentration determined from sensitivity of 178Hf (V) in Plešovice zircon using Hf=11167 ppm (Sláma et al., 2008).

T_{DM} (Ga) are the model Hf ages for the crustal source assuming [2]mafic and [3]felsic crust.

$^{176}Lu/^{177}Hf$ ratios of mafic and felsic crust from Pietranik et al. (2008)

Chapter 3

GEOCHEMICAL AND ND ISOTOPIC DATA FROM VOLCANIC ROCKS OF THE AILLIK GROUP AND DEFORMED GRANITIC INTRUSIONS: IMPLICATIONS ON THE TECTONIC SETTING OF THE AILLIK DOMAIN, MAKKOVIK PROVINCE

ABSTRACT

The Aillik domain is composed of the Aillik Group, a belt of upper greenschist- to lower amphibolite-facies bimodal volcanic and clastic sedimentary rocks, as well as variably deformed plutonic suites and mafic and felsic dykes. Alteration, deformation and metamorphism of the bimodal volcanic and associated sedimentary rocks that form the Aillik Group has complicated the petrographic and geochemical characteristics, making it difficult to determine the tectonic setting in which it was formed more difficult. This study links petrographical features of Aillik Group volcanic rocks and deformed plutonic intrusions occurring within the Aillik domain, with trace and rare earth element geochemistry as well as neodymium isotopic data to elucidate the tectonic environment in which the Aillik Group formed. Two areas are the focus of this study: Middle Head and Pomiadluk Point.

Trace and REE geochemistry demonstrate that felsic volcanic rocks of the Aillik Group, as well as the temporally distinct deformed granitic intrusions of the Aillik domain are 'A-type' in nature. Some felsic volcanic rocks of the Aillik Group have been hydrothermally altered to potassium feldspar. Unaltered felsic volcanic rocks demonstrate a tight range in Nd isotopic signatures ($\varepsilon Nd_{(T)}$ = -1.5 to -2.4) which reflects partial melting of a ca. 2350 to 2590 Ma felsic continental crust. Based on geochemical

signatures, mafic volcanic rocks can be classified into two groups. Group A basalts have geochemical signatures that include a flat rare earth element pattern, consistent with melting of a depleted mantle source, and are composed of primary plagioclase and clinopyroxene and metamorphic amphibole and biotite. Group B basalts and mafic tuff are chemically more evolved, and composed of primary plagioclase and metamorphic amphibole and magnetite. The two distinct REE patterns seen in mafic volcanic rocks are interpreted to reflect a variable amount of crustal contamination. Furthermore, Group A basalts demonstrate systematically more elevated $\varepsilon Nd_{(T)}$ *signatures (+2.8 to +4.6) than Group B basalts and mafic tuff (-3.5 to +2.2). Based on mixing models, mafic magmas of the Aillik Group are determined to have formed by mixing of the depleted mantle with a small to moderate amount (5 to 35%) of the melt residue that formed the felsic volcanic rocks of the Aillik Group.*

The combination of early clastic sedimentation, bimodal volcanism and geochemical signatures of felsic and mafic melts suggests that the Aillik Group formed in a back-arc setting behind an actively subducting continental arc.

3.1 INTRODUCTION

Bimodal volcanism is commonly associated with rifting; in either island arcs or continental rifts, and even at some mid-ocean ridges (Shinjo and Kato, 2000). Although bimodal volcanism is generally attributed to extensional tectonism, structural, metamorphic and alteration processes affecting ancient terranes typically obscure the geological relationships regarding the precise tectonic setting in which the volcanism was generated (Moraes et al., 2003). By combining information about the bulk compositions of the rocks and their mineralogy, it is possible to quantify the amount of alteration, and use trace element (including rare earth element, REE) geochemistry and Nd isotopic data on the least altered samples to evaluate the degree of crustal contamination during magma genesis, the sources of magmas, and the tectonic setting in which ancient volcano-sedimentary belts have formed (eg. Corriveau et al., 2005; Moraes et al., 2003; Menuge et al., 2002).

The Aillik Group of the Makkovik Province of Labrador, Canada, was deposited over at least 31 million years from ca. 1883 to 1852 Ma (Hinchey and Rayner, 2008; LaFlamme, Chapter 2). Bimodal volcanism includes rhyolite flows and felsic pyroclastic units that are widespread and voluminous with lesser basalt flows and mafic pyroclastic units (Marten, 1977; Clark, 1979; Bailey, 1981; Kerr, 1989; Hinchey, 2007). The Aillik Group was deposited and subsequently reworked primarily during the Makkovik orogeny (1900 - 1710 Ma), eradicating many volcanic textures and disrupting stratigraphy (Gower and Ryan, 1986; Kerr et al., 1992; Ketchum et al., 2002; Hinchey, 2007; Hinchey and LaFlamme, 2009)

Two areas that preserve Aillik Group rocks are the focus of this paper: Middle Head and Pomiadluk Point. This paper presents major and trace element geochemistry of basaltic and rhyolitic rocks and deformed intrusions, specifically a syn-volcanic quartz-feldspar porphyritic intrusion and the Cross Lake granite, as well as Sm-Nd isotopic geochemistry, to constrain the magmatic sources and tectonic setting in which the Aillik Group formed. This paper compliments a study addressing the timing of formation and the source of magma generation of felsic rocks of the Aillik Group through detailed mapping and *in situ* U-Pb geochronology and Lu-Hf isotope geochemistry of zircon (Chapter 2).

3.2 REGIONAL GEOLOGY

The Makkovik Province of the Canadian Shield and is a triangular crustal block wedged between the Nain Province to the north and the Grenville Province to the south (Figure 3.1; Ketchum et al., 2002 and references therein). The Makkovik Province is composed of (1) high grade reworked Archean orthogneiss of the Nain Province, (2) four Proterozoic supracrustal sequences, (3) granitoid orthogneisses of the Cape Harrison Metamorphic Suite, (4) foliated and non-foliated plutonic suites of various Proterozoic ages, and (5) abundant deformed and undeformed mafic and felsic dykes (Gower, 1981; Ryan et al., 1983; Kerr et al., 1992). Three domains make up the Makkovik Province, and are termed the Kaipokok domain, Aillik domain and Cape Harrison domain (Figure 3.2).

The Kaipokok domain consists primarily of banded orthogneiss, equivalent to the ca. 2.8 to 3.3 Ga Hopedale Block of the Nain Province that has undergone Paleoproterozoic deformational and metamorphic events (Kerr et al. 1992). The orthogneiss is unconformably overlain by two Early Proterozoic supracrustal sequences termed the Moran Lake Group and the ca. 2178 Ma Post Hill Group, as well as a younger ca. 1649 Ma volcano-sedimentary sequence of the Bruce River Group (Ketchum et al., 2001a; Marten, 1977; Ryan, 1984). Deformed and undeformed plutonic suites intrude the Kaipokok domain (Barr et al., 2001).

The Aillik domain is composed of a slice of reworked orthogneiss, volcano-sedimentary units of the Paleoproterozoic Aillik Group, foliated and non-foliated plutonic suites and variably deformed mafic dykes (Gower et al., 1982; Kerr, 1989; 1994; Kerr et al., 1992; Ketchum et al., 2002; Hinchey, 2007). The Aillik Group structurally overlies the Post Hill Group of the Kaipokok domain. In turn, the Post Hill Group structurally overlies Archean gneiss that forms the basement to its lowest members. Volcanic rocks of the Aillik Group are bimodal, composed dominantly of felsic units and lesser preserved mafic units (Clark, 1973; Gower et al., 1982). Felsic volcanic rocks are dominated by rhyolite and felsic tuff; whereas, mafic volcanic rocks are dominated by basalt and lesser mafic tuff units (Hinchey, 2007). Abundant tuffites occur including primarily tuffaceous sandstone, are also present. Minor volcaniclastic sedimentary rocks outcrop in the area and are dominated by polymictic volcaniclastic breccias. Sedimentary rocks of the Aillik Group include interbedded sandstone-siltstone and less abundant polymictic conglomerate (Hinchey, 2007; Hinchey and LaFlamme, 2009).

The Cape Harrison domain is composed of metamorphosed orthogneiss of the Cape Harrison Metamorphic Suite and minor supracrustal rocks (Kerr, 1989; Kerr and Fryer, 1994; Ketchum et al., 1997, 2002). The Cape Harrison domain is intruded by an abundance of variably deformed plutonic intrusions (Kerr et al., 1992).

Plutonic intrusions are widespread in the Makkovik Province. The deformed ca. 1890—1875 Ma Island Harbour Bay Plutonic Suite (IHBPS) intrudes the Kaipokok domain and is characterized by calc-alkaline 'Ì-type' magmas that Barr et al. (2001) proposed were derived from a mantle wedge above a subducted slab of anomalously hot, post-Archean ocean crust. Nd isotopic data from the IHBPS yield $\varepsilon Nd_{(T)}$ of -2.5 to -7.2 (Kerr and Fryer, 1994; Kerr et al., 1997; Barr et al., 2001). Foliated and non-foliated late-Makkovikian (ca. 1800 Ma) intrusions and non-foliated post-Makkovikian (ca. 1720 Ma) plutonic intrusions are preserved within the Makkovik Province; these intrusions have "A-type" signatures and report variable εNd, ranging from -8 in the west to +4 in the east (Kerr, 1989; Kerr et al., 1992). Undeformed ca. 1650 – 1640 Ma plutonic suites intruding the Makkovik Province are interpreted to be a distal portion of a magmatic arc associated with the Labradorian orogeny (1710-1620 Ma) (Kerr, 1989; Gower et al., 1991).

Various tectonic environments have been suggested for the formation of the Makkovik Province (Kerr, 1989; Culshaw et al., 2000, 2002; Sinclair et al., 2002; Ketchum et al., 2002). The most recent model of Ketchum et al. (2002) suggested that the formation of the Makkovik Province commenced with the collision and subduction of a Paleoproterozoic arc resulting in the formation of the ca. 1895—1870 Ma Island Harbour Bay Plutonic Suite, built on reworked Archean crust. Crust formation continued with the deposition of the Aillik Group (ca. 1860—1850 Ma) on a largely juvenile crust in a rifted-arc or back-arc setting. Northwestwards thrusting of the Aillik Group onto the Archean crust commenced prior to ca. 1802 Ma and may have been driven by the accretion of a second island arc (Cape Harrison Metamorphic Suite?). This was followed by region-wide granitic plutonism from ca. 1815 to 1780 Ma. A single model has not yet been adapted because of stratigraphic disruption and complexity to supracrustal packages, region-wide alteration, and metamorphic overprinting, all of which are attributed to the

Makkovikian orogeny (Gower and Ryan, 1986; Kerr et al., 1992; 1997; Ketchum et al., 2002; Hinchey, 2007).

3.2.1 Metamorphic Evolution, Regional Metasomatism and Local Alteration

Previous work has indicated that volcanic and sedimentary rocks of the Aillik Group preserve upper greenschist- to lower amphibolite-facies metamorphism attributed to the Makkovikian orogeny (Clark, 1973; Bailey, 1981; Gower et al., 1982; Sinclair, 1999; Hinchey, 2007). In some areas, particularly in the northwest, units of the Aillik Group preserve chlorite-grade metamorphism and primary features including cross-bedding, graded bedding and ripple marks (Hinchey, 2007). In other areas, the units of the Aillik Group preserve lower amphibolite- facies metamorphism, locally overprinted by greenschist-facies metamorphism (Hinchey, 2007). In areas of localized high strain, primary features are less readily preserved (Clark, 1973, 1979; Bailey, 1981; Sinclair, 1999; Culshaw et al., 2000; Hinchey, 2007).

The chemical affinity of Aillik Group rocks has remained unclear because of the concentration of geochemical studies on areas of mineralization, where units having undergone localized hydrous alteration associated with uranium mineralization were selected. These studies report lithogeochemical data that has been interpreted as reflecting a variety of tectonic settings (e.g., Gandhi 1978; White and Martin, 1980; Payette and Martin, 1987; Wilton, 1996).

Geochemical data and field observations indicate that sodic and alkalic alteration is widespread throughout the Aillik Group, whereas metavolcanic and sedimentary units to the south of Cape Makkovik are commonly affected by silicification (Gandhi, 1969; Bailey, 1981; Gower and Ryan, 1987; MacDougall, 1988; Sinclair, 1999; Hinchey, 2007;

Hinchey and LaFlamme, 2009). Sinclair (1999) and Sinclair et al. (2002) reported a detailed lithogeochemical study of a highly strained area of the Aillik Group. Sinclair (1999) noted a strong inverse correlation between Na_2O and K_2O contents in the rocks. This "one for one" alkali alteration pattern has also been reported by White and Martin (1980), MacDougall (1988) and Wilton (1996). Sinclair et al. (2002) noted that concentrations of mobile trace elements, Rb, Ba and Sr, demonstrate scatter when plotted against SiO_2. Immobile elements, TiO_2 and Zr, demonstrate less variation with respect to SiO_2 and thus were considered relatively immobile in the Aillik Group rocks not associated with mineralization (Sinclair et al., 2002). Sinclair et al. (2002) reported that amphibolites-facies samples appear to show some Na mobilization. These findings demonstrate that major element geochemistry is suspect in its ability to classify and characterize the Aillik Group, and that immobile REE are more reliable when assessing chemical affinity.

3.3 METHODOLOGY

Samples were collected from Middle Head and Pomiadluk Point. Their UTM coordinates are listed in Appendix B.1. Fifty-eight thin sections from 56 of the samples were cut and polished for transmitted and reflected light microscopy. A subset of these samples was analyzed for major element, trace element and Sm-Nd isotope geochemistry.

3.3.1 Major and trace element geochemistry

Twenty-five samples selected for lithogeochemistry include twelve felsic volcanic rocks, ten mafic volcanic rocks, one sample of quartz-feldspar porphyritic granite and two samples of Cross Lake granite. Analytical details for the geochemical analyses are given in Appendix A.3. Samples weighing 1—2 kg were taken from the host rock outcrop, cleaned of their weathered surfaces and reduced to small fragments directly in the field to avoid contamination. The samples were processed at Memorial University where fresh small fragments were reduced to fine gravel in the jaw crusher and subsequently 20 to 30 grams of said material was ground into powder using a ceramic disk and ring grinder to avoid Ta contamination.

Major and selected trace element analyses were completed at the Geological Survey of Newfoundland by inductively coupled plasma – emission spectrometry (ICP-ES), following the procedures of Finch (2001). Rare earth elements (REE) and other trace element analyses were completed at Memorial University by inductively coupled plasma – mass spectrometry (ICP-MS) following the procedures of Longerich et al. (1990).

3.3.2 Sm-Nd isotope geochemistry

Sixteen of the 25 samples analysed for lithogeochemistry were also analysed for Sm-Nd isotopic composition by thermal ionization mass spectrometry (TIMS). For TIMS analysis, the samples were crushed and prepared in the same manner as for geochemistry at Memorial University (Appendix A.4 for details). Samples were analyzed at Carleton University in the Isotope Geochemistry and Geochronology Research Centre. The principles and systematics of Sm-Nd isotopic geochemistry are described in Chapter 1.

3.4 RESULTS

This section details results obtained from petrographic study, major and trace element geochemistry and Nd isotope analyses completed on the 25 samples of supracrustal rocks of the Aillik Group and deformed granitic intrusions that occur at Middle Head (13 samples) and Pomiadluk Point (12 samples). Table 3.1 lists the locations of the samples, which are also shown on the 1:10, 000 scale geological maps (Figures 3.3, 3.4) that were described in detail in Chapter 2.

Some additional samples that are not the focus of this study, including clastic sedimentary rocks, post-orogenic granites, and diorite and felsic dykes of unknown age were also analysed. Petrographic descriptions of these units are presented in Appendix C.1. Their geochemical compositions, and for one sample its Nd isotope composition, are given in Appendices B.2 and B.3 and briefly described in Appendices C.2 and C.3.

3.4.1 Petrography

The petrographic study documented primary and metamorphic mineral compositions, primary and metamorphic alteration textures, and deformational fabrics. Units are characterized and grouped with respect to degree of alteration and trace element behavior.

The metavolcanic rocks at Middle Head (ca. 1852 Ma; Chapter 2) are dominated by rhyolite, felsic tuff and basalt, whereas the metasedimentary rocks are dominantly arkosic sandstone, tuffaceous sandstone, calcsilicate rock and lesser volcaniclastic breccia. In contrast, Pomiadluk Point is composed primarily of crystal felsic tuff (ca. 1854-1862 Ma; Chapter 2) and polymictic conglomerate, with less abundant preserved rhyolite and basalt. Two deformed plutonic intrusions for which data are presented outcrop in the study areas. At Middle Head, a ca. 1805 Ma (Chapter 2) foliated hornblende-bitotite-monzogranite known as the Cross Lake granite cuts the Aillik Group.

On the west coast of Pomiadluk Point, a ca. 1857 Ma quartz-feldspar porphyritic granite is infolded with the Aillik Group.

3.4.1.1 Felsic tuff

Felsic tuff occurs in the eastern exposed Aillik Group section at Middle Head as lithic felsic tuff (unit 8: Figure 3.3) as well as on the eastern and western coasts of Pomiadluk Point, comprising both crystal-lithic (unit 1: Figure 3.4) and crystal (unit 3: Figure 3.4) varieties. Crystals are composed of quartz, microcline and albite up to 3 mm across and are elongated. At Pomiadluk Point, crystals locally occur as lapilli (Figure 3.5a). Lithic fragments are composed of quartz + plagioclase + potassium feldspar + biotite + chlorite + calcite, elongated, up to 4 mm across, and account for 4% of the rocks. Crystals and lithic fragments occur in a fine-grained matrix composed of potassium feldspar, quartz, plagioclase and minor biotite. Metamorphic minerals locally occurring within the matrix are chlorite and calcite (Figure 3.5b). Zircon and apatite occur as accessory minerals. Bedding in crystal and crystal-lithic felsic tuff is defined by grain size variations in the matrix. A moderate foliation is defined by slightly flattened crystals and/or lithic fragments. Evidence for moderate recrystallization in felsic volcanic rocks includes granoblastic textures in the matrix. Alteration is minor and localized in felsic tuff; it includes potassic alteration of feldspar grains but does not affect all units (Figure 3.5c).

3.4.1.2 Rhyolite

Rhyolite occurs at Middle Head and Pomiadluk Point and is typically interlayered with felsic tuff (unit 7: MH; unit 4: PP). At Middle Head rhyolite is locally porphyritic. Phenocrysts of potassium feldspar, albite and quartz composition, constitute up to 5% of the rocks, are flattened and up to 1 mm wide (Figure 3.5d). The groundmass is made up of potassium feldspar, albite, quartz with minor biotite and hornblende. At Pomiadluk Point, rhyolite is locally flow banded and porphyritic to non porphyritic. Flow banding is defined by darker-coloured layers in outcrop, but is not evident in thin section. Where phenocrysts are present, they are composed of potassium feldspar and plagioclase, are subrounded and up to 2 mm in length, account for 15% of the rocks and define a weak foliation. The rhyolitic matrix is made up of potassium feldspar, quartz and albite with a minor amount of biotite and hornblende. In both areas zircon, apatite and rutile occur as accessory minerals. A weak foliation is developed by elongated phenocrysts in porphyritic rhyolite. In both study areas granoblastic textures are evidence for recrystallization. Alteration is moderate in rhyolite, occurring as potassium feldspar replacement of plagioclase feldspar grains, giving the grains a brown tinge.

3.4.1.3 Basalt (Group A)

Group A basalt (unit 13; Figure 3.3) samples are from a single unit, occurring at Middle Head on a moderately well exposed hill top within several tens of meters of one another. The basalts are characterized by primary plagioclase and clinopyroxene (Figure 3.6a). The clinopyroxene has been partially replaced by green to brown pleochroic amphibole and lesser biotite. A foliation is defined by the alignment of metamorphic amphibole and biotite minerals. Recrystallization textures include a granoblastic matrix. Moderate sericite alteration affects the plagioclase grains in Group A basalts (Figure 3.6b). Evidence for potassic alteration was not observed in Group A basalts.

3.4.1.4 Basalt (Group B)

Fine-grained basaltic rocks, referred to as Group B basalts, occur in both the eastern and western sections of Aillik Group at Middle Head (unit 4: Figure 3.3) and as two thin layers at Pomiadluk Point (unit 2: Figure 3.4). In Group B basalts primary clinopyroxene has been almost completely replaced by green to brown pleochroic amphibole and magnetite, indicating that the basaltic units have undergone amphibolite-facies metamorphism (Figure 3.6c). Such mineralogy differs from that in Group A basalts, which preserve primary clinopyroxene grains. Additionally, magnetite is much more abundant in Group B basalt than in Group A basalt. At both Middle Head and Pomiadluk Point chlorite has replaced amphibole grains along the rims, indicative of locally overprinting greenschist facies metamorphism. Foliation is defined by the alignment of amphibole grains. Evidence for recrystallization includes granoblastic textures in the matrix. Evidence for potassic alteration is not prominent in Group B basalt samples.

3.4.1.5 Mafic tuff

Mafic tuff occurs as thin (up to 20 m wide) discontinuous layers at Pomiadluk Point (unit 6: Figure 3.4). Mafic tuff is fine-grained and plagioclase porphyritic. It is composed of primary plagioclase + clinopyroxene + biotite + quartz. Phenocrysts of plagioclase are recrystallized and less than 2 mm across (Figure 3.6d). Amphibole and magnetite have replaced clinopyroxene, indicating that the mafic tuff has been metamorphosed to amphibolite-facies. Amphibole has been retrogressed in part to chlorite. Mafic minerals are aligned to define a strong foliation. Recrystallization is characterized by granoblastic textures in the matrix. Local and minor calcite alteration occurs as veinlets in mafic tuff.

3.4.1.6 Quartz-feldspar porphyritic granite

Deformed syn-volcanic a quartz-feldspar porphyritic granite occurs on the west coast of Pomiadluk Point (unit 8; Figure 3.4). Phenocrysts, up to 3 mm across, are composed of quartz and lesser plagioclase and occur in a matrix of quartz, potassium feldspar and plagioclase (Figure 3.6e). Flattened and aligned phenocrysts define a weak foliated. Evidence for recrystallization includes granoblastic textures.

3.4.1.7 Cross Lake granite

The Cross Lake granite (unit 9; Figure 3.3) is coarse-grained, hornblende-biotite monzogranite, locally with euhedral phenocrysts of microcline, up to 6 mm across. Hornblende and biotite comprise up to 10% and define a moderate foliation and lineation (Figure 3.6f). Accessory minerals include fluorite, zircon, magnetite and apatite.

3.4.2 Major and trace element geochemistry

The major and trace element composition of the 25 samples included in this study is presented in Table 3.2. Except for the 3 samples of Group A basalts, each of the samples described here was collected from what is interpreted to be separate flow units.

3.4.2.1 Effects of alteration

Alteration can obscure primary magmatic trends by redistributing mobile elements. In the upper greenschist- to lower amphibolite-facies rocks of the Aillik Group, elements cited as mobile include major elements such as Ca, Na, K, Si and large ion lithophile trace elements (LILE) such as Rb, Cs, Sr, Ba (MacKenzie, 1971; Wilton, 1996; Sinclair, 1999; Sinclair et al., 2002). Alteration trends are a function of these mobile elements being lost or gained in the rocks during metamorphic and metasomatic mineral reactions (Large et al., 2001). By understanding the alteration trends in the context of petrographic relationships, it is possible to determine which elements are mobile and which elements were immobile in Aillik Group rocks (Large et al., 2001). Therefore, it is important to understand the style of alteration in the Aillik Group prior to interpreting chemical and isotopic compositions in terms of magmatic processes. Discrimination diagrams plotting mobile elements are suspect when used to determine petrographic affinities and tectonic setting.

All units collected for geochemistry from Middle Head and Pomiadluk Point are plotted on the "alteration box" diagram of Large et al. (2001) in Figure 3.7. The alteration box plot is a graphical representation of two alteration indices: the Ishikawa alteration index (AI), $(K_2O + MgO)/(K_2O + MgO + CaO + Na_2O)$, and the chlorite-carbonate-pyrite index (CCPI), $(MgO + FeO)/(MgO + FeO + Na_2O + K_2O)$. The diagram was developed to distinguish between diagenetic and hydrothermal alteration related to volcanic-hosted massive sulphide mineralization. However, the alteration indices may also be used to measure the intensity of sericite, potassic, chlorite, carbonate and pyrite replacement of feldspar grains and devitrified glass in low- to medium-grade metamorphic rocks affected by metasomatism such as those in the Aillik Group.

Mafic volcanic rocks from the Aillik Group plot in the "least-altered" box of the diagram, in the top left-hand corner of the basalt/andesite field, mostly falling along the carbonate enrichment trend (labeled '5' in the diagram). In thin section, the mafic rock samples have a high proportion of metamorphic minerals (including calcite, along with amphibole and chlorite) in even the least altered rocks, but based on their position in Figure 3.7, the extent of element gain or loss during alteration does not appear to have been extreme. Nonetheless, because many of the mafic samples plot near the top of the least altered field for basalts and andesite, their CCPI may now be somewhat higher than the original magmatic values. This indicates a modest gain of MgO + FeO relative to Na_2O + K_2O during regional metasomatism and/or local hydrous alteration.

Felsic rocks from the Aillik Group tend to be more altered than the mafic rocks with several samples plotting outside of the "least altered" field for rhyolites. The more altered felsic volcanic rocks follow trend 1, weak sericite alteration, and trend 6, potassium feldspar alteration, in Figure 3.7. In hand sample potassium feldspar alteration is evidence by salmon-pink colour and in thin section as localized orthoclase replacement of plagioclase, giving the feldspar grains a brownish tinge. Potassic alteration was first noted in the Aillik Group by Payette and Martin (1987) and reported by Kerr (1989), Sinclair (1999) and Hinchey (2007). Minor sericite alteration is evident in thin section, giving a cloudy appearance to some K-feldspar and plagioclase grains; however, this alteration style is not pervasive. The altered felsic rocks have AI values >60, indicating that they gained significant K_2O + MgO relative to CaO + Na_2O during regional metasomatism and/or local hydrous alteration.

3.4.2.2 Magmatic characteristics of the volcanic rock geochemistry

Major element compositions of the Aillik Group volcanic rocks are plotted as TiO_2, MgO, Al_2O_3, Na_2O, CaO and K_2O against SiO_2 in Figure 3.8. The mafic rocks show a significant amount of scatter in these plots but because the samples show only a modest amount of elemental redistribution in the alteration box diagram (Figure 3.7), it is possible that this scatter reflects primary magmatic variability as well as alteration. This is particularly the case for elements such as titanium and aluminum, which are commonly found to be immobile in altered volcanic rocks (e.g., Winchester and Floyd, 1977). Felsic rocks classified as altered and less altered in the alteration box diagram exhibit dramatic differences only in alkali abundances in Figure 3.8: the altered samples tend to have gained significant K_2O and lost Na_2O relative to the less altered samples.

Figure 3.9 plots elements (Zr, TiO_2, Nb, Y) of the volcanic rocks commonly found to be immobile in altered systems: the Zr/TiO_2 ratio is a measure of the degree of differentiation in magmatic systems and the Nb/Y ratio is a measure of the degree of alkalinity (Winchester and Floyd, 1977; Pearce, 1996). In this diagram the volcanic units are classified as sub-alkalic basalts and rhyolites/dacites, with the exceptions of two felsic tuffs from Middle Head. One of these tuffs (08CL198A-02) plots in the trachyte field of the diagram, and the other (08CL152A-02) plots in the andesite/basalt field. The felsic tuff with the apparent trachytic composition was classified as altered in Figure 3.7, and thus it probably formed with an original, sub-alkalic magmatic affinity like the other felsic volcanic samples but suffered fractionation of Nb/Y during intense alteration. Furthermore, the sample also contains lithic fragments that may represent country rock contaminants added to the magmatic precursor during emplacement. The felsic tuff falling in the andesite/basalt field was not classified as altered in Figure 3.7 but based on petrography is clearly a rhyolitic rock. Thus, Zr may have been lost and/or TiO_2 gained in this sample during metamorphic alteration. Overall; however, these elements appear to have been rather immobile in the samples, with felsic volcanics classified as altered and less altered in Figure 3.7 showing little difference in Figure 3.9.

Additional geochemical characteristics of the felsic and mafic volcanic rocks are described separately below.

3.4.2.2.1 Felsic Volcanic Rocks

Rare earth elements and other trace elements in the felsic volcanic rocks are plotted on chondrite-normalized and primitive mantle-normalized multi-element diagrams in Figure 3.10. REE patterns are strongly fractionated; $[La/Yb]_N$ varies from 2.2 to 15.0 but on average is 7.5 (Figure 3.10a). The felsic volcanic samples display systematic moderate enrichment in light REE (LREE = >100 times chondrite; $[La/Sm]_N = 3.3$), little fractionation in heavy REE ($[Gd/Yb]_N = 1.3$) and strongly negative Eu anomalies ($[Eu/Eu^*]_N = 0.22$). Marked negative Nb and Ti anomalies occur on the multi-element plot (Figure 3.10b). These features are typical of crustal-derived melts (Menuge et al., 2002). One sample of altered felsic tuff from Middle Head (08CL198A-02) demonstrates anomalous geochemistry in that it is strongly depleted in the light REE. This sample is also anomalous because it plots in the trachyte field of Figure 3.9 and, as noted above, intense alteration and/or incorporation of lithic fragment contaminants may have modified its original magmatic geochemistry.

In the Y versus Nb tectonomagmatic discrimination diagram of Pearce et al. (1984), the Aillik felsic volcanic rocks plot mainly in the area of anomalous ocean-ridge granite (ORG) and within-plate granite (WPG) field (Figure 3.11). In the alkalinity diagram of Maniar and Piccoli (1989), the less altered rhyolites of the Aillik Group also straddle the peralkaline and metaluminous fields (Figure 3.12). More altered felsic volcanic rocks tend to be more peraluminous, which likely reflects mobility of Ca, Na and K by secondary processes. Felsic igneous rocks with these compositions are generally considered to be alkaline-rich, 'A-type' magmas (e.g., Eby, 1990). Felsic volcanic rocks of the Aillik Group are enriched in light REE (up to 300x chondrite) and depleted in Sr, Nb, Eu and Ti, which are additional characteristics that are typical of 'A-type' felsic melts (Brewer et al., 2004).

3.4.2.2.2 Mafic Volcanic Rocks

Chondrite normalized REE patterns for mafic units from the Aillik Group (Figure 3.13) display two distinct types of patterns; flat-lying and fractionated. Group A basalts have flat REE patterns ($[La/Yb]_N = 1.0$), similar to chondrites and primitive mantle (Figure 3.12a). Group B basalts and the mafic tuffs, in contrast, are moderately ($[La/Yb]_N = 4.3$) to strongly ($[La/Yb]_N = 11.3$) fractionated with a larger enrichment in light REE ($[La/Sm]_N = 2.9$) than in heavy REE patterns ($[Gd/Yb]_N = 1.6$). They display negative Ti and Nb anomalies as well as minor Zr and Hf depletions (Figure 3.13b). The most fractionated samples are the two mafic tuff samples from Pomiadluk Point. Negative Eu anomalies are less pronounced in both types of mafic volcanic rocks ($[Eu/Eu^*]_N = 0.99$) than in the felsic volcanic rocks.

The Th/Yb versus Ta/Yb diagram of Pearce (1982) differentiates between the tholeiitic, calcalkaline and shoshonitic series in island-arc basalts, as well as between tholeiitic MORB and alkaline OIB series magmas (Figure 3.14). The diagram also defines trends of basalts that are the result of the addition of a crustal contaminant, a subduction component or a within-plate component to MORB-like magmas. In this diagram, Group A basalts from the Aillik Group have compositions similar to N-MORB; whereas, Group B basalt and mafic tuff samples plot in the calc-alkaline field and, with one exception, define a trend indicating crustal contamination. This suggests that the calc-alkaline signature of the Group B basalts and mafic tuffs does not reflect genesis from an island-arc source but rather is the result of crustal contamination of N-MORB basalt magmas, which are preserved in the Aillik Group as the Group A basalts of Middle Head.

The Ta-Hf-Th tertiary diagram of Wood (1980) uses the immobile high field strength elements Ta, Hf and Th to distinguish volcanic arc basalts from within-plate alkali basalt and mid-ocean ridge basalts (Figure 3.15). Here again, Group A basalts of the Aillik Group plot in the N-MORB field, whereas the Group B basalt and mafic tuff samples plot in the calc-alkaline volcanic arc field. A possible trend of crustal contamination, as suggested in the Th/Yb versus Ta/Yb diagram above, is also shown in the Ta-Hf-Th diagram (Figure 3.14).

3.4.2.3 Magmatic characteristics of the geochemistry of deformed granitic intrusions

Two plutonic suites are considered here: a ca. 1857 Ma quartz-feldspar porphyritic granite from Pomiadluk Point, and the 1804 ± 6 Ma Cross Lake granite from Middle Head. The quartz-feldspar porphyritic granite and the Cross Lake granite have SiO_2 concentrations of 76% and 70% respectively and, on the basis of their CIPW normative mineralogy, are classified as monzogranites (Figure 3.16). The Cross Lake granite has a metaluminous composition, whereas the quartz-feldspar porphyritic granite lies at the intersection between a peralkaline and metaluminous fields (Figure 3.12).

In REE diagrams (Figure 3.10A) the Cross Lake granite is moderately fractionated ($[La/Yb]_N = 6.0$) with significant light REE enrichment ($[La/Sm]_N = 3.3$) and relatively flat heavy REE patterns ($[Gd/Yb]_N = 1.3$). The negative Eu anomaly is pronounced with a $[Eu/Eu^*]_N$ ratio of 0.30. The quartz-feldspar porphyritic granite has a REE composition very similar to the Cross Lake granite ($[La/Yb]_N = 6.0$; $[La/Sm]_N = 3.0$; $[Gd/Yb]_N = 1.2$; $[Eu/Eu^*]_N = 0.32$). Both the quartz-feldspar porphyritic granite and Cross Lake granite have negative Nb and Ti anomalies in the primitive mantle-normalized trace element plot (Figure 3.10B).

The Cross Lake granite and the quartz-feldspar granite have chemical compositions that are similar to those of the felsic volcanic rocks of the Aillik Group. In particular these deformed granites display similar REE patterns and similar (but less pronounced) negative anomalies for Nb and Ti. In the Nb versus Y diagram of Pearce et al. (1984), the quartz-feldspar porphyritic granite and the Cross Lake granite plot in the anomalous ocean-ridge granite and within-plate granitoid fields (Figure 3.11), typical of A-type felsic magmas, and similar to the felsic volcanics of the Aillik Group.

3.4.3 Neodymium isotope geochemistry

Fifteen samples of mafic and felsic volcanic rocks of the Aillik Group and one sample of Cross Lake granite were analyzed for Sm-Nd isotopic composition. The data are presented in Table 3.3. An additional Nd isotope analysis of a diorite dyke of unknown age is presented in Appendix C.3.

Calculation of uncertainties on the $^{143}Nd/^{144}Nd$ ratios is based on 2σ of the mean. A bivariate diagram plotting $^{143}Nd/^{144}Nd$ versus $^{147}Sm/^{144}Nd$ for each of the mafic and felsic volcanic rock samples is presented in Figure 3.17. Values for $\varepsilon Nd_{(T)}$ are given in Table 3.3 and plotted in Figure 3.18. They were calculated using the chondritic uniform reservoir of DePaolo (1981) and the measured U-Pb zircon ages for the felsic samples from Chapter 2. For the mafic samples, a crystallization age of 1860 Ma was used for the $\varepsilon Nd_{(T)}$ calculation, based on the assumption that the mafic volcanism was broadly co-magmatic with the felsic volcanism.

Depleted mantle model ages in Table 3.3 are calculated using the depleted mantle reservoir values of Goldstein et al. (1984) and the measured $^{147}Sm/^{144}Nd$ ratios of the samples. Most of the samples have $^{147}Sm/^{144}Nd$ ratios ranging from 0.09 to 0.15, similar to the value for the average continental crust (0.11, Albarède and Brouxel, 1987), except for the three Group A basalts and the felsic tuff from Middle Head with the apparent trachyte composition (08CL198A-02), which have unusually high ratios (0.20 to 0.22). Calculations of model ages for the latter 4 samples have large uncertainties due to the low-angle intersection of the Nd evolution line of the sample with the depleted mantle Nd evolution curve.

The Sm-Nd data for the volcanic rocks plotted in Figure 3.17 define an array, which is very poorly fit by an isochron that gives an age of 1935 ± 390 Ma, calculated using Isoplot/Ex3.0 (Ludwig, 2003). The observed scatter around the isochron is likely due both to disturbance of the Sm-Nd isotope systematics during alteration as well as to multiple sources involved in the petrogenesis of the volcanic rocks.

3.4.3.1 Felsic volcanic rocks

Evidence for post-magmatic disturbance of the Sm/Nd system comes from the $\varepsilon Nd_{(T)}$ values calculated for the felsic volcanic rocks of the Aillik Group. Three felsic volcanic rocks that plot within the less altered field of the alteration box in Figure 3.7 yield $\varepsilon Nd_{(T)}$ values that range from -2.4 to -1.1 with $T_{(DM)}$ that range from 2347 to 2590 Ma. In contrast, two felsic volcanic samples that plot outside the alteration box and are interpreted as having undergone potassic alteration yield $\varepsilon Nd_{(T)}$ values that are considerably more negative, -4.3 and -3.0, with considerably older $T_{(DM)}$ ages of 2771 Ma and 2971 Ma. In the case of the highly altered felsic tuff sample (08CL198A-02) that plots anomalously in the trachyte field in the Zr/TiO_2 – Nb/Y classification diagram (Figure 3.9) and is anomalously poor in light REE abundances (Figure 3.10A), the $\varepsilon Nd_{(T)}$ value is even more negative, -5.5. Its calculated $T_{(DM)}$ age is meaningless, only intersecting the depleted mantle at a future time because its $^{147}Sm/^{144}Nd$ is unusually high (0.2233). The suggestion is that Sm/Nd disturbance in the altered felsic volcanic samples results in$\varepsilon Nd_{(T)}$ values that are more negative than the actual, primary magmatic values.

Kerr and Fryer (1994) reported whole rock $\varepsilon Nd_{(T)}$ data for two ca. 1860 Ma volcanic rocks from the Aillik Group. They found that a rhyolite flow or sill from Ranger Bight has a $\varepsilon Nd_{(T)}$ value of -0.6 and a model age of 2380 Ma, whereas a weakly foliated ash-flow tuff from the Michelin Ridge area yields a $\varepsilon Nd_{(T)}$ value of -6.3 and a model age of 2560 Ma. The former sample is in accordance with the results for the less altered felsic volcanic rocks of this study, whereas the latter sample may have undergone hydrothermal alteration, creating a disturbance in the Sm-Nd isotopic ratio.

3.4.3.2 Mafic volcanic rocks

Group A basalts tend to have more positive $\varepsilon Nd_{(T)}$ values than Group B basalts and mafic tuffs. The three samples of Group A basalt from Middle Head yield $\varepsilon Nd_{(T)}$ that range from +2.6 to +4.3. In contrast, two samples of Group B basalt from Middle Head yield $\varepsilon Nd_{(T)}$ values that are +1.4 and +2.2, and one sample of Group B basalt and two mafic tuff samples from Pomiadluk Point yield $\varepsilon Nd_{(T)}$ that range from -3.5 to -0.3. The $T_{(DM)}$ Nd-model ages of the Group B basalts and mafic tuffs range from 2287 to 2805 Ma, but if these rocks formed by crustal contamination of the their parental mantle-derived magmas, then the crust formation ages represent only an average age of the various sources that contributed to the magmas. The Group A basalts give $T_{(DM)}$ Nd-model ages that are very old (ca. 3.3 and 3.8 Ga) to impossibly old (5.0 Ga) as a result of their unusually high $^{147}Sm/^{144}Nd$ ratios, which were mentioned above.

Sample 08CL159A-02, a Group B basalt from Middle Head, is an exceptional compared to the other basalt samples: it has an $\varepsilon Nd_{(T)}$ value of +6.4, placing it just slightly above the depleted mantle curve of Goldstein et al. (1984) at its assumed crystallization age, 1860 Ma (Figure 3.18), with a $T_{(DM)}$ Nd-model age of 1838 Ma.

3.4.3.3 Deformed Cross Lake granite

The Cross Lake granite, which formed some 50 Ma after the Aillik Group felsic volcanism, yields an $\varepsilon Nd_{(T)}$ value of -4.2 with $T_{(DM)}$ of 2861 Ma. This value is slightly more negative than the accepted $\varepsilon Nd_{(T)}$ values for unaltered felsic volcanic samples of the Aillik Group.

3.5 DISCUSSION

3.5.1 Regional Comparisons

Lithological observations and geochemical data from previous studies of the Aillik Group and syn-volcanic granitic intrusions are compared to the data from the present study to demonstrate that the two study areas, Middle Head and Pomiadluk Point are representative of the Aillik Group, throughout the Aillik domain. The most recent publications describing the lithologies of mafic and felsic volcanic rocks include Hinchey (2007) and Hinchey and LaFlamme (2009) which focus on the (1:50,000 scale) Makkovik Bay and Monkey Hill map sheets, respectively. In these areas the volcanic rocks of the Aillik Group are demonstrated to be bimodal. Basaltic rocks within these areas are described as being fine- to medium-grained, moderately to strongly deformed, locally pillowed and associated with a minor amount of mafic tuff. Felsic volcanic rocks of the Aillik Group are described as being composed primarily of felsic tuff and rhyolite. The felsic tuff includes both crystal and lithic varieties and the rhyolite is porphyritic to equigranular and associated with the felsic tuff. The volcanic rocks within the study areas are lithologically similar to the ones recently described in a regional context.

The geochemistry of the Aillik Group and the Measles' Point granite has previously been studied by Sinclair et al. (2002) and Sinclair (1999). In these reports the author(s) demonstrated that the volcanic rocks within the study areas of Big Head and Big Island-Ranger Bight are representative of the Aillik Group as a whole. Sinclair et al. (2002) reported that the felsic volcanic rocks within the study areas have greater than 70% SiO_2 and mafic volcanic rocks contain less than 55% SiO_2. Sodic and potassium alteration effects were observed by Sinclair et al. (2002), Sinclair (1999) and Payette and Martin (1987). The felsic volcanic rocks in the study areas exhibit moderate LREE enrichment, strong negative anomalies and flat HREE patterns. The Measles' Point granite was determined by the previous authors to have a crustal 'A-type' signature and lie in the within-plate granite field of trace element discrimination diagrams. The mafic volcanic rocks of the study areas display distinct flat REE patterns which were interpreted by the previous authors to be indicative of their formation in a MORB-type setting.

Further studies on the geochemical signature of Aillik Group volcanic rocks include MacDougall (1988), Kerr (1989), MacKenzie (1991) and Wilton (1996). Analyses from felsic volcanic samples are more common in these studies. They plot in the within-plate field of trace element discrimination diagrams and have similar REE patterns to those reported by Sinclair (1999) and Sinclair et al. (2002). Mafic volcanic samples from the

Round Pond area lie stratigraphically above felsic volcanic rocks and possess moderately fractionated REE profiles.

Therefore, the volcanic and granitic samples from the present study areas appear to be representative of the Aillik Group and syn-volcanic granitic intrusions, with regard to both lithological and geochemical characteristics.

3.5.2 Metamorphic grade and alteration style

The mineral assemblages of the volcanic rocks indicate that the Aillik Group at Middle Head and Pomiadluk Point has undergone lower amphibolites-facies metamorphism. Units were subsequently retrograded to greenschist facies, which is reflected in the presence of chlorite in samples of both felsic and mafic volcanic rocks in the study areas. This interpretation is agreement with findings from Hinchey (2007).

Alteration affecting the lithologies at Middle Head and Pomiadluk Point is characterized by localized potassium metasomatism in felsic volcanic rocks and minor sericitization of Group A basaltic units. Potassic alteration of rhyolite and felsic tuff units is evidenced in thin section by potassium feldspar replacement of plagioclase grains, giving them a brown, cloudy appearance. Alteration of Group A basalt includes a minor amount of sericitization of plagioclase grains, giving them a brown tinge in thin section.

The alteration box plot of Large et al. (2001) quantifies alteration based on a chlorite-sericite index and a chlorite-carbonate-pyrite index. In this diagram four out of five rhyolitic and three out of seven felsic tuff samples plot outside of the field of little altered rocks, largely following a potassic feldspar alteration trendline. K_2O and Na_2O appear to have been particularly mobile during regional metasomatism and/or local alteration, resulting in potassium feldspar replacement of plagioclase grains. MgO, FeO and CaO may also have redistributed. Thus, many of the major elements are not reliable when assessing the tectonomagmatic affinity and magmatic sources for the Aillik Group. Because Paleoproterozoic terranes have undergone extended and multiple periods of metasomatism and alteration, it is important to identify and quantify the nature and amount of the element redistribution prior to interpreting geochemical signatures in terms of magmatic processes and tectonic setting.

3.5.3 Petrogenesis of Felsic Volcanic Rocks of the Aillik Group

Major and trace element signatures of the less altered felsic volcanic rocks have compositions of metaluminous to peralkaline 'A-type' rhyolites; whereas, only the more altered rhyolite and felsic tuff samples plot as peraluminous in Figure 3.16. When felsic volcanic samples are plotted in multi-element diagrams, REE patterns show LREE enrichment with marked negative Eu anomalies and flat HREE profiles, which is typical of the compositions of melts derived by partial melting of sialic crust (Menuge et al., 2002; Brewer et al., 2004). Felsic volcanic samples also display strongly negative Nb, and Ti anomalies, typical of crustally derived melts (Arculus, 1991; Kemp and Hawkesworth, 2003).

Less altered felsic volcanic rocks have $\varepsilon Nd_{(T)}$ values that range from -2.4 to -1.1 with $T_{(DM)}$ model ages that range from 2347 Ma to 2590 Ma. The results suggest that the felsic volcanic rocks were derived by partial melting sialic crust of predominantly Paleoproterozoic age. Altered felsic volcanic rocks have somewhat more negative $\varepsilon Nd_{(T)}$ values (-3.0 to -5.5) and older $T_{(DM)}$ model ages (2771 and 2971 Ma, excluding sample 08CL198A-02, which gives a meaningless age). This suggests there has been post-magmatic disturbance of the Sm-Nd system during alteration whereby the calculated $\varepsilon Nd_{(T)}$ values for the altered rocks are more negative than the actual, primary magmatic values. However, comparison of the Nd whole rock model ages with Hf zircon model ages in three samples of felsic tuffs where both types of analyses were performed (Chapter 2) presents an alternative hypothesis (Figure 3.19). In this diagram, the Nd whole rock model age of 2.77 Ga for the one altered felsic tuff analysed (08CL458A-02) corresponds well with the Hf zircon model ages of 2.63 to 2.83 Ga. Thus it may be that the Nd model ages for the altered felsic volcanic rocks reflect derivation from older, Neoarchean crustal sources, up to 2.97 Ga in age, distinct from the less altered felsic volcanic rocks which were derived from Paleoproterozoic sources. The range in eNd model ages, overlaps with the eHf model ages in Chapter 2, which supports the interpretation that the felsic volcanic rocks were derived from crustal sources ranging in age from 2400 to 3000 Ma.

3.5.4 Petrogenesis of Mafic Volcanic Rocks of the Aillik Group

Two distinct primitive mantle-normalized multi-element patterns arise when mafic volcanic samples are plotted in multi-element diagrams. Group A basalts are flat-lying, indicative of a MORB-like signature. Group B basalt and mafic tuff samples are moderately to strongly fractionated, with incompatible element enrichments and negative Ti and Nb anomalies as well as Hf and Zr depletions. In tectonomagmatic discrimination diagrams for mafic volcanic samples, Group A basalts plot in the N-MORB field; whereas, Group B mafic volcanic samples plot in subduction-related fields. The differences in geochemical signatures between Group A and Group B mafic volcanic rocks may be attributed to the effects of contamination of early N-MORB basalts by felsic magma or rock from sialic crust, as has been reported in terranes elsewhere (Brewer et al., 2004; Brown et al., 2002; Saunders and Tarney, 1991). This model indicates that the apparent calc-alkaline signature of the Group B basalts and mafic tuff of the Aillik Group is a result of crustal contamination.

Variable degrees of crustal contamination explain much of the large spread in $\varepsilon Nd_{(T)}$ from -0.33 to +4.6 (excluding sample 08CL159A-02 as explained below) found in all the mafic volcanic rocks of the Aillik Group. In general, Group B basalts have undergone more crustal contamination, which is indicated by their negative $\varepsilon Nd_{(T)}$ values; whereas, Group A basalts are more primitive in nature and have positive $\varepsilon Nd_{(T)}$ values. Figure 3.20 is bivariate diagram plotting $\varepsilon Nd_{(T)}$ against 1/Nd concentration (ppm) for mafic and felsic volcanic rocks of the Aillik Group and the Cross Lake granite. Magmatic rocks related by simple two component mixing (mafic magma with felsic magma or felsic rock) fall along lines connecting the two end member components in this diagram. The felsic rocks are scattered in the diagram indicating that they are not related by two component mixing. However, when mafic volcanic rocks are plotted on the same diagram a distinct linear trend is observed in the form of a simple mixing line for six of the samples, including three Type A basalts, two Type B basalts and one mafic tuff. Thus, the large spread of $\varepsilon Nd_{(T)}$ values within these mafic volcanic samples is interpreted as the product of variable degrees of mixing between a primitive mafic magma derived from depleted mantle and a felsic magma or rock derived from sialic crust. Based on the depleted mantle of DePaolo (1981), the primitive mafic magma model end-member for the mixing line (labeled DM in Figure 3.20) has an $\varepsilon Nd_{(T)}$ value of 6.21, which is the value for depleted mantle at ca. 1852 Ma. Its Nd concentration is based on the average value of four Iceland picrites thought to be primitive mantle melts (Chauvel and Hemonde, 2000), and is equal to 2.97 ppm. Based on a line of best fit to the six mafic samples, the end-member representing felsic crust (labeled FC in Figure 3.20) is assumed to have a $\varepsilon Nd_{(T)}$ value of -1.1 and a Nd concentration of 103.6 ppm. Because compositions of some felsic volcanic rocks of the Aillik Group plot near the felsic crust endmember of the mixing line, it is likely that they were the contaminant of the mafic magmas that formed the mafic volcanic rocks of the Aillik Group. The possibility of a Neoarchean felsic crustal contaminant is ruled out based on its expected composition ($\varepsilon Nd_{(T)}$ = -12.0 and Nd = 25 ppm, Kerr, 1989), which would plot well below the mixing line in Figure 3.20.

Three of the Group B basalts and mafic tuffs analyzed from the Aillik Group do not fall along the model mixing line in Fig. 3.20. However, they follow the general trends of crustal contamination in the trace element plots of Figure 3.13 and 3.14, suggesting that they had an origin similar to the other six samples of mafic volcanic rocks analysed here. Two of the samples, a Group B basalt (08CL398A-02) and a mafic tuff (08CL454A-02) from Pomiadluk Point plot below the mixing line. It is possible that their parental magmas were affected by crustal contamination by felsic magma or felsic rock with a more negative $\varepsilon Nd_{(T)}$ value than the other Group B basalt and mafic tuff samples. Sample 08CL159A-02, a Group B basalt from Middle Head, plots above the mixing line: its $\varepsilon Nd_{(T)}$ value of +6.4 is very close to the value for the depleted mantle at 1860 Ma, the presumed crystallization age of the sample, but its Nd concentration is much higher than predicted by the model for primitive mafic magma from the depleted mantle. It is possible that the Nd concentration or isotopic composition of the sample has been affected by alteration but there is no other evidence that the sample is more altered than any of the other basaltic rocks of this study. Instead, the most likely explanation is that sample 08CL159A-02 was derived from the same depleted mantle source as the primitive mafic magmas assumed for the mixing model in Figure 3.20 but that it formed by unusually small degrees of partial melting. At melt fractions of less than 10%, incompatible elements such as Nd and the other light REE will be enriched in the magma relative to the source, and could explain the eNd value of +6.4 and high Nd concentration in this sample.

3.5.5 Origin of Deformed Felsic Intrusive Suites

Compositions of the deformed intrusive suites are similar to those of the unaltered felsic volcanic rocks of the Aillik Group in that both are metaluminous to peralkaline, 'A-type' felsic rocks. The ca. 1805 Ma Cross Lake granite plots as a monzogranite in the QAP diagram and demonstrates a metaluminous signature. The ca. 1857 Ma quartz-feldspar porphyritic granite plots as a monzogranite and demonstrates a peralkaline to metaluminous signature. In multi-element plots, the Cross Lake granite and the quartz-feldspar porphyritic granite mimic the profile of the felsic volcanic rocks occurring at Middle Head and Pomiadluk Point, and have the same negative Eu, Nb and Ti anomalies, indicative of 'A-type' melts. The data thus point to similar sialic sources for the felsic volcanic rocks and the deformed granitic intrusive suites. In the case of the Cross Lake granite, the data indicate that the thermal conditions due to subduction and underplating of the depleted mantle causing partial melting of the crust persisted for over 50 million years, which is the difference in age between the Cross Lake granite and the felsic volcanic rocks of the Aillik Group.

The U-Pb zircon age of the Cross Lake granite suggests that it is a member of the Kennedy Mountain Intrusive Suite (Chapter 2). Kerr (1989) noted that the felsic volcanic rocks of the Aillik Group displayed strong geochemical similarities to the Kennedy Mountain Intrusive Suite, indicating that they likely formed in the same way that the felsic melts of the Aillik Group formed, via mafic underplating and partial melting of the upper continental crust.

The Cross Lake granite has an $\varepsilon Nd_{(T)}$ value of -4.2 and $T_{(DM)}$ Nd model age of 2.86 Ga similar to the altered felsic volcanic rocks measured in this study and is consistent with derivation from a crustal source. The Hf zircon model ages for the granite are somewhat younger; however, ranging from 2.42 to 2.59 Ga (Fig 3.19). An easy explanation for the discrepancy between the Hf and Nd model ages is not readily apparent; however, the results suggests that the crustal source of the granite may have been heterogeneous in age with Neoarchean minerals carrying the bulk of the Nd and Paleoproterozoic minerals (probably zircon) carrying the bulk of the Hf. A source containing clastic sedimentary rocks would be compatible with this interpretation and could possibly have been the Aillik Group metasandstone units.

3.5.6 Crustal contamination model

A spreadsheet program, FC-AFC-FCA (Ersoy and Helvaci, 2009), was used to model two possible contamination processes in the mafic volcanic rocks of the Aillik Group: (1) simple two component magma mixing and (2) combined assimilation fractional crystallization (AFC). For simple mixing, the model involves mixing a picritic magma derived from depleted mantle with a magma having the composition of a felsic tuff of the Aillik Group. For AFC, fractional crystallization of the picritic magma is combined with assimilation of Aillik Group felsic volcanic rocks.

3.5.6.1 Simple Mixing

When modeling simple mixing between two separate magmas, trace element concentrations for magma derived from depleted mantle (C_a) are chosen based the average values from the four Iceland picrites presented above (Chauvel and Hemonde, 2000). The second end member (C_b) is an unaltered Aillik Group felsic tuff (08CL452A-02). Six further mafic volcanic samples are modeled. Simple mixing within each model is demonstrated in Figure 3.21a. The model plots the Nd isotopic tracer $^{144}Nd/^{143}Nd$ against the elemental concentration of Nd. A second model uses trace elements Nb and Y for modeling because of the empirical link that exists between Nb - Y and tholeiitic - calc-alkalic compositional affinities (Figure 3.21b). The relationship is based on the depletion of Nb during magnetite fractionated and depletion of Y during amphibole fractionation, both of which are characteristic of hydrous, low temperature, oxidized, calc-alkaline magma systems (Wobus et al., 2001). In both models, the resultant mixing line requires a small to moderately significant amount of felsic material component (5 to 35%) to mix with the primitive magma from the depleted mantle. Simple mixing is determined to be a likely mechanism by which mafic volcanic rocks of the Aillik Group formed.

3.5.6.2 Assimilation fractional crystallization (AFC)

Fractional crystallization processes are generally thought to occur during the assimilation of solid wall rocks surrounding a magma chamber; the process is known as assimilation-fractional crystallization (AFC; DePaolo, 1981). When modeling AFC, the same primitive mafic magma and felsic tuff described above are used as C_o and C_a

respectively as well as the same six mafic volcanic samples. The best line of fit occurs when 1) the F value (representing the incremental amount of melt remaining, ranging from 1 to 11%) is set to 2%, meaning that crystallization starts at 2% and reaches up to 18% (namely, F = 0.98, 0.96, ..., 0.82), and 2) the r value (representing the ratio of fractionating material to assimilated material) is set to 0.8. Assimilated fractional crystallization is modeled for $^{143}Nd/^{144}Nd$ versus Nd and Y versus Nb in Figure 3.21. Crystallization ends at 18% of magma consumed, leaving 82% of the melt. In each case, the general model calculations match the analytical data most closely at r = 0.8 and when crystallization begins at 2% and ends at 18% magma consumed.

Such a high r value (0.8) is indicative of the rate of assimilation-fractional crystallization needed to generate the level of incompatible trace elements and Nd isotopic ratios that are typical of lower crustal conditions (Lassen et al., 2004). This is because higher temperatures and pressures are needed to produce the high rates of assimilation relative to fractional crystallization (Lassen et al. 2004; DePaolo, 1981). It is unlikely that Aillik Group mafic magmas were formed by assimilation fractional crystallization given that, in this case, the assimilant is interpreted as occurring as partial melt of the upper continental crust based on the models presented in Figure 3.21.

3.5.7 Interpretation of Tectonic Setting

3.5.7.1 Previous interpretations

Several different tectonic models for formation of the Aillik Group, and Makkovik Province have been proposed (ie. Kerr, 1989; Culshaw et al., 2000, 2002; Sinclair et al., 2002; Ketchum et al., 2002). Based on trace element data from the least altered outcrops, Kerr (1989) proposed that the formation of the Aillik Group commenced in a continental back-arc setting and continued in a continental arc setting following a pre-1800 Ma collision of a composite arc-type terrane with the North Atlantic Craton, followed by an extended period of post-collisional magmatism. Based on field and isotopic evidence for a sialic basement, geochemistry of volcanic and intrusive units, argon-argon cooling ages, normal faulting and the presence of mafic dykes, Culshaw et al. (2000; 2002) and Sinclair et al. (2002) interpreted the Aillik Group as having formed in a distal back-arc to rifted arc setting following the extension and erosional unroofing of an Andean-type convergent plate margin. Culshaw et al. (2000) proposed that the Aillik Group was then thrust onto the attenuated margin of the North American craton following basin inversion before 1810 Ma. Ketchum et al. (2002) interpreted the lithology, major and trace element geochemistry, and Sm-Nd isotopic geochemistry of deformed plutonic intrusions in the Aillik Group to indicate that the group was deposited in a back arc basin. The back arc basin is interpreted to have formed following a collision of an island arc (of unknown age) with the reworked Archean rocks and IHBPS of the Kaipokok domain (Ketchum et al., 2002). The back-arc basin of Ketchum et al. (2002) and differs from models of Kerr (1989), Culshaw et al. (2000; 2002), and Sinclair (1999), in that it forms in a post-collisional basin, rather than behind an actively subducting island or continental arc.

3.5.7.2 Proposed Model

The production of bimodal volcanism is generally documented in four tectonic settings: mid-ocean ridge, continental rift, rifted arc and back-arc systems. However, a back-arc setting behind an actively subducting continental arc is favoured for the origin of the Aillik Group, as explained below.

The volcano-sedimentary sequences of the Aillik Group and their possible plutonic counterparts have geological features that are inconsistent with mid-ocean ridge, continental-rift and rifted-arc models. Although bimodal volcanism can occur in mid-ocean ridge and continental-rift environments, the dominance of felsic volcanism as seen in the Aillik Group make it inconsistent with either of these tectonic settings. Furthermore, the coeval (or slightly younger) high-level granites in the Aillik Group and the intrusion of ca. 1800 Ma granites is not consistent with a mid-ocean ridge setting. Also, in a continental-rift environment, mafic volcanism is more common in the earlier stage of volcanism, resulting in widespread flood basalts and the presence of gabbroic and anorthositic intrusions (Moraes et al. 2003), which are not seen in the Aillik Group.

The sedimentary record preserved in the Aillik Group is not consistent with a rifted-arc model. In a rifted-arc, a large amount of mudstone and limestone is produced in a largely subaqueous environment. However, the Aillik Group lacks abundant pelite, marble and calc-silicate rocks, the products of metamorphosed very fine-grained mudstone, limestone and dirty limestone.

Bimodal volcanism, voluminous explosive rhyolite eruptions, the transitional nature of lesser basalts, the abundance of mafic dykes and sills and rapid resedimentation into a subaqueous environment are characteristic of extension or rifting in an arc environment (Brown et al., 2002; Neder et al., 2002; Kearey and Vine, 1994). Extension in arc environments may occur due to: 1) slab roll-back/break-off, resulting in a back-arc basin or 2) the development of a mantle plume, causing rifting. Both scenarios have been demonstrated to result in bimodal volcanism (Brewer et al., 2004); however, in the latter explanation the temperature anomaly required to form the plume at the crust-mantle boundary would result in the voluminous production of basaltic melts compared to rhyolitic melts (Menuge et al., 2002; Griffiths and Campbell, 1990). In the Aillik Group, felsic volcanism is much more commonly preserved (Clark, 1979; Kerr, 1989; Ketchum et al., 2002; Hinchey, 2007; Hinchey and LaFlamme, 2009).

Back-arc basins of the Cenozoic western Pacific Ocean form as a result of slab roll-back or slab break-off in a collisional belt, commencing extension and a weakening of the lithosphere, followed by upwelling of asthenosphere, and leading to the remelting of arc-type crust (Saunders and Tarney, 1991; Rollinson, 1993; Coulon et al., 2002). As continental crust thins, the upwelling of asthenosphere supplies sufficient heat to initiate melting in the mantle and lower crust (e.g., Reid, 2003). The ability of such mafic melts to rise through the continental crust will control the occurrence of both basaltic and silicic volcanic activity (Chichorro et al., 2008). In continental back-arc extension it is possible that large volumes of mafic material are stored at the base of the crust in lower crustal magma chambers, rather than be erupted, and thus provide the heat source to cause extensive crustal melting to produce relatively large volumes of metaluminous to peraluminous 'A-type' rhyolites and associated 'co-magmatic' granitic plutons (Rivers, 1997; Menuge et al., 2002; Brewer et al. 2004). The production of felsic magma may also bar the ascent of mafic magmas, leading to the abundance of felsic magmatism, as is observed in the Aillik Group (e.g., Pankhurst et al., 1998; Menuge et al., 2002; Brewer et al., 2004). In such environments, the sedimentary record is dominated by early immature clastic sediments, followed by periods of sedimentation interspaced with volcanism (Brewer et al., 2004). Polymictic conglomerate occurs at Pomiadluk Point, and a large package and several small layers potassium feldspar-rich, immature sandstone occur interspaced with mafic and felsic volcanic rocks at Pomiadluk Point.

The geochemical composition of magma extracted from the mantle at spreading centers can yield information about mantle source materials as well as about melting and extraction processes (Hichey-Vargas et al., 2006). Early basaltic volcanism is more fractionated than subsequent episodes because earlier magmas have resided in chambers for a prolonged period in time and later magmas rise through the crust through conduits that have been isolated from contamination by crystallization products of earlier magmas (Brewer et al., 2004; Moraes et al., 2003). The difference in mineral assemblages, variation in trace element data and spread in Nd isotope signatures of mafic volcanic rocks, can be defined by the amount of crustal contamination (Moraes et al., 2003). Within the Aillik Group this process is demonstrated in the study areas by two distinct groups of mafic rocks. Based on enriched REE signatures, trace element data and negative Nd isotope geochemistry, Group A basalts ($\varepsilon Nd_{(T)} = +2.8$ to $+4.6$), occurring at Middle Head, which have undergone little crustal contamination and are interpreted as being a close representation of the magmas from the depleted mantle. Group B basalt and mafic tuff ($\varepsilon Nd_{(T)} = -0.33$ to $+2.2$), are interpreted to have formed by mixing of the primitive magmas derived from depleted mantle with the partial melts involved in the formation of the Aillik Group felsic volcanic rocks. Back-arc basins have often been associated with bimodal magmas with transitional geochemical and compositional affinities that vary greatly up stratigraphy and even along strike (Sandeman et al., 2006; Saunders and Tarney, 1984).

The Aillik Group at Pomiadluk Point and Middle Head is lithologically varied. Pomiadluk Point (ca. 1854 to 1862 Ma) preserves a thick package of immature polymictic conglomerate and felsic volcanic rocks; whereas, Middle Head (ca. 1852 Ma) preserves arkosic sandstone and mafic volcanic rocks. Based on REE pattern and trace element signatures, the felsic magmatism of the Aillik Group and deformed intrusions are characterized by 'A-type' felsic melts with within plate granite signatures. These signatures are inferred to reflect their formation via partial melting of the upper continental crust.

The presence of 'A-type' felsic volcanism has, in the past, been recognized as anorogenic in nature; however, metaluminous to peralkaline 'A-type' rhyolites frequently occur in post-orogenic extensional settings (e.g., Sylvester, 1989; Eby, 1992; Rivers, 1997; Menuge et al., 2002). Furthermore, Lentz (1998) demonstrated that the change from compressional to extensional regimes in arc settings may lead to the emplacement of magmas with an 'A-type' signature. Therefore, 'A-type' felsic volcanic rocks of the Aillik Group did not necessarily form in an anorogenic, within-plate setting.

The enrichment in incompatible elements and especially LREE of the felsic rocks of the Aillik Group are interpreted as reflecting the partial melting of a crustal source. Rhyolites from modern back-arc settings are generally not as enriched in REE as the Aillik Group rhyolites, and are modeled as fractionates of the comagmatic basalt (e.g., Fryer et al., 1990). Because rhyolitic melts were generated during the early phases of rifting, they demonstrate a within-plate granite signature in tectonomagmatic discrimination diagrams. The fact that felsic melts of the Aillik Group are enriched in incompatible elements is evidence for their formation via partial melting of the continental crust and subsequent crustal contamination.

The Aillik Group is proposed here to have formed in a back-arc basin, in a continental setting. Extension would have been initiated by the underplating of mantle at the base of the crust. Heat production from mafic magmas would have melted the upper continental crust producing A-type felsic melts and possibly temporarily barring the ascent of mafic magmas. Earlier episodes of basalt volcanism would have been crustally contaminated, followed by later MORB-like basalts. The abundance of felsic volcanism is evidence for extension occurring in an active arc setting. Following the convective removal of the lithosphere, decompressional melting generates firstly asthenospheric melts and secondly crustal melts (Turner et al., 1999). The sedimentary record in the Aillik Group is in agreement with a back-arc basin tectonic setting, preserving large successions of immature polymictic conglomerate and arkosic sandstone. A model depicting the formation of the Aillik Group is presented in Figure 3.22.

No known exposed rocks within the Aillik domain represent basement to the felsic volcanic rocks of the Aillik Group (Kerr and Fryer, 1994; Culshaw et al., 2000; Hinchey, 2007), and the Nd model ages of the felsic volcanic rocks of the Aillik Group are not represented by ages opf known units preserved in the Makkovik Province. The Nd model ages of the felsic volcanic rocks of the Aillik Group (ca. 2.35 to 2.59 Ga) are reported within two continental fragments known as the Sask Craton and Meta Incognita microcontinent (Lewry et al., 1994; St. Onge et al., 2000). The Sask Craton is predominantly formed of 2.4 to 2.5 Ga felsic to mafic igneous rocks (Rayner et al., 2005), and the Meta Incognita microcontinent comprises an older 2.7 to 2.6 Ga Neoarchean crust and 2.4 to 2.5 Ga magmatism (Corrigan et al., 2009). Therefore, these terranes may have linkages with the basement rocks of the Aillik Group.

3.6 CONCLUSIONS

(1) Volcanic and sedimentary rocks of the Aillik Group at Middle Head and Pomiadluk Point have undergone amphibolites-facies metamorphism. Units have subsequently retrogressed to greenschist facies.

(2) Based on REE and trace element geochemistry, felsic melts of the Aillik Group and deformed intrusions are determined to be 'A-type' and to have within-plate granite characteristics. This signature is inferred to reflect their formation via partial melting of a felsic crust.

(3) Mafic rocks have transitional trace and REE patterns. Group A basalts are non-fractionated and demonstrate mineral assemblages of amphibole + plagioclase + clinopyroxene + magnetite. Group B basalt and mafic tuff are composed of amphibole + plagioclase ± quartz ± biotite and moderately to strongly fractionated.

(4) Neodymium isotope geochemistry illustrates that mafic and felsic magmas of the Aillik Group were not formed by the same mechanism. Felsic volcanic rocks ($\varepsilon Nd_{(T)}$ = -1.1 to -5.5) formed by the partial melting of a felsic crust. The broad range of isotopic signatures is interpreted as resulting from post-magmatic alteration. Mixing models demonstrate that the basaltic melts of the Aillik Group formed via mixing of the depleted mantle with the same source that formed the felsic volcanic rocks of the Aillik Group. Non-fractionated Group A basalts ($\varepsilon Nd_{(T)}$

= 2.8 to + 4.6) have undergone less crustal contamination than Group B basalt and mafic tuff ($\varepsilon Nd_{(T)}$ = -3.5 to +2.2).

(5) Nd depleted mantle model ages range from 2350 to 2590 Ma for unaltered felsic volcanic samples of the Aillik Group. These ages are not correlated with known units of the Makkovik Province.

(6) Trace and REE geochemistry combined with Nd isotope data indicate that the Aillik Group likely formed in a back-arc basin behind an actively subducting continental arc.

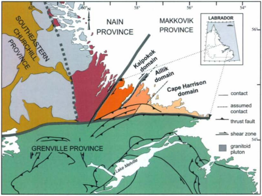

Figure 3.1: Simplified tectonic framework of south-central Labrador after Wardle *et al.* (1997). The map shows the three domains of the Makkovik Province, the Kaipokok, Aillik and Cape Harrison domains.

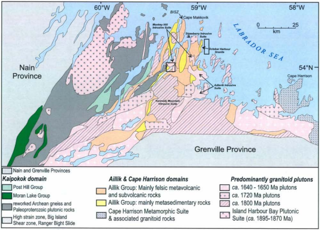

Figure 3.2: Simplified geology of the Makkovik Province after Ketchum et al. (2002). Figure highlights volcano-sedimentary packages as well as plutonic and metamorphic suites mentioned in text. Locations of study areas enclosed

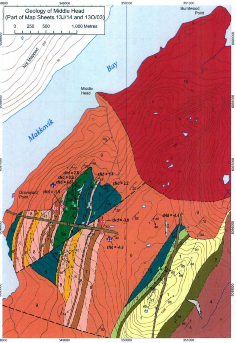

Figure 3.3: Geological map of the Middle Head area (1:10,000 scale) with location of samples taken for geochemistry and εNd data plotted. Sample numbers identified in Table 3.1.

Intrusive Rocks

Dykes (Age Unknown)

- 12 Granitic pegmatite dykes
- 11 Hornblende diorite dykes

Non-foliated Intrusive Unit *ca.* 1640 Ma

- 10 Medium-grained, leucocratic, undeformed bt-hbl monzogranite *(Monkey Hill Granite, part of Monkey Hill Intrusive Suite)*

Foliated Intrusive Unit 1805 ± 6 Ma

- 9 Coarse-grained, foliated hbl-bt monzogranite *(Cross Lake granite)*

Volcanic and Sedimentary Rocks

Aillik Group *ca.* 1883 - 1852 Ma (tectonostratigraphy, no stratigraphic order implied)

- 8 Crystal and crystal-lithic felsic tuff
- 7 Porphyritic to equigranular rhyolite
- 6 Arkosic sandstone interbedded with minor tuffaceous sandstone, containing <4% mafic minerals
- 5a Basalt (Group A)
- 5 Basalt (Group B)
- 4 Tuffaceous sandstone
- 3 Volcaniclastic breccia having subangular felsic and mafic volcanic clasts
- 2 Calc-silicate rock
- 1 Arkosic sandstone, containing 7% mafic minerals

Symbols

- ★ Geochronology (zircon U-Pb age)
- Station
- Lineation (generation unknown)
- Fold Axis (generation unknown)
- Bedding (tops known, tops unknown)
- Flow Contact (generation unknown)
- Foliation or Cleavage (generation unknown)
- Contact (defined, approximate, assumed)
- Fault (assumed)
- Altered rhyolite
- Unaltered felsic tuff
- Altered felsic tuff
- Basalt
- Cross Lake granite

Legend for Figure 3.3

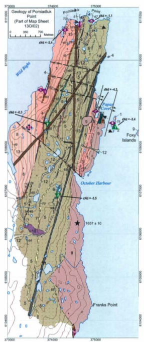

Figure 3.4: Geological map of the Pomiadluk Point area (1:10,000 scale) with location of samples taken for geochemistry and εNd data plotted. Sample numbers identified in Table 3.1.

Intrusive Rocks

Dykes (Age Unknown)

13 Undeformed plagioclase porphyritic gabbro dykes

12 Undeformed potassium feldspar porphyritic felsic dykes

11 Schistose plagioclase porphyritic diabase dyke

Non-foliated Intrusive Unit *ca.* 1650 Ma

10 Medium-grained, undeformed bt-hbl gabbro *(Adlavik Intrusive Suite)*

9 Coarse-grained, undeformed bt-fl monzogranite *(October Harbour Granite 1657 ± 10 Ma (Cox et al. 2003))*

Foliated Intrusive Unit *ca.* 1857 Ma

8 Medium-grained quartz feldspar - porphyritic granite

Volcanic and Sedimentary Rocks

Aillik Group *ca.* 1883 - 1852 Ma (tectonostratigraphy, no stratigraphic order implied)

7 Laminated siltstone

6 Mafic tuff

5 Polymictic conglomerate having subrounded, poorly sorted clasts of granite, granodiorite, mafic tuff, felsic tuff, rhyolite and sandstone. Variations in degree of strain.

4 Porphyritic to equigranular, locally flow banded rhyolite

3 Crystal felsic tuff

2 Crystal-lithic felsic tuff

1 Basalt

Symbols

★ Geochronology (zircon U-Pb age)

Station

Fold Axial Plane (generation unknown)

Linear Fabric (generation unknown)

Fold Axis (generation unknown)

Bedding (tops unknown)

Foliation or Cleavage (generation unknown)

Contact (defined, approximate, assumed)

Limit of mapping

Anticlinal Axis (defined)

Synclinal Axis (defined)

Strike-slip Fault (approximate, sinistral, dextral)

◆ Altered rhyolite

◇ Unaltered rhyolite

Unaltered felsic tuff

Altered felsic tuff

▽ Mafic tuff

△ Basalt

Qtz-fd porphyritic granite

Legend for Figure 3.4

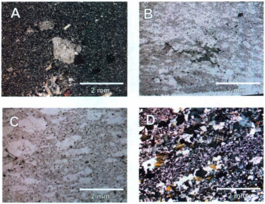

Figure 3.5: Representative photomictographs of units within the Aillik Group: a) feldspar crystals occurring within crystal-lithic felsic tuff as lapilli; b) secondary chlorite and calcite occurring within felsic tuff matrix; c) potassic alteration of feldspar within felsic tuff; and d) elongated phenocrysts in porphyritic rhyolite.

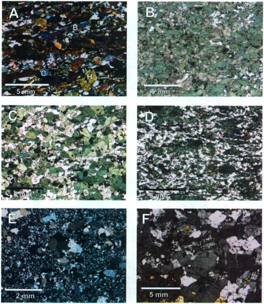

Figure 3.6: Representative photomictographs of units within the Aillik Group: a) primary plagioclase and clinopyroxene in Group A basalt (B-biotite, C-clinopyroxene, H-hornblende); b) sericite alteration in Group A basalt; c) secondary magnetite and hornblende in Group B basalt; d) mafic tuff; e) quartz and feldspar phenocrysts in porphyritic granite; and f) foliation in Cross Lake granite.

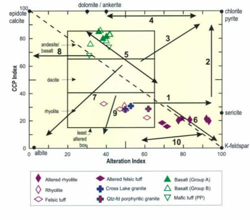

Figure 3.7: Alteration box encompassing field of least altered volcanic rocks for felsic, intermediate, and mafic compositions modified after Large et al. (2001). Field for diagenetic alteration (lower left) and hydrothermal alteration (upper right). Arrows demonstrate the common trends. 1: weak sericitic alteration, 2: intense sericite-chlorite ± pyrite alteration, 3: chlorite ± sericite ± pyrite, 4: chlorite-carbonate alteration, 5: sericite-carbonate alteration, 6: potassium feldspar-sericite alteration, 7: albite-chlorite alteration, 8: epidote-calcite ± albite alteration, 9: potassium feldspar-albite alteration, 10: paragonitic sericite-albite alteration.

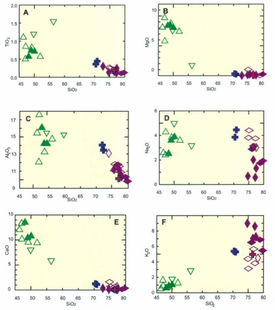

Figure 3.8: Harker variation diagrams for major element oxides in silicic and mafic volcanic rocks of the Aillik Group, intrusive suites and dykes. Legend is as in Figure 3.7: a) TiO_2; b) MgO; c); Al_2O_3 d); Na_2O e) CaO; and f) K_2O.

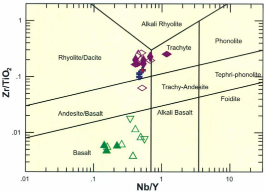

Figure 3.9: Plots X vs. Y (Winchester and Floyd, 1977; Pearce, 1996) for silicic and mafic volcanic rocks and deformed granitic intrusive rocks of the Aillik Group. Legend is as in Figure 3.7.

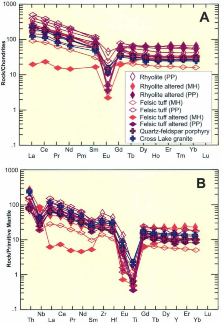

Figure 3.10: Multi-element REE plots for felsic volcanic and deformed granitic samples: a) Chondrite-normalized rare earth element diagram normalizing values after Sun and McDonough (1989); b) Primitive mantle-normalized rare earth element diagram after Sun and McDonough (1989).

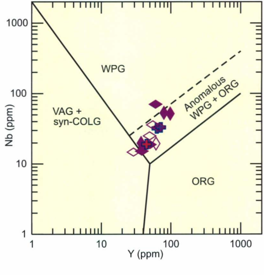

Figure 3.11: Felsic discrimination diagram Y versus Nb (Pearce et al. 1984). The diagram is divided into four fields: within-plate granite (WPG), volcanic-arc granite and syn-collisional granite (VAG + syn-COLG), ocean ridge granite (ORG), and within-plate granite and ocean ridge granite. The dashed line divides a field where anomalous ORG overlaps with WPG. Legend for samples as in Figure 3.7.

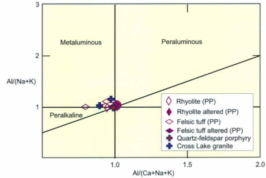

Figure 3.12: Al/(Ca+Na+K) versus Al/(Na+K) diagram of rock alkalinity from Maniar and Piccoli (1989) for felsic volcanic and granitic samples from the Aillik domain.

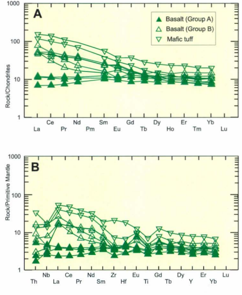

Figure 3.13: Multi-element REE plots for mafic volcanic samples: a) Chondrite-normalized rare earth element diagram normalizing values after Sun and McDonough (1989); b) Primitive mantle-normalized rare earth element diagram after Sun and McDonough (1989).

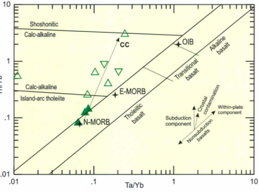

Figure 3.14: Ta/Yb vs. Th/Yb diagram from Pearce (1982). Normal (N) mid-ocean-ridge basalt (MORB), enriched (E) MORB, and ocean-island basalt (OIB) normalizing values are after Sun and McDonough (1989). The arrow depicts crustal contamination (CC). Legend is as in Figure 3.7.

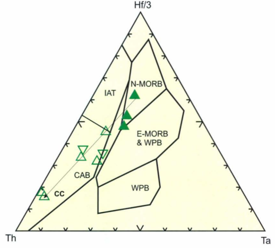

Figure 3.15: Ta-Hf-Th tectonomagmatic discrimination diagram after Wood (1980) for mafic volcanic samples from the Aillik Group. Fields are for IAT -island-arc tholeiite; WPB -within-plate basalt; MORB -mid-ocean-ridge basalt, E enriched and N - normal; CAB -calc-alkaline basalt. Legend for samples as in Figure 3.12. Arrow shows trend for crustal contamination (CC) of basaltic magmas of the Aillik Group with N-MORB compositions.

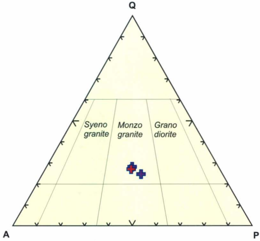

Figure 3.16: CIPW normative mineralogy for granitic samples from the Aillik domain plotted on the classification diagram of Streckeisen (1976), assuming that A = normative orthoclase and P = normative albite + anorthite. Legend is as in Figure 3.7.

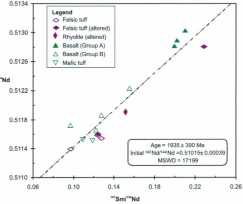

Figure 3.17: $^{147}Sm/^{144}Nd$ versus $^{143}Nd/^{144}Nd$ plot for mafic and felsic volcanic samples from the Aillik Group. A very poorly defined isochron regressed through the data using Isoplot/Ex3.0 (Ludwig, 2003) is shown only for reference.

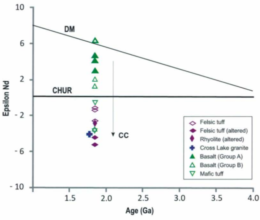

Figure 3.18: Initial εNd (CHUR) values for mafic and felsic volcanic samples from the Aillik Group, and the associated Cross Lake granite, plotted on the Nd isotopic evolution diagram. CHUR = chondritic uniform reservoir (DePaolo, 1981), DM = depleted mantle (Goldstein et al., 1984). A trend line for sialic crustal contamination (CC) of mafic magmas derived from DM is shown.

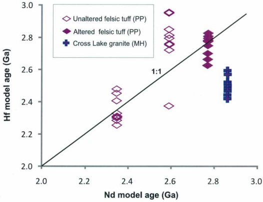

Figure 3.19: Nd vs. Hf model age for three felsic volcanic samples from Pomiadluk Point and the Cross Lake granite. Hf model ages are after Pietranik et al. (2008) and Nd model ages are after Goldstein et al. (1984).

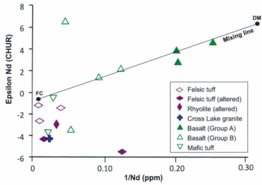

Figure 3.20: 1/Nd vs. Epsilon Nd of mafic and felsic volcanic rocks of the Aillik Group showing a model mixing line between a hypothetical primary mafic magma (represented by Icelandic picrite) derived by depleted mantle (DM) and felsic crust (FC, represented by felsic tuff 08CL452A-02).

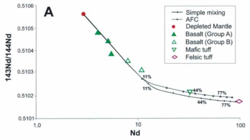

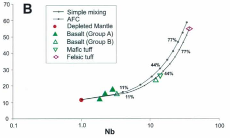

Figure 3.21: Models of simple mixing and assimilated fractional crystallization (AFC) for (a) Nd vs. $^{143}Nd/^{144}Nd$ (b) Nb vs. Y for Group A basalts and Group B basalts and mafic tuffs from the Aillik Group. Mixing end members as in Figure 3.20. AFC modeled using the software FC-AFC-FCA spreadsheet program by Ersoy and Helvaci (2009). The proportions of the felsic crust endmember in the mixtures are shown by tick marks along the model curves.

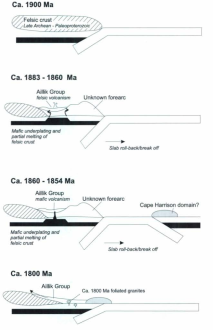

Figure 3.22: Model depicting tectonic setting of the Aillik Group.

Table 3.1: Location of samples selected for major and trace element geochemistry

Sample	Location	Number	Lithology
08CL099B-02	MH	1	Group B basalt
08CL107A-02	MH	2	Group A basalt
08CL159A-02	MH	3	Group B basalt
08CL179A-02	MH	4	Group B basalt
08CL195A-02	MH	5	Group A basalt
08CL266A-02	MH	6	Group A basalt
08CL268A-02	MH	7	Group B basalt
08CL152A-02	MH	8	felsic tuff
08CL198A-02	MH	9	felsic tuff
08CL153A-02	MH	10	rhyolite
08CL197A-02	MH	11	rhyolite
08CL199A-02	MH	12	CLG
08CL265A-02	MH	13	CLG
08CL398A-02	PP	1	Group B basalt
08CL371A-02	PP	2	mafic tuff
08CL454A-02	PP	3	mafic tuff
08CL346A-02	PP	4	felsic tuff
08CL398B-02	PP	5	felsic tuff
08CL452A-02	PP	6	felsic tuff
08CL453A-02	PP	7	felsic tuff
08CL458A-02	PP	8	felsic tuff
08CL346B-02	PP	9	rhyolite
08CL389A-02	PP	10	rhyolite
08CL400A-02	PP	11	rhyolite
08Cl388A-02	PP	12	q-f porphyry

Table 3.2: Chemical data and CIPW normative mineralogy for samples from the Aillik Group, a quartz-feldspar porphyritic granite and the Cross Lake granite.

Sample No.	099B-02	107A-02	159A-02	179A-02	195A-02	266A-02
Lithology	basalt	basalt	basalt	basalt	basalt	basalt
No. in Fig 3.3	1	2	3	4	5	6
SiO_2	47.03	48.97	47.12	51.92	48.10	50.04
Al_2O_3	12.07	14.22	17.60	14.74	16.08	14.21
FeO	6.61	7.55	6.84	6.46	6.47	7.60
Fe_2O_3	2.89	3.55	3.45	3.24	2.54	3.80
MgO	9.71	8.47	5.80	7.41	8.40	8.04
CaO	13.30	10.42	10.15	9.41	13.50	10.78
Na_2O	2.40	3.59	4.28	3.59	2.52	3.89
K_2O	1.62	0.90	0.91	1.26	0.62	1.04
TiO_2	0.50	0.74	0.85	0.57	0.57	0.71
MnO	0.18	0.18	0.15	0.21	0.15	0.20
P_2O_5	0.04	0.05	0.27	0.23	0.04	0.05
LOI	0.97	1.00	1.20	1.31	0.75	0.60
Total	97.3	99.6	98.6	100.3	99.7	101.0
V	222	267	190	182	231	359
Cr	615	333	124	227	519	325
Ni	186	111	69	47	115	107
Zn	131	98	125	131	63	212
Sc	40	47	29	34	48	46
Cu	1	15	1	15	126	47
As			3		2	
Rb	75	41	33	53	18	28
Sr	388	280	688	588	154	350
Y	23	15	12	13	12	15
Zr	38	44	52	65	27	41
Nb	12.0	2.2	3.1	5.2	1.8	3.4
Ba	107	106	444	547	85	183
La	18.5	2.7	11.7	12.3	1.6	2.9
Ce	31.0	6.8	27.1	31.9	4.3	7.0
Pr	3.1	1.0	3.7	4.1	0.7	1.1
Nd	10.9	5.1	17.1	18.3	4.0	5.4
Sm	2.48	1.65	3.64	4.01	1.57	1.91
Eu	0.64	0.69	1.33	1.12	0.56	0.62
Gd	2.96	2.32	3.33	3.29	1.77	2.39
Dy	6.93	3.03	2.64	2.61	2.15	2.62
Tb	0.53	0.43	0.48	0.47	0.34	0.40
Ho	0.80	0.66	0.49	0.50	0.49	0.59
Er	2.55	1.94	1.37	1.37	1.38	1.79
Tm	0.38	0.27	0.20	0.20	0.20	0.25
Yb	2.50	1.81	1.24	1.28	1.44	1.78
Lu	0.35	0.26	0.17	0.22	0.23	0.27
Hf	0.89	1.28	1.39	1.71	0.90	1.50
Ta	0.03	0.11	0.13	0.23	0.12	0.15
Pb	13	7	29	11	4	12
Th	1.37	0.15	0.79	3.38	0.21	0.45

Table 3.2 cont

Sample No.	268A-02	152A-02	198A-02	153A-02	197A-02	199A-02	265A-02
Lithology	basalt	felsic tuff	felsic tuff	rhyolite	rhyollite	CLG	CLG
No. in Fig 3.3	7	8	9	10	11	12	13
SiO_2	49.12	74.83	78.79	74.64	77.11	70.80	70.36
Al_2O_3	13.24	11.08	10.33	11.21	10.63	13.47	14.06
FeO	9.05	1.12	1.22	1.23	1.14	1.81	1.94
Fe_2O_3	4.31	0.96	1.11	1.23	1.10	1.79	1.80
MgO	8.76	1.01	0.01	0.12		0.27	0.34
CaO	9.52	1.62	0.14	0.14	0.06	1.12	1.28
Na_2O	3.84	3.81	1.73	0.67	0.58	4.45	3.85
K_2O	0.76	4.37	6.85	8.97	8.59	5.28	5.37
TiO_2	0.82	0.28	0.11	0.14	0.12	0.45	0.36
MnO	0.13	0.07		0.01		0.08	0.03
P_2O_5	0.06	0.09	0.01	0.03	0.01	0.09	0.05
LOI	0.99	0.69	0.29	0.21	0.39	0.49	0.98
Total	100.6	99.9	100.6	98.6	99.7	100.1	100.4
V	265	6	10	3	19		3
Cr	209	21	5	2	2	2	2
Ni	98	9	1	2	2	4	4
Zn	59	48	22	39	12	72	21
Sc	48	6		1		7	4
Cu	55				1		4
As	3	21	5	13	6	3	4
Rb	35	110	228	260	264	155	178
Sr	219	119	34	50	23	113	214
Y	18	29	60	94	79	63	72
Zr	45	174	272	233	271	384	397
Nb	2.8	14.8	70.3	50.2	51.6	32.0	33.0
Ba	127	985	56	67	137	982	495
La	12.4	21.7	4.8	42.1	32.4	43.2	81.3
Ce	18.9	50.9	14.6	124.0	78.7	102.4	168.2
Pr	2.0	6.0	1.5	12.5	8.1	11.5	18.3
Nd	7.9	24.0	7.0	51.1	31.0	45.6	67.9
Sm	2.27	4.82	2.60	12.3	8.19	10.7	12.8
Eu	1.02	0.85	0.13	0.21	0.29	1.51	1.10
Gd	2.66	4.32	4.04	12.7	10.7	10.1	11.0
Dy	2.93	4.82	7.25	14.4	15.5	10.0	10.8
Tb	0.45	0.77	0.94	2.23	2.16	1.58	1.74
Ho	0.66	1.00	1.64	2.97	3.37	2.10	2.25
Er	1.96	2.89	5.18	8.85	10.6	6.11	6.76
Tm	0.31	0.42	0.84	1.35	1.60	0.94	1.02
Yb	2.06	2.76	5.68	8.42	10.5	6.30	6.78
Lu	0.32	0.37	0.79	1.19	1.52	0.94	1.04
Hf	1.37	3.72	8.27	6.27	7.39	8.74	10.3
Ta	0.16	0.70	3.84	3.53	3.31	1.71	1.69
Pb	3	10	14	27	23	41	11
Th	0.25	12.8	6.99	30.1	21.8	20.1	22.2

Note: Analyses are below detection limit where no data is given for element

Table 3.2 cont

Sample No.	398A-02	371A-02	454A-02	346A-02	398B-02	452A-02
Lithology	basalt	mafic tuff	mafic tuff	felsic tuff	felsic tuff	felsic tuff
No. in Fig 3.4	1	2	3	4	5	6
SiO_2	46.34	49.84	56.20	76.04	76.58	75.01
Al_2O_3	15.46	15.48	15.28	11.78	11.56	11.82
FeO	8.25	6.87	7.39	1.06	1.15	1.83
Fe_2O_3	3.18	4.06	4.51	1.04	1.05	1.46
MgO	8.11	7.34	1.49		0.28	0.32
CaO	12.07	7.67	5.59	0.07	0.62	1.06
Na_2O	2.59	4.86	3.61	2.87	3.14	4.41
K_2O	0.51	1.50	2.66	6.51	5.62	3.11
TiO_2	1.10	1.15	1.50	0.16	0.17	0.24
MnO	0.18	0.15	0.16		0.03	0.05
P_2O_5	0.44	0.54	0.52	0.01	0.02	0.03
LOI	0.72	1.05	0.17	0.30	0.45	0.85
Total	99.0	100.5	99.1	99.8	100.7	100.2
V	181	159	206		5	10
Cr	239	105	330	9		2
Ni	138	43	120	24		
Zn	153	156	122	129	9	61
Sc	31	29	28	1	3	1
Cu						
As	54	8	25	32	7	54
Rb	11	56	79	152	136	74
Sr	634	436	500	29	83	75
Y	15	19	36	46	49	55
Zr	40	84	242	264	364	474
Nb	5.7	10.3	12.3	19.6	25.0	36.6
Ba	165	793	1279	265	48	211
La	12.1	28.1	36.9	50.6	62.7	118.4
Ce	26.4	61.0	86.6	100.5	126.4	239.1
Pr	3.7	8.1	10.6	12.0	15.9	27.6
Nd	16.9	32.7	44.0	44.5	59.1	99.0
Sm	3.63	6.03	8.59	8.29	12.3	16.1
Eu	1.40	1.69	2.15	0.62	0.30	0.22
Gd	3.53	4.81	7.67	7.50	10.0	11.6
Dy	3.06	3.60	6.42	7.38	9.89	8.99
Tb	0.50	0.66	1.07	1.19	1.59	1.52
Ho	0.55	0.70	1.31	1.40	1.89	1.89
Er	1.59	1.87	3.78	4.39	5.77	5.64
Tm	0.22	0.26	0.51	0.66	0.88	0.88
Yb	1.47	1.78	3.38	4.52	5.96	5.68
Lu	0.26	0.26	0.53	0.70	0.97	0.89
Hf	1.29	2.12	5.78	5.89	10.2	10.5
Ta	0.22	0.37	0.45	0.99	1.57	1.64
Pb	4	38	20	17	12	9
Th	0.60	1.14	2.87	8.23	14.9	15.4

Note: Analyses are below detection limit where no data is given for element

Table 3.2 cont

Sample No.	08CL	458A-02	346B-02	389A-02	400A-02	388A-02
Lithology	felsic tuff	felsic tuff	rhyolite	rhyolite	rhyolite	q-f porphyry
No. in Fig 3.4	7	8	9	10	11	12
SiO_2	77.13	79.63	77.42	72.72	76.45	76.53
Al_2O_3	10.89	9.82	10.34	13.09	11.25	10.43
FeO	1.81	0.63	1.10	1.88	1.06	1.75
Fe_2O_3	1.48	0.51	1.00	1.86	1.00	1.50
MgO	0.11	0.23	0.09	0.02	0.21	0.02
CaO	0.18	0.36	0.16	0.35	0.11	0.05
Na_2O	3.85	1.92	1.32	4.96	2.00	3.06
K_2O	3.81	5.45	7.24	4.67	7.02	5.03
TiO_2	0.20	0.13	0.15	0.30	0.16	0.20
MnO	0.03			0.03		0.02
P_2O_5	0.02	0.01	0.01	0.03	0.01	0.01
LOI	0.29	0.44	0.35	0.28	0.36	0.25
Total	99.8	99.2	99.2	100.2	99.6	98.9
V						3
Cr	4		2	1	1	1
Ni	4			2	2	
Zn	65	30	29	32	47	53
Sc		1	1	2	1	
Cu		11	7		1	5
As	9	28	10	4	20	5
Rb	130	127	155	125	174	113
Sr	65	56	32	105	31	60
Y	67	38	39	48	37	43
Zr	536	251	263	503	307	252
Nb	33.3	15.4	17.6	19.8	19.8	19.1
Ba	509	327	378	1281	773	140
La	94.4	52.9	60.6	51.2	58.0	43.6
Ce	195.0	118.3	116.2	107.3	104.1	110.0
Pr	23.9	13.6	13.6	12.6	14.4	11.1
Nd	92.2	55.0	52.0	49.2	53.8	45.8
Sm	18.5	11.2	9.41	10.2	8.55	9.38
Eu	1.45	0.89	0.69	1.73	0.63	0.93
Gd	16.4	9.74	7.31	8.54	6.89	7.80
Dy	16.7	8.52	7.56	8.27	7.10	8.02
Tb	2.56	1.40	1.19	1.35	1.07	1.25
Ho	3.59	1.79	1.53	1.62	1.57	1.52
Er	10.3	5.30	4.81	4.66	4.74	4.66
Tm	1.53	0.78	0.71	0.70	0.74	0.74
Yb	9.70	5.31	5.02	4.72	5.16	4.99
Lu	1.41	0.80	0.72	0.82	0.76	0.88
Hf	11.0	5.70	5.99	10.3	6.96	5.93
Ta	1.87	0.87	0.95	1.08	1.03	1.11
Pb	20	25	28	25	29	27
Th	13.9	7.70	8.20	4.64	8.24	6.70

Note: Analyses are below detection limit where no data is given for element

Table 3.3: Whole rock Nd isotope data. Measured $^{143}Nd/^{144}Nd$ and $^{147}Sm/^{144}Nd$ for chosen mafic and felsic rocks from Middle Head and Pomiadluk Point.

Sample Number	Lithology	Age (Ma)	Sm (ppm)	Nd (ppm)	$^{147}Sm/^{144}Nd$ (measured)	$^{143}Nd/^{144}Nd$ (measured)	±2SE	$^{143}Nd/^{144}Nd$ (initial)	eNd CHUR (T)[c]	T_{DM}* (Ma)
Middle Head										
08CL197A-02	rhyolite	1852	8.41	33.74	0.1507	0.511926	4.5E-05	0.510090	-2.97	2971
08CL198A-02	felsic tuff	1852	2.92	7.91	0.2233	0.512680	6.5E-05	0.509958	-5.53	-7881
08CL152A-02	felsic tuff	1852	4.20	20.88	0.1215	0.511649	3.6E-05	0.510167	-1.46	2492
08CL199A-02	CLG	1805	10.11	44.54	0.1372	0.511718	4.1E-05	0.510089	-4.19	2861
08CL099B-02	Group B basalt	1860	2.68	12.71	0.1276	0.511866	3.8E-05	0.510312	1.35	2287
08CL159A-02	Group B basalt	1860	3.04	19.14	0.0959	0.511738	2.9E-05	0.510571	6.42	1838
08CL107A-02	Group A basalt	1860	1.70	5.10	0.2015	0.512894	5.9E-05	0.510441	3.86	3342
08CL195A-02	Group A basalt	1860	1.27	3.65	0.2097	0.513030	6.1E-05	0.510477	4.57	5012
08CL266A-02	Group A basalt	1860	1.69	5.11	0.1999	0.512817	5.9E-05	0.510384	2.76	3778
08CL268A-02	Group B basalt	1860	2.23	8.66	0.1554	0.512246	4.6E-05	0.510355	2.18	2385
Pomiadluk Point										
08CL452A-02	felsic tuff	1862	16.85	103.63	0.0983	0.511378	3.0E-05	0.510173	-1.06	2347
08CL453A-02	felsic tuff	1861	19.23	94.71	0.1228	0.511610	3.7E-05	0.510106	-2.42	2590
08CL458A-02	felsic tuff	1854	11.92	57.30	0.1258	0.511556	3.8E-05	0.510021	-4.25	2771
08CL398A-02	Group B basalt	1860	3.98	17.73	0.1356	0.511717	4.0E-05	0.510057	-3.39	2805
08CL454A-02	mafic tuff	1860	8.98	45.29	0.1199	0.511518	3.6E-05	0.510051	-3.52	2657
08CL371A-02	mafic tuff	1860	6.69	37.06	0.1092	0.511553	3.3E-05	0.510217	-0.33	2338

* T_{DM} = Nd depleted mantle model age - calculated using $^{143}Nd/^{144}Nd$ 0.513163; and $^{147}Sm/^{144}Nd$ of 0.2137 (Goldstein et al., 1984)
[c]calulated using present day chondritic uniform reservoir with $^{143}Nd/^{144}Nd$ = 0.512638 & $^{147}Sm/^{144}Nd$ = 0.1967 (DePaolo, 1981) and a ^{147}Sm decay constant (λ) = 6.54 * 10^{-12} (Lugmair and Marti, 1978)

Chapter 4

Summary and Conclusions

4.0 INTRODUCTION

The purpose of this thesis, as presented in Chapter 1, is to unravel the history of the volcanism that formed the Aillik Group, by a) constraining the timing of volcanism, (b) determining the source of the magma, (c) evaluating the nature of volcanism, and (d) interpreting the tectonic setting in which the Aillik Group was formed. This study will aid in unravelling the geodynamic history of the Makkovik Province. Two areas are the focus of this study; they are used as case studies that represent the various lithologies present in the Aillik Group to meet the objectives presented in this thesis. Analytical work completed on each study area includes: lithologic and tectonostratigraphic analyses, U-Pb geochronology and Hf isotope geochemistry of target rocks, in addition to petrographic, major and trace element geochemistry and Nd isotope geochemistry analyses.

4.2 SUMMARY

In order to accomplish the objectives outlined above, field analyses were combined with detailed analytical work. The two study areas, Middle Head and Pomiadluk Point, were mapped at the 1:10,000 scale using both traditional and modern mapping methods, where observations and data were entered and digitized in the field using hand-held computers and ArcGIS software. Field data are complimented by: 1) detailed maps and tectonostratigraphic columns, 2) *in situ* U-Pb SHRIMP zircon geochronology 3) *in situ* Hf isotopic analyses of target rocks, 4) whole-rock major and trace element geochemistry, and 5) whole-rock Nd-isotope geochemistry. Although Chapters 2 and 3 are "stand alone" papers, they complement one another in their conclusions and analytical methods. An overview of the principle objectives and conclusions in Chapter 2 and 3 are presented in this section.

4.2.1 Chapter 2 - Geology and *in situ* zircon U-Pb and Lu-Hf isotope systematics from Paleoproterozoic magmatic rocks of the Aillik domain, Makkovik Province, Labrador

This paper focuses on the timing of volcanism and the source of magma generation of the Aillik Group via lithological and petrographic studies, combined with U-Pb SHRIMP geochronology and Lu-Hf LA-MC-ICPMS isotope geochemistry. This paper seeks to further constrain the timing of formation and deposition of the Aillik Group. Furthermore, it provides information regarding the nature of the magmatic source rocks necessary for evaluating the evolution of the Aillik Group and subsequently the Makkovik Province, discussed in Chapter 3.

The two study areas differ lithologically. Middle Head is composed of arkosic sandstone, felsic tuff, rhyolite and basalt. Pomiadluk Point is composed primarily of felsic tuff and polymictic conglomerate. These rocks are metamorphosed to lower amphibolite-facies and discreet areas are retrograded to greenschist facies. U-Pb SHRIMP zircon geochronology is completed on four felsic tuff samples. Magmatic ages range from ca. 1852 Ma at Middle Head to ca. 1854 - 1862 Ma at Pomiadluk Point. When combined with previous geochronology, the duration of volcanism within the Aillik Group is extended to 31 million years. Inherited zircon grains, interpreted to be xenocrystic, occur in the felsic volcanic rocks of the Aillik Group, ranging in age from ca. 1880 to 1920 Ma.

A foliated Paleoproterozoic monzogranite known as the Cross Lake Granite yields a magmatic date of 1805 ± 6 Ma. Because of its similar petrology and age, the Cross Lake granite it is interpreted as being part of the Kennedy Mountain Intrusive Suite, intruding the Aillik Group during the final compressional stages of the Makkovikian orogeny and constraining the timing of deformation to have continued after its emplacement at ca. 1805 Ma.

Two trends are observed in Hf isotope analyses and differ by location. At Middle Head, $\varepsilon Hf_{(t)}$ in magmatic zircon grains from the ca. 1852 Ma lithic felsic tuff and the ca. 1805 Ma Cross Lake granite range from -1.7 to -5.1. A crystal-lithic felsic tuff and a crystal felsic tuff preserved on the west and east coasts of Pomiadluk Point yield $\varepsilon Hf_{(t)}$ in magmatic zircon grains that range from -11.9 to -4.8. A crystal-lithic felsic tuff occurring between two conglomerate units on the northern coast of Pomiadluk Point yields $\varepsilon Hf_{(t)}$ that range from -1.9 to +2.1. The isotopic heterogeneity observed between samples is interpreted to result from heterogeneity in age of the crust from which the samples were formed. The range of crust formation ages for all of the analyzed magmatic zircons spans from 2260 to 2970 Ma, or some 700 m.y., indicating that the Aillik Group was formed from crust with both Paleoproterozoic and Neoarchean components.

Similarity exists in Hf isotope crust formation ages for the magmatic and inherited zircon in each sample. This phenomenon is interpreted to indicate that the inherited zircon formed from the same basement sources as the Aillik Group and the later foliated granitic intrusions, meaning that a similar crustal source existed beneath the Aillik Group for at least 115 m.y.

4.2.2 Chapter 3 - Geochemical and isotopic data from volcanic rocks of the Aillik Group and deformed granitic intrusions: Implications for the tectonic setting of the Aillik domain, Makkovik Province

The purpose of this paper is to interpret the tectonic setting in which the Aillik domain was formed. Analyses include major and trace element and Nd isotopic compositions combined with petrographical observations. The two discrete study areas of Middle Head and Pomiadluk Point are compared. This paper compliments Chapter 2, as it uses the results with regards to timing of volcanism and nature of the magmatic source to define a tectonic model.

Petrographical observations reveal that the Aillik Group at Middle Head and Pomiadluk Point has undergone amphibolite-facies metamorphism subsequently retrograded to greenschist-facies. Volcanism in the Aillik domain is bimodal, being dominantly composed of felsic tuff and rhyolite, with less abundant basalt and mafic tuff. Some felsic lithologies in both study areas demonstrate a moderate amount of potassic alteration. For these reasons, major element geochemistry is treated as suspect in interpreting the geochemical nature of Aillik Group rocks. Therefore, this paper focuses mainly on the trace and rare earth element geochemistry to characterize the Aillik Group supracrustal rocks and foliated granitic intrusions.

Felsic volcanic rocks and deformed granitic intrusions all have similar multi-element profiles and are strongly fractionated with marked negative Nb, Ti and Eu anomalies.

Such geochemical signatures are interpreted as indicating that felsic volcanic rocks of the Aillik Group, high-level porphyritic granite and the Cross Lake granite formed via partial melting of a felsic crust. Aillik Group felsic volcanic rocks and the Cross Lake granite demonstrate $\varepsilon Nd_{(T)}$ that range from -5.5 to -1.1, indicative of crustal contamination. The broad range in $\varepsilon Nd_{(T)}$ is interpreted as being a result of a heterogeneous source, rather than disequilibrium in the melt.

Mafic volcanic rocks of the Aillik Group are classified as two separate groups based on petrography, and trace, rare earth element and isotopic data. Group A basalts are non-fractionated and demonstrate mineral assemblages of plagioclase + clinopyroxene + amphibole + magnetite. Group B basalt and mafic tuff are composed of plagioclase ± amphibole + quartz ± biotite and moderately to strongly fractionated. Furthermore, Group A basalts (occurring at Middle Head) have the most elevated $\varepsilon Nd_{(T)}$ (+2.8 to +4.6) signatures while Group B basalts occurring at Pomiadluk Point and Middle Head have the most crustal $\varepsilon Nd_{(T)}$ values (-3.5 to +2.2). The two varying geochemical and isotopic signatures of Group A and Group B mafic volcanic rocks may be attributed to the effects of contamination of early N-MORB basalts by felsic magma or rock from sialic crust. Both mixing and AFC models were investigated as mechanisms for the formation of the basaltic rocks. Mixing models demonstrate that the basaltic melts of the Aillik Group formed via mixing of the depleted mantle with the same source that formed the felsic volcanic rocks of the Aillik Group.

The formation of the Aillik Group occurred following a change from a compressional to extensional regime, the depleted mantle was injected in the base of the crust, generating the heat necessary to melt the felsic crust and form and eject large volumes of 'A-type' rhyolitic melt rocks. Basaltic melts were initially barred from ascent. Early flows are fractionated due to crustal contamination and mixing with the Aillik Group felsic volcanic rocks, later flows have a more pronounced depleted mantle signature, as they have not undergone mixing. The petrographical, geochemical and isotopic characteristics of the Aillik Group, combined with the observed lithologies demonstrate that it was formed in a back-arc basin at a continental margin.

References

Anderson, T., Andersson, U.B., Graham, S., Aberg, G., Simonsen, S.L. 2009. Granitic magmatism by melting of juvenile continental crust: new constraints on the source of Paleoproterozoic granitoids in Fennoscandia from Hf isotopes in zircon. *Journal of the Geological Society*, **166**: 233-247.

Albarède, F., Brouxel, M. 1987. The Sm/Nd secular evolution of the continental crust and the depleted mantle. *Earth and Planetary Science Letters*, **82**: 25-35.

Arculus, R.J., Banno, S., Charvet, J., Kushiro, I. 1994. Tectonics, metamorphism and magmatism in island arcs. *Lithos*, **33**: 1-223.

Bailey, D.G. 1981. Kaipokok Bay - Big River, Labrador. Newfoundland Department of Mines and Energy, Map 81-18.

Barbero, L., Villaseca, C., Rogers, G., Brown, P.E. 1995. Geochemical and isotopic disequilibrium in crustal melting: An insight from the anatectic granitoids from Toledo, Spain. *Journal of Geophysical Research*, **100**: 745-765.

Barr, S.M., White, C.E., Culshaw, N.G., Ketchum, J.G.W. 2001. Geology and tectonic setting of Paleoproterozoic granitoid suites in the Island Harbour Bay area, Makkovik Province, Labrador. *Canadian Journal of Earth Science*, **38**: 441-463.

Barr, S.M., White, C.E., Ketchum, J.W.F. 2007. Field relations, geochemistry, and age of Paleoproterozoic igneous rocks in the northeastern Kaipokok Bay area, Makkovik Province, Labrador. *Atlantic Geology*, **43**: 121-136.

Belousova, E.A., Griffin, W.L., O'Reilly, S.Y. 2006. Zircon crystal morphology, trace element signatures and Hf isotope composition as a tool for petrogenetic modelling: Examples from eastern Australian granitoids. *Journal of Petrology*, **47**: 329-353.

Black, L.P., Kamo, S.L., Allen, C.M., Davis, D.W., Aleinikoff, J.N., Valley, J.W., Mundil, R., Campbell, I.H., Korsh, R.J., Williams, I.S., Foudoulis, C. 2004. Improved $^{206}Pb/^{238}U$ microprobe geochronology by monitoring of a trace-element-related matrix effect; SHRIMP, ID-TIMS, ELA-ICP-MS and oxygen isotope documentation for a series of zircon standards. *Chemical Geology*, **205**: 115-140.

Bouvier, A., Vervoort, J.D., Patchett, P.J., 2008. The Lu-Hf and Sm-Nd isotopic composition of CHUR: Constraints from unequilibriated chondrites and implication for the bulk composition of terrestrial planets. *Earth and Planetary Science Letters*, **273**: 48-57.

Bowen, N. L. 1928. *The evolution* of the *igneous rocks*. New Jersey: Princeton University Press, 334 pp.

Brewer, T.S., Ahall, K.I., Menuge, J.F., Storey, C.D. and Parrish, R.R. 2004. Mesoproterozoic bimodal volcanism in SW Norway, evidence for recurring pre-Svenconorwegian continental margin tectonism. *Precambrian Research*, **134**: 249-173.

Brown, S.J.A., Barley, M.E., Krapez, B., Cas, R.A.F. 2002. The Late Archaean Melita Complex, Eastern Goldfields, Western Australia: shallow submarine bimodal volcanism in a rifted arc environment. *Journal of Volcanology and Geothermal Research*, **115**: 303-327.

Chadwick, B., Coe, K. 1983. Geological map of Greenland, 1:100,000 scale, Buksefjorden, 63 V.1 Nord, with text, Copenhagen.
Chauvel, C., Hemonde, C. 2000. Melting of a complete section of recycled oceanic crust: Trace element and Pb isotopic evidence from Iceland. *G^3: Geochemistry, Geophysics, Geosystems*, **1**: 1-22.
Chavagnac, V., Nägler, T.F., Kramer, J.D. 1999. Migmatization by metamorphic segregation at subsolidus conditions: implications for Nd–Pb isotope exchange. *Lithos*, **46**: 275–298.
Christie, A.M., Roscoe, S.M., Fahrig, W.F. 1953. Central Labrador coast, Newfoundland (descriptive notes). Geological Survey of Canada, Paper 53-14, 3 pp.
Clark, A.M.S. 1973. A re-interpretation of the stratigraphy and structure of the Aillik Group, Makkovik, Labrador. Unpublished Ph.D. thesis, Department of Earth Sciences, Memorial University of Newfoundland, St. John's, Nfld.
Clark, A.M.S. 1979. Proterozoic deformation and igneous intrusions in part of the Makkovik sub-province, Labrador. *Precambrian Research*, **10**: 95-114.
Clement, S.W., Compston, W. 1989. SIMS at high sensitivity and high mass resolution. *In*: Proceedings of the International Secondary Ion Mass Spectrometry Conference. *Edited by*: C.A. Evans, K.D. McKeegan, H.A. Storms, H.W. Werner: New York. 815-819.
Cocherie, A., Robert, M. 2008. Laser ablation coupled with ICP-MS applied to U-Pb zircon geochronology: a review of recent advances. *Gondwana Research*, **14**: 597-608.
Condie, K.C., Beyer, E., Belousova, E., Griffin, W.L., O'Reilly, S.Y. 2005. U–Pb isotopic ages and Hf isotopic composition of single zircons: The search for juvenile Precambrian continental crust. *Precambrian Research*, **139**: 42–100.
Corfu, F. Hanchar, J.M., Hoskin, P.W.O., Kinny, P. 2003. Atlas of zircon textures. *In*: Zircon. Reviews in Mineralogy and Geochemistry. *Edited by*: J.M. Hanchar, P.W.O. Hoskin, 53: 469-499.
Corrigan, D., Pehrsson, S., Wodicka, N., DeKemp, E. 2009. The Paleoproterosoic Trans-Hudson Orogen: a prototype of modern accretionary processes. *In:* Ancient Orogens and Modern Analogues. *Edited by*: J.B. Murphy, J.D. Keppie, A.J. Hynes. Geological Sociey, London, Special Publications, **327**: 457-479.
Coulon, C. 2002. Post-collisional transition from calc-alkaline to alkaline volcanism during the Neogene in Oranie (Algeria); magmatic expression of a slab breakoff. *Lithos*, **62**: 87-110.
Cox, R.A., Wilton, D.H.C., Kosler, J. 2003. Laser-ablation U-Th-Pb *in situ* dating of zircon and allanite: An example from the October Harbour Granite, central coastal Labrador, Canada. *Canadian Mineralogist*, **41**: 273-291.
Crowley, J.L. 2002. Testing the model of late Archean terrane accretion in southern West Greenland: a comparison of the timing of geological events across the Qarliit nunaat fault, Buksefjorden region. *Precambrian Research*, **116**: 57-79.
Culshaw, N., Reynolds, P, Sinclair, G., Barr, S. 2002. Amphibole and mica 40Ar/39Ar ages from the Kaipokok and Aillik domains, Makkovik Province, Labrador: towards a

characterization of back-arc processes in the Paleoproterozoic. *Canadian Journal of Earth Science*, **39**: 749-764.

Culshaw, N., Ketchum, J., and Barr, S. 2000. Structural evolution of the Makkovik Province, Labrador, Canada: Tectonic Processes during 200 Myr at a Paleoproterozoic active margin. *Tectonics*, **19**: 961-977.

Culshaw, N.G., Ketchum, J. F., Barr, S.M., and Sinclair, G.S. 1998. A history of the Makkovik Province. ESCOOT Transect Meeting, Lithoprobe Report No. 68, pp 20-37.

Davis, D.W. and Krogh, T.E. 2003. Historical development of zircon geochronology. *Reviews in Mineralogy and Geochemistry*, **53**: 145-181.

DePaolo, D.J., Wasserberg, G.J. 1976a. Inferences about magma sources and mantle structure from variations of Nd-143/Nd-144. *Geophysical Research Letters*, **3**: 743-746.

DePaolo, D.J., Wasserberg, G.J. 1976b. Nd isotopic variations and petrogenetic models. *Geophysical Research Letters,* **3**: 249-252.

DePaolo, D.J. 1981. A neodymium and strontium isotopic study of the Mesozoic calc-alkaline granitic batholiths of the Sierra Nevada and Peninsula ranges, *Journal of Geophysical Research,* **86**: 10470–10488.

DePaolo, D.J. 1988. *Neodymium Isotope Geochemistry: An Introduction*, Springer-Verlag, New York. 264 pp.

Dickin, A. 1995. *Radiogenic Isotope Geology*, Cambridge: Cambridge University Press. 490 pp.

Douglas, G.V. 1953. Notes on localities visited on the Labrador coast in 1946 and 1947. Geological Survey of Canada, Paper 53-1, 67 pp.

Eby, G.N. 1990. The A-type granitoids: a review of their occurrence and chemical characteristics and speculations of the peterogenesis. *Lithos*, **26**: 115-134.

Eby, G.N. 1992. Chemical subdivision of the A-type granitoids: petrographic and tectonic implications. *Geology* ,**20**: 641–644.

Ermanovics, I., and Ryan, B. 1990. Early Proterozoic orogenic activity adjacent to the Hopedale Block of the Southern Nain Province. *Geoscience Canada*, **17**: 293-297.

Ermanovics, I.F. 1993. Geology of the Hopedale Block, southern Nain Province, and the adjacent Proterozoic terranes. Geological Survey of Canada, Memoir 431.

Ersoy, Y., Helvaci, C. 2010. FC–AFC–FCA and mixing modeller: A Microsoft® Excel© & spreadsheet program for modeling geochemical differentiation of magma by crystal fractionation, crustal assimilation and mixing. *Computers & Geosciences*, **36**: 383–390.

Faure, G., Mensing, T. 2005. , John Wiley, New Jersey, 898 pp.

Finch, C.J. 1998. Inductively coupled plasma-emission spectrometry (ICP-ES) at the geochemical laboratory. Newfoundland Department of Miners and Energy, Geological Survey, Report 98-1, 179-193.

Finn, G.C. 1991. Major-, trace-, and rare-earth-element geochemistry of the Archaean Maggo Gneisses, southern Nain Province, Labrador. *Canadian Journal of Earth Sciences*, **28**: 44-57.

Flowerdew, M.J., Millar, E.L., Vaughan, A.P.M., Horstwood, M.S.A., Fanning, C.M. 2006a. The source of granitic gneisses and migmatites in the Antarctic Peninsula: a combined U-Pb SHRIMP and laser ablation Hf isotope study of complex zircons. *Contributions to Mineralogy and Petrology*, **151**: 752-768.

Flowerdew, M.J., Chew, D.M., Daly, J.S., Millar, I.L. 2009. Hidden Archean and Paleoproterozoic crust in NW Ireland? Evidence from zircon Hf isotopic data deom granitic intrusions. *Geological Magazine*, **146**: 903-916.

Foley, S.F. 1982. Mineralogy, geochemistry, petrogenesis and structural relationships of the Aillik Bay alkaline intrusive suite, Labrador, Canada. Unpublished M.Sc. thesis, Memorial University of Newfoundland, St. John's, Newfoundland, 210 pp.

Foley, S.F. 1996. Trace element partition coefficients for clinopyroxene and phlogopite in an alkaline lamprophyre from Newfoundland by LAM-ICP-MS. Geochimica et Cosmochimica Acta, **60**: 629-638

Friend, C.R.L., Nutman, A.P. 2001. U–Pb zircon study of tectonically bounded blocks of 2940–2840 Ma crust with different metamorphic histories, Paamiut region, South-West Greenland: implications for the tectonic assembly of the North Atlantic craton. *Precambrian Research*, **105**: 143–164.

Gandhi, S.S., Grasty, R.L., Grieve, R.A.F. 1969. The geology and geochronology of the Makkovik Bay area, Labrador. *Canadian Journal of Earth Sciences*, **6**: 1019-1034.

Gandhi, S.S. 1978. Geological setting and genetic aspects of uranium occurrences in the Kaipokok Bay – Big River area, Labrador. *Economic Geology*, **73**, 1492-1522.

Gorton, M.P., Schandl, E.S. 2000. From continents to island arcs: A geochemical index of tectonic setting for arc-related and within-plate felsic to intermediate volcanic rocks. *The Canadian Mineralogist*, **38**: 1065-1073.

Goldstein, S.L., O'Nions, R.K., Hamilton, P.J. 1984. A Sm-Nd isotopic study of atmospheric dusts and particulates from major river systems. *Earth and Planetary Science Letters*, **70**: 221-236.

Govindaraju, K. 1989. Compilation of working values and sample description for 272 geostandards. *Geostandards Newsletter*, **13**: 113 pp.

Gower, C. F. 1981. The geology of the Benedict Mountains, Labrador. Newfoundland Department of Mines and Energy, Mineral Development Division, Report 81-3.

Gower, C.F., Krogh, T.E. 2002. A U-Pb geochronological review of the Paleoproterozoic history of the eastern Grenville Province. *Canadian Journal of Earth Science*, **39**: 795-829.

Gower, C.F., Heaman, L.M., Loveridge, W.D., Schurer, U., Tucker, R.D. 1991. Grenvillian magmatism in the eastern Grenville Province, Canada. *Precambrian Research*, **51**: 315-336.

Gower, C.F., Ryan, B. 1987. Two stage felsic volcanism in the Lower Proterozoic upper Aillik Group, Labrador, Canada: its relationship to syn- and post-kinematic plutonism. *In* Geochemistry and Mineralization of Proterozoic Volcanic Suites, Geological Society of London Special Publication No. 33, 201-210.

Gower, C.F., Ryan, B. 1986: Proterozoic evolution of the Grenville Province and adjacent Makkovik Province in east-central Labrador. *In* The Grenville Province. *Edited by* J.M. Moore. Geological Association of Canada, Special Paper 31, pp. 281-296.

Gower, C.P., Flanagan, M.J., Kerr, A., Bailey, D.G. 1982. Geology of the Kaipokok Bay - Big River area, Central Mineral Belt, Labrador. Newfoundland and Labrador Department of Mines and Energy, Report 82-7, 77 pp.
Griffin, W.L., Pearson, N.J., Belousova, E., Jackson, S.E., Van Achterbergh, E., O'Reilly, S.Y., Shee, S.R. 2000. The Hf isotope composition of cratonic mantle: LAM-MC-ICPMS analysis of zircon megacrysta in kimberlites. *Geochimica et Cosmochimica Acta*, **64**: 133-147.
Griffiths, R.W., Campbell, I.H., 1990. Stirring and structure in mantle starting plumes. *Earth Planet Science Letters,* **99**: 66–78.
Hall, J., Wardle, R.J., Gower, C.F., Kerr, A., Coflin, K., Keen, C.E., Carroll, P. 1995. Proterozoic orogens of the northeastern Canadian Shield: new information from the Lithoprobe ECSOOT crustal reflection seismic survey. *Canadian Journal of Earth Sciences*, **32**: 1119–1131.
Hancher, J.M., Miller, C.F. 1993. Zircon zonation patterns as revealed by cathoduminescence and backscattered electron images: implication for interpretation of complex crustal histories. *Chemical Geology,* **110**: 1-13.
Hawkins, D.W. 1976: Emplacement, petrology and geochemistry of ultrabasic to basic intrusives at Aillik Bay, Labrador. Unpublished M.Sc. thesis, Memorial University of Newfoundland, St. John's, Newfoundland, 236 pp.
Hawkesworth, C.J. and Kemp, A.I.S. 2006. Using hafnium and oxygen isotopes in zircons to unravel the record of crustal evolution: *Chemical Geology*, **226**: 144–162.
Hickey-Vargas, R., Savov, I.P., Bizimis, M., Ishii, T., Fujioka, K. 2006. Origin od diverse geochemical signatures in igneous rocks from the West Philippine basin: Implications for tectonic models. *In*: Back-arc Spreading Systems: Geological, Biological, Chemical and Physical Interactions. *Edited by*: Chistie, D.M., Fisher, C.R., Lee, S., Givens, S. Geophysical Monograph 166. 287-303.
Hinchey, A.M. 2007. The Paleoproterozoic metavolcanic, metasedimentary and igneous rocks of the Aillik Domain, Makkovik Province, Labrador (NTS Map Area 13O/03). Newfoundland Department of Natural Resources Geological Survey, 7-01, pp. 25-44.
Hinchey, A.M., LaFlamme, C. 2009. The Paleoproterozoic volcano-sedimentary rocks of the Aillik Group and associaed plutonic suites of the Aillik domain, Makkovik Province, Labrador (NTS map area 13J/14). Newfoudland Department of Narural Resources Geological Survey, 9-01, pp. 159-182.
Hinchey A.M., Rayner, N. 2008. Timing constraints on the Paleoproterozoic, bi-modal metavolcanic rocks of the Aillik Group, Aillik domain, Makkovik Province, Labrador. *In* GAC-MAC 2008, Abstract Volume 33.
Inger, S., Harris, N.B.W. 1993. Geochemical constraints on leucogranite magmatism in the Langtang valley, Nepal Himalaya. *Journal of Petrology*. **34**: 345-368.
Jacobsen, S.B., Wasserburg, G.J. 1979. *Lunar and Planetary Science,* **11**: 502.
Jaffey, A.H., Flynnm K.F., Glendenin, L.E., Bentley, W.C. and Essling, A.M. 1971. Precision measurement of the half-lives and specific activities of U^{235} and U^{238}. *Phys Rev. C* **4**: 1889-1907.

James, D., Kamo, S. and Krogh, T. 2002. Evolution of 3.1 and 3.0 Ga volcanic belts and a new thermotectonic model for the Hopedale Block, North Atlantic craton (Canada). *Canadian Journal of Earth Science*, **39**: 687-710.

Jenner, G.A., Longerich, H. P., Jackson, S. E., Fryer, B. J. 1990. ICP-MS; a powerful tool for high-precision trace-element analysis in earth sciences; evidence from analysis of selected U.S.G.S. reference samples *Chemical Geology*, **83**: 133-148.

Kearey, P., Vine, F.J. 1996. *Global Tectonics*. Blackwell, Oxford.

Kemp, A.I.S, Hawkesworth, C.J. 2003. Granitic Perspectives on the generation and secular evolution of the continental crust. *In* Treatise on Geochemistry. *Edited* by Holland, H.D. and Turekian, K.K. Elsevier Science. 350-404.

Kerr, A. 1989. Early Proterozoic granitoid magmatism and crustal evolution in the Makkovik Province of Labrador: A geochemical and isotopic study. Unpublished PhD thesis, Memorial University of Newfoundland, St. John's, Nfld.

Kerr, A. 1994. Early Proterozoic magmatic suites of the eastern Central Mineral Belt Makkovik Province, Labrador: Geology, geochemistry and mineral potential. Newfoundland Department of Miners and Energy, Geological Survey, Report 94-3, 149 pp.

Kerr, A., Krogh, T.E., Corfu, F., Scharer, U. Gandhi, S.S., Kwok, Y.Y. 1992. Episodic Early Proterozoic granitoid plutonism in the Makkovik Province, Labrador: U-Pb geochronological data and geological implications. *Canadian Journal of Earth Sciences,* **29**: 1166-1179.

Kerr, A., Ryan B., Gower, C.F., Wardle, R.J. 1996. The Makkovik Province: extension of the Ketilidian Mobile Belt in mainland North America. *In:* Precambrian Crustal Evolution in the North Atlantic Region. *Edited by:* T.S. Brewer. Geological Society of London, Special Publication No. 112, pp. 155-177.

Kerr, A., Fryer, B.J. 1994. The importance of late- and post-orogenic crustal growth in the early Proterozoic: Evidence from Sm-Nd isotopic studies of igneous rocks in the Makkovik Province, Canada. *Earth and Planetary Science Letters,* **125**: 71-88.

Kerr, A., Hall, J., Wardle, R.J., Gower, C.F., Ryan, B. 1997. New reflections on the structure and evolution of the Makkovikian-Ketilidian orogen in Labrador and southern Greenland. *Tectonics*. **16**: 942-965.

Ketchum, J.W.F., Culshaw, N.G., Dunning, G.R. 1997. U-Pb geochronologic constraint on Paleoproterozoic orogenesis in the northwestern Makkovik Province, Labrador, Canada. *Canadian Journal of Earth Sciences*, **34**: 1072-1088.

Ketchum, J.W.F., Jackson, S.E., Barr, S.M., Culshaw, N.G. 2001a. Depositional and tectonic setting of the Paleoproterozoic Lower Aillik Group, Makkovik Province, Canada: Evolution of a passive margin-foredeep sequence based on U-Pb (TIMS and LAM-ICP-MS) geochronology. *Precambrian Research,* **105**: 331-356.

Ketchum, J.W.F., Barr, S.M., Culshaw, N.G., White, C.E. 2001b. U-Pb ages of granitoid rocks in the northwestern Makkovik Province, Labrador: evidence for 175 million years of episodic synorogenic and postorogenic plutonism. *Canadian Journal of Earth Sciences*, **38**: 359-372.

Ketchum, J.W.F., Culshaw, N.G., Barr, S.M. 2002. Anatomy and orogenic history of a Paleoproterozoic accretionary belt: the Makkovik Province, Labrador, Canada. *Canadian Journal of Earth Sciences*, **39**: 711-730.
King, A.F. 1963. Geology of the Cape Makkovik Peninsula, Aillik, Labrador. Unpublished M.Sc. thesis, Memorial University of Newfoundland, St. John's, Newfoundland, 114 pp.
King, A.F., McMillan, N.J. 1975. A Mid-Mesozoic breccia from the coast of Labrador. *Canadian Journal of Earth Sciences*, **12**: 44-51.
Kinny, P., Mass, R. 2003. Lu-Hf and Sm-Nd isotope systems in zircon. *Reviews in Mineralogy and Geochemistry*. **53**: 327-341.
Košler, J., Forst L., Sláma, J. 2008. LamDate and LamTool: spreadsheet-based data reduction for laser ablation ICP-MS. Mineralogical Association of Canada Short Course 40. *In:* Laser-Ablation-ICP-MS in the Earth Sciences: Current Practices and Outstanding Issues. *Edited by:* P. Sylvester. Appendix A4.
Kosler, J., Sylvester, P. 2003. Present trends and the future of zircons in geochronology; laser ablation ICP-MS. Reviews in Mineralogy and Geochemistry, **53**: 243-275.
Kranck, E.H. 1939. Bedrock geology of the seaboard region of Newfoundland and Labrador. Geological Survey of Newfoundland, Bulletin 19, 44 pp.
Kranck, E.H. 1953. Bedrock geology of the seaboard of Labrador between Domino Run and Hopedale, Newfoundland. Geological Survey of Canada, Bulletin 26, 41 pp.
Kurhila, M., Andersen, T., Rämö, O.T. 2010. Diverse sources of crustal granitic magma: Lu–Hf isotope data on zircon in three Paleoproterozoic leucogranites of southern Finland. *Lithos*, **115**: 263–271.
Large, R.R., Gemmell, J.B., Paulick, H., Huston, D.L. 2001. The Alteration Box plot: A simple approach to understanding the relationship between alteration mineralogy and lithogeochemistry associated with volcanic-hosted massive sulphide deposits. *Economic Geology*, **96**: 957-971.
Lassen, B., Bridgwater, D., Berstein, S., Rosing, M. 2004. Assimilation and high-pressure fractional crystallization (AFC) recorded by Paleoproterozoic mafic dykes, Southeast Greenland. *Lithos*, **72**: 1-18.
Leat, P. T., Livermore, R. A., Millar, I. L., Pearce, J. A. 2000. Magma supply in back-arc spreading centre segment E2, East Scotia Ridge. *Journal of Petrology*, **41**: 845-866.
Lentz, D.R. Petrogenetic evolution of felsic volcanic sequences associated with Phanerozoic volcanic-hosted massive sulphide systems: the role of extensional geodynamics. *Ore Geology Reviews*, **12**: 289–327.
Lewry, J.F., Hajnal, Z., Green, A., Lucas, S.B., White, D., Stauffer, M.R., Ashton, K.E., Weber, W., Clowes, D. 1994. Structure of a Paleoproterozoic continent-continent collision zone: a lithoprobe seismic reflection profile across the trans-Hudson Orogen, Canada: *Tectonophysics*, **232**: 143-160.
Licthe, F.E., Golightly, D.W., Lamothe, P.J. 1987. Inductively Coupled Plasma-Atomic Emission Spectrometry. *In*: Methods for Geochemical Analysis. US Geological Survey Bulletin 1770, pp. B1-B10.

Longerich, P., Jenner, G.A., Fryer, B.J., Jackson, S.E. 1990. Inductively coupled plasma – mass spectrometric analysis of geological samples: an overview. *Chemical Geology*, **83**: 105–118.
Ludwig, K.R. 2003. User's manual for Isoplot/Ex rev. 3.00: A Geochronological Toolkit for Microsoft Excel. Special Publication, 4, Berkeley Geochronology Center, Berkeley, 70 pp.
Lugmair, G.W., Marti, K. 1978. Lunar initial $^{143}Nd/^{144}Nd$: Differential evolution of the lunar crust and mantle. *Earth and Planetary Science Letters*, **39**: 349-35.
Lyons, P. 1971. Staining of feldspars on rock-slab surfaces for modal analyses. *Mineralogical Magazine*, **38**: 518-519.
MacDougall, C.S. 1988. A metallogenic study of polymetallic granophile mineralization within the early Proterozoic Upper Aillik Group, Round Pond area, Central Mineral Belt, Labrador. Unpublished M.Sc. thesis, Memorial University of Newfoundland, 245 pp.
MacKenzie and O-nions, 1991. Partial melt distributions from inversion of rare earth element concentrations. *Journal of Petrology*: **32**, 1021–1091.
MacLean W. H., Barrett, T. J. 1993. Lithogeochemical techniques using immobile elements. *Journal of Geochemical Exploration*, **48**: 109-133.
Malpas, J., Foley, S.F., King, A.F. 1986. Alkaline mafic and ultramafic lamprophyres from the Aillik Bay area, Labrador. *Canadian Journal of Earth Sciences*, **23**: 1902-1918.
Maniar, P.D., Piccoli, P.M. 1989. Tectonic discrimination of granitoids. *Geological Society of America Bulletin.* **101**: 635-643.
Marsh, J. 1989. Geochemical constraints on coupled assimilation and fractional crystallization involving upper crustal compositions and continental tholeiitic magma. *Earth and Planetary Science Letters*, **92**: 70–80.
Marten, B.E. 1977. The relationship between the Aillik Group and the Hopedale gneiss, Kaipokok Bay, Labrador. Unpublished Ph.D. thesis. Memorial University of Newfoundland, St. John's NFLD.
Matteini, M., Junges, S.L., Dantas, E.L., Pimentel, M.M., Buhn, B. 2010. In situ zircon U-Pb and Lu-Hf systematic on magmatic rocks; insights on the crustal evolution of the Neoproterozoic Goias magmatic arc, Brasilia Belt, central Brazil. *Gondwana Research*, **17**: 1-12.
Menuge, J.F., Brewer, T.S., Seeger, C.M. (2002). Petrogenesis of metaluminous A-type rhyolites from the St Francois Mountains, Missouri and the Mesoproterozoic evolution of the southern Laurentian margin. *Precambrian Research*, **113**: 269–291.
Metzger, E.P., Miller, R.B., Herper, G.D. (2002). Geochemistry and Tectonic Setting of the Ophiolitic Ingalls Complex, North Cascades, Washington: Implications for Correlations of Jurassic Cordilleran Ophiolites. *Journal of Geology*, **110**: 543-560.
Moreas, R., Fuck, R.A., Pimentel, M.M., Gioia, S.M., Figueiredo, A.M.G. (2003). Geochemistry and Sm–Nd isotopic characteristics of bimodal volcanic rocks of Juscelândia, Goiás, Brazil: Mesoproterozoic transition from continental rift to ocean basin. *Precambrian Research*, **125**: 317–336

Murphy, J.B., Dostal, J., Keppie, J.D. 2008. Neoproterozoic–Early Devonian magmatism in the Antigonish Highlands, Avalon terrane, Nova Scotia: Tracking the evolution of the mantle and crustal sources during the evolution of the Rheic Ocean. *Tectonophysics*, **461**: 181-201.

Murphy, J.B., Keppie, J.D., Davis, D., Krogh, T.E. 1997. Regional significance of new Neoproterozoic igneous units in Avalonian rocks of northern mainland Nova Scotia, Canada, *Geological Magazine* **134**: 113–120.

Neder, R.D., Leite, J.A.D., Figueiredo, N.J., McNaughton, N.J. 2002. 1.76 Ga volcano-plutonism in the southwestern Amazonian craton, Aripuanã-MT, Brazil: tectono-stratigraphic implications from SHRIMP U- Pb zircon data and rock geochemistry. *Precambrian Research*, **119**: 171-187

Pankhurst, R.J., Leat, P.T., Sruoga, P., Rapela, C.W., Márquez, M., Storey, B.C., Riley, T.R. 1998. The Chon-Aike silicic igneous province of Patagonia and related rocks in West Antarctica: a silicic LIP. *Journal of Volcanology and Geothermal Research*, **81**: 113–136.

Payette, C., Martin, R.F. 1987. The glass inclusions and mineralogy of the rhyolites, Upper Aillik Group, Labrador. Geological Survey of Canada, Ottawa, Ont., Project 24 ST-23233-6-1281, unpublished report.

Pearce, J.A. (1996). A user's guide to basalt discrimination diagrams. *In* Trace Element Geochemistry of Volcanic Rocks. *Edited by* D.A. Wyman. Geological Association of Canada Short Course Notes ,12, 79-114.

Pearce, J.A. 1982. Trace element characteristics of lavas from destructive plate boundaries. *In* Andesites: Orogenic Andesites and Related Rocks. *Edited by* R.S. Thorpe. John Wiley & Sons, Chichester, U.K. 525-548.

Piercey, S.J. 2005. A Simple and Systematic Approach to Processing Lithogeochemical Datasets. *Unpulished.*

Pietranik, A.B., Hawkesworth, C.J. Storey, C.D., Kemp, A.I.S., Sircombe, K.N., Whitehouse, M.J., Bleeker, W. 2008. Episodic, mafic crust formation from 4.5 to 2.8 Ga: New evidence from detrital zircons, Slave craton, Canada. *Geology*, **36**: 875-878.

Rapp, R., Watson, E.B., Miller, C.F. 1991. Partial melting of amphibolite/eclogite and the origin of Archean trond-hjemites and tonalities. *Precambrian Research*, **51**: 1–25.

Rayner, N., Stern, R.A., Bickford, M.E. 2005. Tectonic implications of new SHRIMP and TIMS U-Pb geochronology of rocks from the Sask Craton, Peter Lake Domain and Hearne margin, Trans-Hudson Orogen, Saskatchewan. *Canadian Journal of Earth Sciences*, **42**: 635-657.

Reagan, M.K., Sims, K.W.W., Erich, J., Thomas, R.B., Cheng, H., Edwards, R.L., Layne, G., Ball, L. 2003. Time scales of differentiation from mafic parents to rhyolite in North America from continental arcs. *Journal of Petrology*, **44**: 1703-1726.

Reid, M.R. 2003. Timescales of Magma Transfer and Storage in the Crust. *In*: Treatise on Geochemistry: The Crust. *Edited by*: R.L. Rudnick. **3**: 167-193.

Richard, P., Shimizu, N. and Allègre, C.J. 1976. $^{143}Nd/^{146}Nd$, a natural tracer: an application to oceanic basalts. *Earth Planetary Science Letters*, **31**: 269-278.

Rivers, T. 1997. Lithotectonic elements of the Grenville Province: review and tectonic implications. *Precambrian Research*, **86**: 117–154.

Rollinson, H.R. 1993. *Using Geochemical Data: Evaluation, Presentation, Interpretation,* Longman, UK. 352 pp.
Ryan, A.B. 1984. Regional geology of the central part of the Central Mineral belt, Labrador. Newfoundland Department of Mines and Energy, Mineral Development Division, Memoir 3.
Ryan, A. B., Kay, A., Ermanovics, I. 1983. The geology of the Makkovik Subprovince between Kaipokok Bay and Bay of Islands, Labrador. Newfoundland Department of Mines and Energy, Mineral Development Division, Maps 83-38 and 83-41.
Sandeman, H.A., Hanmer, S., Tella, S., Armitage, A.A., Davis, W.J., Ryan, J.J. 2006. Petrogenesis of Neoarchaean volcanic rocks of the MacQuoid supracrustal belt: a back-arc setting for the northwestern Hearne subdomain, western Churchill Province, Canada. *Precambrian Research*, **144**: 140-165.
Saunders, A.D., Tarney, J. 1984. Geochemical characteristics of basaltic volcanism within back-arc basins. *Geological Society, London, Special Publications*, **16**: 59-76.
Saunders, A. D., Tarney, J. 1991. Back-arc basins. *In*: Oceanic Basalts. *Edited by*: Floyd, P. A. Glasgow: Blackie, 219–263.
Schärer, U., Krogh, T.E., Wardle, R., Ryan, A.B., Gandhi, S.S. 1988. U-Pb ages of early and middle Proterozoic volcanism and metamorphism in the Makkovik orogen, Labrador. *Canadian Journal of Earth Sciences*, **25**: 1098-1107.
Shervais, J. W., 1982. Ti-V plots and the petrogenesis of modern and ophiolitic lavas. *Earth and Planetary Science Letters*, **59**: 101-118.
Shinjo, R., Kato, Y. 2000. Geochemical constraints on the origin of bimodal magmatism at the Okinawa Trough, an incipient back-arc basin. *Lithos*, **54**: 117–137.
Sinclair, G.S. 1999. Geochemistry and argon thermochronology of the upper Aillik Group and associated granitoid rocks in the Makkovik Bay Area, Aillik Domain, Makkovik Province, Labrador. Unpublished MSc thesis, Dalhousie University, Halifax, Nova Scotia, Canada, 294 pp.
Sinclair, G.S., Barr, S.M., Culshaw, N.G., Ketchum, J.W.F. 2002. Geochemistry and age of the Aillik Group and associated plutonic rocks, Makkovik Bay area, Labrador: Implications for the tectonic development of the Makkovik Province. *Canadian Journal of Earth Sciences,* **39**: 1089-1107.
Söderlund, U., Patchett, J., Vervoort, J., Isachsen, C. 2004. The ^{176}Lu decay constant by Lu-Hf and U-Pb isotope systematic of Precambrian mafic intrusions. *Earth and Planetary Science Letters,* **222**: 311-324.
Stern, R.A. 1997. The GSC Sensitive High Resolution Ion Microprobe (SHRIMP): analytical techniques of zircon U-Th-Pb age determinations and performance evaluation: *in* Radiogenic Age and Isotopic Studies, Report 10, Geological Survey of Canada, Current Research 1997-F, pp. 1-31.
Stern R. 1999. In situ zircon trace element analysis by high mass-resolution SIMS. Ninth Annual V.M. Goldschmidt Conference, pp. 284-285.
Stern, R.A., Amelin, Y. 2003. Assessment of errors in SIMS zircon U-Pb geochronology using a natural zircon standard and NIST SRM 610 glass. *Chemical Geology*, **197**: 111-146.
St. Onge, M.R., Scott, D.J., Lucas, S.B. 2000. Early partitioning of Quebec:

microcontinent formation in the Paleoproterozoic. *Geology*, **28**: 323-326.
Sun, S.S., McDonough, W.F. 1989. Chemical and isotopic systematics of oceanic basalts: implications for mantle composition and processes. *In* Magmatism in the ocean basins. *Edited by* A.D. Saunders and M.J. Norry. Geological Society Special Publication (London), No. 42, 313–345.
Sutton, J.S., Marten, B.E., Clark, A.M.S. 1971. Structural history of the Kaipokok bay area, Newfoundland. Proceedings of the Geological Association of Canada, Volume 24, pp. 103-106.
Sylvester, P.J. 1989. Postcollisional alkaline granites. *Journal of Geology*, **97**: 261-280.
Tappe, S., Foley, S.F., Jenner, G.A., Heaman, L.M., Kjarsgaard, B.A., Romer, R.L., Stracke, A., Joyce, N., Hoefs, J. 2006. Genesis of ultramafic lamprophyres and carbonatites of Aillik Bay, Labrador: A consequence of incipient lithospheric thinning beneath the North American craton. *Journal of Petrology*, **47**: 1261-1315.
Tappe, S., Foley, S.F., Stracke, A., Romer, R.L., Kjarsgaard, B.A., Heaman, L.M., Joyce, N. 2007. Craton reactivation on the Labrador Sea margins: $^{40}Ar/^{39}Ar$ age and Sr–Nd–Hf–Pb isotope constraints from alkaline and carbonatite intrusives. *Earth and Planetary Science Letters*, **256**: 433–454.
Taylor, S.R., McLennan, S.M. 1985. *The continental crust: its composition and evolution*, Blackwell: Oxford. 312 pp.
Turner, S., Platt, J.P., George, R.M., Kelley, S.P., Pearson, D.G., Nowell, G.M., 1999. Magmatism assocated with orogenic collapse of the Betic-Alboran domain, SE Spain. *Journal of Petrology*, **40**: 1011-1036.
Vervoort, J., Blichert-Toft, J. 1999. Evolution of the depleted mantle; Hf isotope evidence from juvenile rocks through time. *Geochimica et Cosmochimica Acta*, **63**: 533-556.
Wang, K-L., Chung, S-L., O'Reilly, S.Y., Sun, S-S., Shinjo, R., Chen, C-W. 2004. Geochemical constraints for the genesis of post-collisional magmatism and the geodyamic evolution of the northern Taiwan region. *Journal of Petrology*, **45**: 975-1011.
Wardle, R. J., Bailey, D. G. 1981. Early Proterozoic sequences in Labrador. Geological Survey of Canada, Special Paper 81-10: 331–359.
Wardle, R.J., Gower, C.F., Ryan, B., James, D., Nolan, L., Nunn, G.A.G., Kerr, A. 1997. A new geological map of Labrador. Report of Activities - Newfoundland. Newfoundland Department of Mines and Energy, Geological Survey, Report of Activities 1997, 61-62.
Wardle, R., Gower, C., James, D., St-Onge, M., Scott, D., Garde A., Culshaw, N., van Gool, J., Connelly, J., Perreault, S., Hall, J. 2002. Correlation chart of the Proterozoic assembly of the northeastern Canadian – Greenland Shield. *Canadian Journal of Earth Science*, **39**: 895.
Watson E.B., Harrison, T.M. 1983. Zircon saturation revisited: temperature and composition effects in a variety of crustal magma types. *Earth and Planetary Science Letters*. **64**: 295-304.
Wedepohl, K.H. 1995. The compositions of the continental crust, *Geochimica and Cosmochimica Acta*. **59**: 1217-1232.

White, M.V.W., Martin, R.F. 1980. The metasomatic changes that occur with uranium mineralization in the nonorogenic rhyolites of the Upper Aillik Group, Labrador. *Canadian Mineralogist*, **18**: 459–479.

Wilton, D.H.C. 1996. Metallogeny of the Central Mineral Belt and adjacent Archean basement, Labrador. Newfoundland and Labrador Department of Mines and Energy, Geological Survey Mineral Resource Report 8, 178 pp.

Winchester, J.A., Floyd, P.A. 1977. Geochemical discrimination of different magma series and their differentiation products using immobile elements. *Chemical Geology.* **20**: 325-343.

Wobus, R.A., Folley, M.J., Wearn, K.M., Noblett, J.B. 2001. Geochemistry and tectonic setting of Paleoproterozoic metavolcanic rocks of the southern Front Range, lower Arkansas River Canyon and northern Wet Mountains, central Colorado. *Rocky Mountain Geology*, **36**: 99-118.

Wood, D.A. 1980. The application of a Th–Hf–Ta diagram to problems of tectonomagmatic classification, and to establishing the nature of crustal contamination of basaltic lavas of the British Tertiary volcanic province. *Earth Planetary Science Letters*, **50**: 11-30.

Zanetti, A., Massimo, Tiepolo, M., Oberti, R., Vanucci, R. 2004. Trace element partitioning in olivine; modelling of a complete data set from a synthetic hydrous basanite melt. *Lithos*, **75**: 39-54.

Appendix A

A.1 GEOCHRONOLOGY

Samples, 40–50 kg in weight, were collected and cleaned of their weathered surfaces in the field. Care was taken to avoid veins, fractures, alteration and fragments where possible. Rocks were crushed and zircon separated by traditional Wifley table and heavy liquid concentrate methods and divided into magnetic fractions with a Franz separator. Zircon grains of various sizes, textures and morphologies were chosen optically for mounting.

Analysis of zircon grains was performed on the sensitive high resolution ion microprobe (SHRIMP) – II at the Geological Survey of Canada in Ottawa (Clement and Compston, 1989). Analytical procedures followed those described by Stern (1997), with standards and U-Pb calibration methods following Stern and Amelin (2003). Briefly, zircons were cast in 2.5 cm diameter epoxy mounts along with fragments of the GSC laboratory standard zircon (z6266, with $^{206}Pb/^{238}U$ age = 559 Ma). The mid-sections of the zircons were exposed using 9 µm, 6 µm, and 1 µm polishing diamond compound, and the internal features of the zircons (such as zoning, structures, alteration, etc.) were characterized in back-scattered electron mode (BSE) and cathode luminescence (CL) utilizing a Zeiss Evo 50 scanning electron microscrope.

Mount surfaces were evaporatively coated with 10 nm of high purity Au. Analyses were conducted using an $^{16}O^{-}$ primary beam, projected onto the zircons at 10 kV. The sputtered area used for analysis was 15 µm in diameter with a beam current of 3.4-6.0 nA. The count rates at ten masses including background were sequentially measured over 6 scans with a single electron multiplier and a pulse counting system with deadtime of 27 ns. Off-line data processing was accomplished using customized SQUID 2 software. The 1σ external errors of $^{206}Pb/^{238}U$ ratios reported in the data table incorporate a ± 1.3% or 1.5% error in calibrating the standard zircon. The change in error occurred at the 36 hours interval of 89 hour run time. No fractionation correction was applied to the Pb-isotope data. Common Pb correction utilized the Pb composition of the surface blank (Stern, 1997). Isoplot v. 3.00 (Ludwig, 2003) was used to generate concordia plots and calculate weighted means. The error ellipses on the concordia diagrams and the weighted mean errors are reported at 2σ.

Analyses of a secondary zircon standard (1242) were interspersed between the sample analyses to verify the accuracy of the $^{207}Pb/^{206}Pb$ calibration. The weighted mean $^{207}Pb/^{206}Pb$ age of sixteen analyses of 1242 zircon is 2679.5 ± 0.5 Ma (95% conf.). The accepted $^{207}Pb/^{206}Pb$ age of the 1242 standard is 2679.5 ± 0.5 Ma. Therefore the weighted means of the $^{207}Pb/^{206}Pb$ age of unknown zircon were corrected and the error propagated.

Pits made by SHRIMP analysis were re-imaged in BSE on a FEI Quanta 400 Scanning Electron Microscope at Memorial University.

A.2 HF ISOTOPE GEOCHEMISTRY

Mounts for geochronological zircon analyses were used for *insitu* Hf isotope analyses. A spot size of 49 μm was ablated at a rate of 10 Hz corresponding to energy densities of 5 J/cm^2. Gas blank was acquired for 30 s followed by 60 s (600 pulses) of laser ablation. The typical signal intensities of ^{178}Hf varied between 1.5 and 2.9 V over 35-50 integration cycles, depending on duration. The $^{176}Hf/^{177}Hf$, $^{175}Lu/176$mass and $^{173}Yb/176$mass data were corrected for gas blank and normalised to $^{179}Hf/^{177}Hf = 0.7325$

(Patchett and Tatsumoto, 1981), using an exponential correction for mass bias (Slama et al., 2008). The signal measured for the 176mass is a combination of ^{176}Lu, ^{176}Yb, ^{176}Hf. In order to determine ^{176}Hf, the interferences from Yb and Lu must be subtracted using the recommended values of $^{176}Lu/^{175}Lu = 0.02656$ (Chu et al., 2002), and $^{176}Yb/^{173}Yb = 0.7952$ (Lapen et al. 2004). The Plešovice natural zircon standard (Slama et al., 2008) was periodically analysed as a quality control standard. Their reported value for $^{176}Hf/^{177}Hf$ is 0.282481 ± 0.000013 (2σ).

In a closed system the basic age equation for the Lu-Hf dating method is as follows:

$$(^{176}Hf/^{177}Hf)_t = (^{176}Hf/^{177}Hf)_{initial} + (^{176}Lu/^{177}Hf)_t \cdot (e^{\lambda t} - 1)$$

Where t is the elapsed time and λ is the ^{176}Lu decay constant.

To calculate the elipson depleted mantle values (ε_0 and ε_t) the following constants were used: Age of the Earth = 4.56 Ga; $^{176}Lu/^{177}Hf = 0.0388$; $^{176}Hf/^{177}Hf = 0.28325$; (Griffin et al., 2000; updated by Andersen et al., 2009).

Mantle extraction ages were calculated after: $\varepsilon Hf_{DM}{}^{(T)} = 0.1 * T^2 - 4 * T + 16$, applied to the equation of LILE depletion of chondritic mantle (DePaolo and Wasserberg, 1976) with $\varepsilon Hf_{MORB} = 16$ (Mean value of the MORB field; Nowell et al. 1998); $\varepsilon Hf_{2.7Ga} = 6$ (Corfu and Noble, 1992; Vervoort et al., 1999); chondritic values of $^{176}Hf/^{177}Hf =$ 0.282785 and $^{176}Lu/^{177}Hf = 0.0336$ (Bouvier et al., 2009). Mafic and felsic crust ratios; $(^{176}Lu/^{177}Hf)_t = 0.022$ and $(^{176}Lu/^{177}Hf)_t = 0.01$ respectively (Pietranik et al., 2008).

A.3 MAJOR AND TRACE ELEMENT GEOCHEMISTRY

A variety of units were sampled in both the study areas for whole rock geochemistry based on their lithology and field relationships; 24 samples from Middle

Head and 18 from Pomiadluk Point (some of which are presented in Appendix C.1). Care was taken to obtain samples from surfaces that were devoid of veining and alteration. At Middle Head 9 samples of mafic pyroclastic rocks and basalt, 4 samples of felsic pyroclastic rocks and rhyolite, 1 sample of tuffaceous sandstone, 2 samples of sandstones, 2 samples of calcsilicate rock, 4 samples of granite, 1 sample of granitic pegmatite and 3 samples of dioritic/granodioritic dykes were analyzed for major and trace element geochemistry. At Pomiadluk Point 4 samples of mafic pyroclastic rocks and basalt, 9 samples of felsic pyroclastic rocks and rhyolite, 2 samples of granite, 1 sample of a gabbroic sill and 2 samples of felsic dykes were sampled for major and trace element geochemistry.

Samples weighing 3-5 kg were taken from the host rock, cleaned of their weathered surfaces and reduced to small fragments directly in the field to avoid contamination. The samples were processed at Memorial University where fresh small fragments were reduced to a fine gravel in the jaw crusher and subsequently 20 to 30 grams of said material was made into powder using a ceramic disk and ring grinder to avoid Ta contamination.

Major elements as well as the following trace elements; As, Ba, Be, Cd, Ce, Co, Cr, Cu, Dy, Fe, La, Li, Mn, Mo, Nb, Ni, P, Pb, Rb, Sc, Sr, Ti, V, Y, Zn; were analyzed by inductively coupled plasma – emission spectrometry (ICP-ES) at the Geochemical Laboratory of the Newfoudland and Labrador Department of Natural Resources (Finch, 2001). Preparations for these processes are after Finch (1998) and are as follows. 1) Major element analyses: 0.1 g of <180 micron material is weighed into a graphite crucible with 0.5 g of lithium metaborate. The samples and flux are mixed thoroughly and placed in a 1000 °C furnace and fused. The samples are removed after one hour and tipped into a mixture of 4% hydrochloric acid and concentrated hydrofluoric acid contained in a polycarbonate digestion bottle. The caps are immediately sealed and samples are placed in a water bath at 90 °C. After 90 minutes, the samples are removed and 50 mL of 50 g/L boric acid solution is added, after which the samples are returned to the digestion bath. Following another 90 minutes the sample are removed, cooled and transferred to 100 mL volumetric flasks. 2) Trace element analyses: 1 g of material is weighed into a 125 mL Teflon beaker. Five mL of concentrated hydrochloric acid, 15 mL of hydrofluoric acid and 5 mL of 1:1 perchloric acid is added to each sample. The samples are placed on a hotplate at 200 °C and evaporated to dry, after which the beakers are half filled with 10% hydrochloric acid and returned to the hot plate at 100 °C. When the residue is completely dissolved the samples are removed, cooled and transferred to 50 mL volumetric flasks. One mL of 50 g/L boric acid is added to each sample to compile any residual hydrofluoric acid. The sample are made to volume and analyzed by ICP-ES after Licthe et al. (1987).

Further trace element work was completed by inductively coupled plasma – mass spectrometry (ICP-MS) at Memorial University to analyze Y, Zr, Nb, Ba, La, Ce, Pr, Nd, Sm, Eu, Gd 157, Gd 160, Tb, Dy, Ho, Er, Tm, Yb, Lu, Hf, Ta, Th. These samples were prepared in the following manner: (1) sintering of a 0.2 g sample aliquot with sodium peroxide, (2) dissolution of the sinter cake, separation and dissolution of REE hydroxide-bearing precipitate, (3) analysis by ICP-MS using the method of internal standardization to correct for matrix and drift effects. Duplicate data was collected for Ba, Ce, Dy, La, Nb and Y. ICP-ES data was used for Ba, Ce, Dy and La while ICP-MS data was used for

Nb and Y. Full details of the procedure are given in Longerich et al. (1990). A pure quartz reagent blank (BLANK) and three certified geological reference standards were prepared and analyzed for comparison with recommended values given by Govindaraju (1989), and average values determined by Jenner et al. (1990). Reagent blank concentrations are generally insignificant and have not been subtracted from sample concentrations. Five samples were prepared and analyzed in duplicate. Sample detection limits in ppm (3 standard deviations of the background) are quoted for each analytical run. Several inter-element interferences are present in ICP-MS analysis. The instrument is optimized such that for most rock types the interferences are at a sufficiently low level to be adequately corrected.

A.4 ND ISOTOPE GEOCHEMISTRY

Sixteen samples for Sm-Nd isotopic analyses were chosen, crushed and prepared in the sample manner sample for geochemistry at Memorial University (see Appendix C). These samples include two felsic tuff, one rhyolite, one monzogranite, one mafic dyke and six basalt samples from Middle Head and three felsic tuff, two mafic tuff and one basalt samples from Pomiadluk Point. Samples were analysed at Carleton University in the Isotope Geochemistry and Geochronology Research Centre. Between 100 and 200 mg of sample powder is dissolved in 0.26N HCl and loaded onto Eichrom Ln Resin chromatographic columns containing Teflon powder coated with HDEHP [di(2-ethylhexyl) orthophosphoric acid; Richard et al. 1976]. Nd is diluted using 0.26N HCl, followed by Sm in 0.5N HCl. Sm and Nd concentrations were measured by ICP-MS, with precision estimated at ±5% (2σ). Ratios of $^{147}Sm/^{144}Nd$ and $^{143}Nd/^{144}Nd$ were measured directly by high-precision thermal ionization mass spectrometry (TIMS), with precision estimated at ± 0.5% (2σ) and ± 0.000020 (2σ) respectively. The analytical results are presented in Table 3.2.

Total procedural blanks for Nd are < 50 picograms; < 6 picograms for Sm. Samples are spiked with a mixed ^{148}Nd-^{149}Sm spike prior to dissolution. Concentrations are precise to ± 1%, but $^{147}Sm/^{144}Nd$ ratios are reproducible to 0.5%. Samples are loaded with H_3PO_4 on one side of a Re double filament, and run at temperatures of 1700-1800 °C. Isotope ratios are normalized with respect to $^{146}Nd/^{144}Nd$ = 0.72190. Analyses of the USGS standard BCR-1 yield Nd = 29.02 ppm, Sm = 6.68 ppm, and $^{146}Nd/^{144}Nd$ = 0.512668 ± 20 (n=4). The international La Jolla standard produced: TRITON: $^{143}Nd/^{144}Nd$ = 0.511847 ± 7, n = 26. Internal lab standard = 0.511818 ± 8, n = 28 and 0.511819 ± 10 n = 94.

A.5 FC-AFC-FCA and Mixing Modeler

Parameters are set in the FC-AFC-FCA and Mixing Modeler (Ersoy and Hevaci, 2010) to control the model curves. Parameters include the selection of elements (and isotopes), fractionating minerals, partition coefficient (Kd) dataset prepared for acid, intermediate, and basic melt compositions, assimilant rock compositions, ratio of fractionating material to assimilated materials (r), and fraction of melt remaining (F) . For this study trace elements Y and Nb are modeled against each other, as well as Hf to $^{176}Hf/^{177}Hf$ and Nd to $^{143}Nd/^{144}Nd$.

An acidic melt is chosen for felsic volcanic rocks of the Aillik Group in Chapter 2. A basic melt is chosen for mafic volcanic rocks of the Aillik Group in Chapter 3, and fractionating minerals are olivine (20%), clinopyroxene (20%) and plagioclase (60%). The ratio of concentrations of an element in the solid material to concentration in the melt phase (Kd) for each fractionating mineral are presented in below. To model AFC the depleted mantle (based on an average of 4 pickrites from Chauvel and Hemonde, 2000) is assimilated with felsic tuff sample 08CL453A-02. To model AFC in Chapter 3 we require an 'r' value of 0.8 and an 'F' value of 2%.

	Olivine	Clinopyroxene	Plagioclase	Reference
Hf	0.0037	0.2630	0.0510	Zanetti et al. 2004
Y	0.0038	0.4380	0.0300	Foley et al. 1996
Nb	0.0017	0.0027	0.0100	Rollinson, 1993
Nd	0.0010	0.1730	0.1400	MacKenzie and O-Nions, 1991

Appendix B.1: Location of representative, geochemical and geochronological samples

Station ID	Easting	Northing	Sample ID	Field Name
08CL058	374292.06	6110681.76	08CL058A-01	felsic tuff
			08CL058B-01	diabase dyke
08CL059	374367.05	6110837.01	08CL059C-01	amphibolite dyke
08CL060	374429.89	6110953.83	08CL060A-01	felsic tuff
08CL061	374570.95	6110881.00	08CL061A-01	felsic lapillituff
08CL062	374661.68	6110829.08		
08CL063	374735.67	6110847.23	08CL063A-01	conglomerate
			08CL063A-04	clasts in conglomerate
			08CL063A-04	clasts in conglomerate
08CL064	374869.26	6110792.07	08CL064B-01	conglomerate
08CL088	349424.95	6096951.04		
08CL089	349759.97	6097435.76	08CL089A-01	CL hbl-bt monzogranite
08CL090	350118.57	6097817.98	08CL090A-01	MH bt-monzogranite
08CL091	350427.18	6097998.65		
08CL092	350863.78	6097728.85	08CL092A-01	MH bt-monzogranite
08CL093	350801.75	6097324.23	08CL093A-01	MH bt-monzogranite
08CL094	350868.88	6096892.84		
08CL095	351502.14	6096766.34		
08CL096	349389.43	6096932.38	08CL096A-01	CL bt-syenogranite
			08CL096B-01	basalt
			08CL096A-02	basalt - CLG contact
08CL097	349049.97	6096890.73	08CL097A-01	
08CL098	349172.03	6096617.83	08CL098A-01	basalt
08CL099	349482.03	6096712.83	08CL099B-01	basalt
			08CL099B-02	basalt
08CL100	349594.57	6096664.12		
08CL101	350158.35	6096724.83		
08CL102	350391.11	6096738.21		
08CL103	350603.29	6096541.41		
08CL104	350198.16	6096247.02		
08CL106	349456.60	6096179.09		
08CL107	349144.04	6096408.28	08CL107A-01	basalt
			08CL107A-02	basalt
08CL150	349440.58	6095985.10	08CL150A-01	felsic tuff
			08CL150B-01	hbl diorite dyke
			08CL150B-02	hbl diorite dyke
08CL151	349233.53	6096042.56	08CL151A-01	tuffaceous sandstone
			08CL151B-01	metabasalt
08CL152	348974.71	6096336.40	08CL152B-01	felsic lapilli tuff
			08CL152B-02	felsic lapilli tuff
08CL153	348863.11	6096305.83	08CL153A-01	rhyolite
			08CL153A-02	rhyolite
08CL154	348735.56	6096280.26	08CL154A-01	hbl diorite dyke
08CL155	348339.78	6096190.82		
08CL156	348464.50	6095908.90		
08CL157	348759.22	6095966.68	08CL157A-01	felsic tuff
08CL158	348887.33	6095828.34		
08CL159	348932.59	6095610.37	08CL159A-02	basalt
			08CL159A-01	basalt

08CL160	348915.59	6095489.37	08CL160A-01	sandstone
			08CL160A-02	sandstone
08CL161	348980.48	6095416.27	08CL161A-01	felsic tuff
08CL162	349075.91	6095457.60		
08CL163	349357.46	6095681.44		
08CL164	349732.67	6095825.30		
08CL165	350379.22	6096082.81		
08CL166	350644.09	6095925.47		
08CL167	350811.99	6095951.24	08CL167A-01	hbl diorite dyke
08CL168	350999.58	6096011.25		
08CL169	351112.20	6095835.25		
08CL170	351148.14	6095815.31		
08CL171	351119.66	6095748.32	08CL171A-01	sandstone
			08CL171A-02	calcsilicate layer
08CL172	351059.19	6095522.02		
08CL173	350774.76	6095234.70		
08CL174	350763.00	6094907.66	08CL174A-01	calcsilicate layer in sandstone
08CL175	350477.37	6094710.78	08CL175A-01	hbl diorite dyke
08CL176	350320.61	6094674.63	08CL176A-01	mafic tuff
08CL177	350309.53	6094952.87		
08CL178	350462.27	6095121.50	08CL178A-01	sandstone
08CL179	350551.37	6095337.93	08CL179A-01	basalt
			08CL179A-02	basalt
			08CL179C-01	
08CL180	350141.97	6095760.91		
08CL191	349883.26	6096136.92		
08CL192	349862.22	6096371.69		
08CL193	349641.44	6096204.06	08CL193A-01	CL monzogranite
08CL194	349366.02	6096195.88	08CL194A-01	fault rock, brecciated felsic tuff
08CL195	349176.41	6096364.68	08CL195A-01	basalt
			08CL195A-02	basalt
08CL196	349298.52	6096029.61	08CL196A-01	mafic tuff
			08CL196A-02	mafic tuff
08CL197	349600.67	6096108.91	08CL197A-01	porphyritic rhyolite
			08CL197A-02	porphyritic rhyolite
			08CL197A-03	porphyritic rhyolite
08CL198	349589.37	6095956.71	08CL198A-01	crystal-lithic felsic tuff
			08CL198A-02	crystal-lithic felsic tuff
			08CL198A-03	crystal-lithic felsic tuff
08CL199	350305.30	6095439.52	08CL199A-01	CL hbl-bt monzogranite
			08CL199A-02	CL hbl-bt monzogranite
			08CL199A-03	CL hbl-bt monzogranite
08CL200	350538.11	6095273.22		
08CL201	350534.13	6095086.99	08CL201A-01	volcaniclastic sandstone
08CL202	350848.18	6094676.70	08CL202A-01	calcsilicate rock
			08CL202A-02	calcsilicate rock
08CL203	351032.97	6094509.43	08CL203A-01	felsic tuff
			08CL203A-02	felsic tuff
08CL204	351173.43	6094736.41	08CL204A-01	granitic pegmitite
			08CL204A-02	

08CL205	351162.60	6095213.43		
08CL206	350964.20	6095769.09		
08CL207	351137.33	6096035.81		
08CL265	348829.10	6096673.21	08CL265A-01	CL hbl-bt monzogranite
			08CL265A-02	CL hbl-bt monzogranite
08CL266	349025.18	6096298.32	08CL266A-01	basalt
			08CL266A-02	basalt
08CL267	349143.91	6095565.19		
08CL268	349483.33	6096237.59	08CL268A-01	basalt
			08CL268A-02	basalt
08CL269	350725.91	6097098.07	08CL269A-01	MH bt monzogranite
			08CL269A-02	MH bt monzogranite
08CL270	349046.29	6095644.54		
08CL321	350657.01	6095215.23	08CL321A-01	sandstone
			08CL321A-02	sandstone
08CL322	350460.85	6098744.09	08CL322A-01	MH bt monzogranite
			08CL322A-02	MH bt monzogranite
08CL323	351048.59	6099301.93	08CL323A-01	MH bt monzogranite
08CL324	348976.46	6094711.79		
08CL325	349060.91	6094651.58	08CL325A-01	felsic tuff
08CL326	349517.91	6094322.87	08CL326A-01	CL hbl-bt monzogranite
08CL327	349637.12	6094260.95	08CL327A-01	CL hbl-bt monzogranite
08CL346	373829.04	6109336.42	08CL346A-01	felsic tuff
			08CL346B-01	metarhyolite
			08CL346A-02	rhyolite
			08CL346B-02	rhyolite
08CL347	374058.05	6109227.13	08CL347A-01	porphyritic rhyolite
08CL348	374124.96	6109302.62	08CL348A-01	shear zone
			08CL348B-01	felsic tuff
08CL349	374439.30	6109243.09	08CL349A-01	conglomerate
			08CL349B-01	gabbro dyke
08CL350	374778.27	6109132.41	08CL350A-01	granite clast
			08CL350B-01	lapillistone
08CL351	374930.64	6109346.18	08CL351A-01	plag phyrric diabase dyke
08CL352	374894.10	6109401.03		
08CL353	374997.54	6109834.97	08CL353A-01	strained conglomerate
08CL354	375238.70	6110095.07	08CL354B-01	plag phyrric gabbro dyke
			08CL354C-01	rhyolite
08CL355	374868.98	6110214.19		
08CL356	374566.04	6110389.36		
08CL357	374346.29	6110266.95		
08CL359	374646.20	6110811.70		
08CL360	374720.43	6110736.50		
08CL361	374616.84	6110309.06	08CL361A-01	mafic tuff
08CL362	374370.19	6109877.67	08CL362B-01	felsic dyke
08CL363	374508.86	6109797.68	08CL363A-01	felsic dyke
08CL364	374685.88	6109621.59		
08CL365	374404.46	6109440.97		
08CL366	374260.95	6109375.80		
08CL367	374290.84	6109160.98	08CL367B-01	mafic lapillistone

08CL368	374267.69	6108838.36		
08CL369	374196.80	6108731.24		
08CL370	374194.28	6108706.07	08CL370A-01	felsic dyke
			08CL370A-02	felsic dyke
08CL371	373845.99	6108477.27	08CL371A-01	mafic tuff
			08CL371A-02	mafic tuff
08CL372	373713.53	6108619.64		
08CL373	374666.42	6107405.24	08CL373B-01	OH bt-fl monzogranite
08CL374	374959.85	6107752.38	08CL374A-01	OH bt-fl monzogranite
			08CL374A-02	OH bt-fl monzogranite
			08CL374B-01	OH bt-fl monzogranite
08CL375	375066.46	6108446.78		
08CL376	375063.89	6108692.74	08CL376A-01	felsic tuff
08CL377	374990.46	6109305.91	08CL377A-01	felsic tuff
			08CL377B-01	plag-phyrric diabase dyke
08CL378	375084.54	6109721.37	08CL378A-01	plag phyrric diabase dyke
08CL379	375163.19	6109985.10		
08CL380	375029.40	6110697.38	08CL380A-01	strained conglomerate
08CL381	374335.28	6107375.40	08CL381B-01	conglomerate
08CL382	374037.71	6106703.66		
08CL383	373704.44	6106597.28		
			08CL384B-01	plag phyrric gabbro dyke
08CL384	373337.91	6106227.06	08CL384B-02	plag phyrric gabbro dyke
08CL385	373475.12	6106801.43	08CL385B-01	felsic dyke
08CL386	373640.75	6107354.21		
08CL387	373952.14	6107655.86		
08CL388	373462.38	6108466.80	08CL388A-01	q-f porphyritic granite
			08CL388A-02	q-f porphyritic granite
08CL389	374498.07	6103719.42	08CL389A-01	felsic tuff
08CL389			08CL389A-02	felsic tuff
08CL390	374376.52	6104168.59	08CL390B-01	OH bt-fl monzogranite
			08CL390A-01	OH bt-fl monzogranite
08CL391	374080.62	6104611.37	08CL391A-04	clasts in conglomerate
08CL392	373610.02	6104996.20		
08CL393	373751.64	6105944.76		
08CL394	373393.56	6105948.97		
08CL395	373404.36	6106854.28	08CL395A-01	conglomerate
08CL396	373332.01	6107521.82		
08CL397	373066.73	6107948.04		
08CL398	375464.05	6108493.00	08CL398A-01	basalt
			08CL398A-02	basalt
			08CL398B-01	felsic tuff
			08CL398B-02	felsic tuff
08CL399	376143.30	6108327.84	08CL399A-01	OH bt-fl monzogranite
			08CL399A-02	OH bt-fl monzogranite
08CL400	374619.48	6110878.71	08CL400A-01	flow banded rhyolite
			08CL400A-02	flow banded rhyolite
08CL401	374906.82	6110899.02	08CL401A-01	contact
08CL451	374405.27	6110880.29		
08CL452	374899.39	6110895.52	08CL452A-01	tuffaceous sandstone

Appendix B.1 cont

			08CL452A-02	tuffaceous sandstone
			08CL452A-03	tuffaceous sandstone
08CL453	375033.18	6108819.05	08CL453A-01	crystal felsic tuff
			08CL453A-02	crystal felsic tuff
			08CL453A-03	crystal felsic tuff
08CL454	374128.09	6106923.06	08CL454A-01	mafic tuff
			08CL454A-02	mafic tuff
08CL455	350375.89	6094804.75	08CL455A-01	sandstone
08CL456	374180.90	6108194.44	08CL456A-01	porphyritic felsic dyke
			08CL456A-02	porphyritic felsic dyke
08CL457	374229.20	6107677.92	08CL457B-01	strained conglomerate
08CL458	374338.34	6110829.47	08CL458A-01	felsic tuff
			08CL458A-02	felsic tuff
			08CL458A-03	felsic tuff
08CL459	374410.00	6110874.00		
08CL460	374649.00	6110840.00		
08CL461	373207.00	6105929.00		
08CL462	350454.00	6095040.00	08CL462A-01	volcaniclastic breccia
08CL463	349474.00	6096054.00		
08CL464	349216.00	6096295.00		
08CL465	374122.00	6108309.00	08CL465A-01	strained conglomerate
			08CL465A-02	strained conglomerate
08CL466	374228.00	6108160.00		
08CL467	374328.00	6108000.00		
08CL468	374297.00	6107927.00		
08CL469	374293.00	6107724.00		
08CL470	374139.00	6107484.00		
08CL471	374070.00	6107430.00		

Appendix B.2: Petrographic descriptions of samples from study Pomiadluk Point and Middle Head

POMIADLUK POINT		
08CL058A-01	felsic tuff	Foliated felsic tuff. Coarser grained fragments of felsic tuff in fine grained quartzofeldspathic matrix. Porphyroclasts contains quartz-plag-bt. Moderately foliated defined by elongated fragments. Porphyroblasts of undulatory quartz. Calcite alteration in fragments.
08CL060A-01	felsic tuff	Fined grained homogeneous felsic tuff. Foliation is moderate and parallel to bedding. Rare crystals and lithic fragments in felsic tuff. Crystals are subrounded Kspar, plag and quartz and fragments are coarser grained felsic tuff. All are less than 1 mm wide.
08CL346A-01	felsic tuff	Felsic tuff with quartzofeldspathic matrix. Foliated parallel to bedding. Fragments are of coarser grained felsic tuff. Contains quartz veinlets. Fragments take up 5% of rock. Apatite accessory minerals.
08CL346B-01	rhyolite	Silicified porphyritic rhyolite with feldspathic porphyries. Mostly recrystallized to quartz. Foliated weakly and parallel to bedding. Apatite accessory minerals.
08CL348A-01	conglomerate	Foliated conglomerate that resembles siltstone. Layers are very strung out. Mostly felsic layers with elongated fragments of felsic tuff and granite. 2 fragments are very mafic containing alteration minerals of chloritoid and cpx. Silicified.
08CL349A-01	conglomerate	Polymictic conglomerate. Difficult to tell foliation since clasts are so large. Quartzo-feldspathic matrix. Clast taking up most of thin section has a very large garnet crystal. Odd alteration on some plagioclase crystals. Clast is also calcite altered.
08CL353A-01	conglomerate	Epidote altered heterogeneous polymictic conglomerate. Strongly foliated. Clasts are elongated (volcanic) to subrounded (granitoids). Volcanic layers are hornblend-opaque rich and bend around granitoid clasts. Sheared // foliation. Demonstrated en echelon.
08CL370A-01	felsic dyke	Felsic dyke with quartzofeldspathic groundmass which has been slightly silicified. Rare (4%) porphyry crystals of k-feldspar (microcline) rimmed by finer grained quartz. Porphyries are up to 3 mm wide, and are have antiperthite textures. Biotite, hbl, zircon occur in groundmass. Fluorite replaces some minerals. Non foliated and undeformed.
08CL371A-01	mafic tuff	Foliated hbl-bt mafic tuff. Fine to medium grained, recrystallized with amygdules filled with plagioclase, altered by hornblend
08CL374A-01	OHG	Non foliated bt-monzogranite (October Harbour). Equigranular. Medium to coarse grained. Plagioclase grains are occasionally perthitic. Minor sericitization on plagioclase grains.
08CL381B-01	conglomerate	Sheared conglomerate, ressembling sandstone. Pseudo-mylonitic. Clasts are very elongated, forming layers. Layers of hbl-mafic and felsic. Some les competant clasts are granitic 1) plag rich anorthosite, 2) sericitized hbl granodiorite, 3) syenogranite. Matrix is quartzfeldspathic and very fined grained.

08CL384B-01	gabbro dyke	Non foliated, undeformed bt-hbl-gabbro dyke. Euhdral lath like grains of twinned plagioclase. Medium grained, homogeneous, equigranular. Lots of opaque crystals in groundmass as well.
08CL388A-01	qtz-fd porph. granite	Quartz-feldspar porphyritic granite. Matrix is Quartz-orthoclase-plagioclase with porphyries of undulatory quartz and minor sercitized plagioclase. Weakly foliated.
08CL389A-01	felsic tuff	Fine grained, weakly foliated crystal felsic tuff. Quartz veining. Matrix is kspar-quartz rich that is heavily silicified. Lithic fragments include medium grained quartz altered plagioclase porphyroblasts.
08CL395A-01	conglomerate	Polymictic conglomerate that is strained. Fragments are stretched out in a porphyroblastic matrix. Matrix supported with 20 % clasts. Clasts are granitic and contain hbl-bt-opaques. Other more competant clasts are felsic tuff and rhyolite. Matrix is quartz dominated (silicified?) Elongated clasts define foliation.
08CL398A-01	basalt	Foliated fine grained hbl metabasalt with epidote veining. Relic bt and cpx are recrystallized to hbl. Heterogeneous with layers that are more hbl rich.
08CL398B-01	felsic tuff	Fine grained matrix that is quartz dominated. Fragments up to 2mm wide are crystal and lithic. Lithic fragments are composed of qtz-plag-orthoclase-hbl. Weakly foliated.
08CL399A-01	OHG	Non foliated bt-monzogranite (October Harbour). Equigranular. Medium to coarse grained. Minor sericitization on plagioclase grains.
08CL400A-01	rhyolite	Silicified flow banded rhyolite. Flow bands are defined by coarser layers of quartz crystals in bands (recrystallized) againt finer grained mostly quartz bands. Foliation is subparallel to flow banding. Recrystallized and very fine to fine grained. Accessory apatite and rutile.
08CL452A-01	felsic tuff	Fine grained felsic tuff. Foliation is strong, parallel to bedding and defined by biotite grains in matrix. Has a quartz-biotite matrix with few (5%) fragments and crystals. Fragments resemble granite and are likely derived from the proximal conglomerate. Fragments have calcite alteration, they are up to 3mm wide and subrounded.
08CL453A-01	felsic tuff	Silicified crystal felsic tuff. Crystals make up 15% of the unit and are rounded and 2 mm wide. They are Quartz, k-spar and plagioclase. Foliation is parallel to bedding. Matrix is homogeneous and very fine grained. Quartz crystals havegranoblastic texture. Some plagioclase crystals are perthitic.
08CL454A-01	mafic tuff	Foliated fine grained hbl-mafic tuff. Recrystallized. Qtz nodules have sericite alteration. Nodules are elongated in direction of foliation
08CL458A-01	felsic tuff	Heterogeneous, fine grained, silicifed, felsic tuff. Calcite and chloritoid alteration. Folation is parallel to bedding. Slightly coarser grained felsic tuff clasts in a finer grained matric. Recrystallized.

Appendix B.2 cont

08CL465A-01	conglomerate	Pseudomylonitic conglomerate. Epidote altered. Clasts stretched and straightened due to shearing. Mafic hbl rich layers, qtz + plag rich felsic layers.

Appendix B.2 cont

MIDDLE HEAD		
08CL096A-02	CLG/basalt	Contact between Cross Lake Granite and metabasalt. Contact is interfingered and sheared. Shearing is parallel to foliation in basalt. Basalt is recrystallized and silicified. CLG does not appear to be silicified, although demonstrates sericitization on plagioclase and kspar crystals. Epidote abundant at contact.
08CL099B-01	basalt	Fine to medium grained hbl-bt metabasalt. Strongly foliated, defined by hbl-bt laths. Recrystallized. No evidence of chlorite.
08CL107A-01	basalt	Weakly foliated hbl-metabasalt. Minor chlorite + epidote alteration. Quartz veinlets are 1 mm wide. Hbl grains are subhedral and have a lath-like nature. Hbl grains are locally twinned. Inequigranular, silicified and recrystallized. Alteration evident along rims of hbl grains.
08CL150A-01	felsic tuff	Very fine grained felsic tuff with crystal porphyroblasts of kspar-plag-quartz in quartzofeldspathic matrix. Crystals are elongated and up to 5mm wide. Recrystallized. Foliated and defined by elongate crystals. Crystals have jigsaw puzzle texture at intersections.
08CL150B-01	diorite dyke	Undeformed, non foliated medium grained hbl diorite dyke. Sericitized, eudral grained. Some calcite veining. Hbl sees to be replacing pyroxene? Hbl is appinitic (euhedral)
08CL151A-01	tuffaceous sandstone	Silicified bt-tuffaceous sandstone. Hbl recrystallized, fine grained. Strongly foliated defined by hbl-bt laths.
08CL152B-01		
08CL153A-01	rhyolite	Homogeneous, silicified rhyolite (weakly flow banded, defined by bt-laths which in places are being replaced by hbl). Weakly foliated in direction of flow banding. Very fine grained. Quartz grains are anhedral blebs.
08CL159A-01	basalt	Fine grained, foliated metabasalt. Epidote - chlorite - amphibole alteration. Calcite veining and some calcite replacement. Silicified and recrystallized. Foliation defined by hbl laths.
08CL160A-01	sandstone	Silicified, recrystallized, homogeneous sandstone. Foliated, hbl altered. Fine to medium grained.
08CL171A-01	MHG	Equigranular hbl-monzogranite (Monkey Hill). Medium grained, recrystallized, homogeneous. Minor sericitization on plagiooclase and K-feldspar.
08CL179A-01	diorite dyke	Medium grained, non foliated hbl-diorite dyke. Hbl is appinitic 1mm-5mm long. Some twinning in hbl grains.
08CL194A-01	fault rock	Fault rock. Brecciated, k-spar altered felsic tuff. Olivine, garnet, epidote, hbl are alteration minerals. Recrystallized. Abundant sericite alteration on igneous minerals.
08CL195A-01	basalt	Fine to medium grained, sericite altered hbl-metabasalt. Foliated. Grain ize coarsening is metamorphic feature of hbl recrystallization
08CL196A-01	mafic tuff	Foliated fine grained calc-silicate . Quartz veins. Undulatory extinction in quartz. Calcite veining.

Appendix B.2 cont

08CL197A-01	rhyolite	Foliated porphyritic rhyolite. Fine grained groundmass that has been silicified with large porphyry crystals of microcline, quartz and plagioclase. Recrystallized, inequigranular. Crystals are up to 1 mm wide and define the weak foliation (elongated).
08CL198A-01	felsic tuff	Inequigranular, foliated felsic tuff. Fragments of coarser grained felsic tuff in finer grained matrix. Elongated fragments, defining foliation. Matrix is quartzofeldspathic. Recrystallized. K-spar grains have triple junctions. Silicified.
08CL199A-01	CLG	Strongly foliated hbl-bt syenogranite. Hbl and bt define foliation. Coarse grained, inequigranular. Recrystallized.
08CL202A-01	mafic tuff	Fine to medium grained calc-silicate. Silicified and foliated. Recrystallized. Some sericitization on plagioclase crystals (locally)
08CL203A-01	felsic tuff	Foliated tuffaceous sandstone . Foliation is parallel to bedding. Bedding defined by slight coarsening in matrix. Very fine grained quartzofeldspathic matrix. Crystals of mostly elongated quartz and minor plagioclase, altered by bt and hbl. Recrystallized. Crystals are up to 4mm wide.
08CL204A-01	pegmitite	Very coarse grained granitic pegmitite. Large euhedral plagioclase crystals with perthitic texture. Massive. Inequigranular.
08CL265A-01	CLG	Medium to coarse grained hbl-bt syenogranite. Hbl - bt define foliation. Inequigranular and recrystallized.
08CL266A-01	basalt	Foliated, fine grained hbl-bt basalt. Quartz and epidote veining. Foliation is defined by hbl - bt laths. Recrystallized and silicified.
08CL268A-01	basalt	Fine to medium grained basalt. Sulfide (pyrite) rich. Veinlets of finer grained quarts. Silicified and recrystallized. Weakly foliated defined by hbl laths.
08CL269A-01	MHG	Hbl-bt monzogranite. Recrystallized, sericite altered. medium grained. Alteration of hbl - bt (igneous) to chlorite - epidote - chloritoid.
08CL321A-01	sandstone	Quartzofeldspathic (arkosic) sandstone. Bedding parallel to foliation. Moderately defined foliating defined by subhedral hbl grains. Recrystallized, medium grains, homogeneous, inequigranular. Q-F grains are reworked and anhedral. Some sercire alteration on plagioclase grains.
08CL322A-01	MHG	Medium grained, equiranular, underformed bt- monzogranite. Sericite alteration on kspar and plagioclase crystals. Chloritoid replacing biotite crystals (Monkey Hill Granite)

Appendix C.1: Major oxide (wt %) and trace element (ppm) geochemistry of samples not directly relevant to this paper

Sample No.	08CL203A-02	08CL160A-02	08CL321A-02	08CL196A-02	08CL202A-02
Lithology	tuffaceous ss	sandstone	sandstone	c-s rock	c-s rock
SiO_2	76.89	76.45	68.08	62.29	60.55
Al_2O_3	11.34	9.95	15.17	15.58	14.58
FeO	1.85	1.44	2.01	3.09	3.63
Fe2O3	1.55	1.28	1.68	1.86	2.53
MgO	0.11	0.64	1.52	2.08	3.18
CaO	0.48	0.73	2.85	5.96	7.80
Na_2O	7.74	2.34	5.71	4.42	6.19
K_2O	0.16	6.12	2.66	1.37	0.99
TiO_2	0.25	0.24	0.41	0.52	0.61
MnO	0.06	0.07	0.08	0.14	0.14
P_2O_5	0.03	0.02	0.10	0.15	0.09
LOI	0.25	0.51	0.44	0.76	0.47
Total	100.7	99.8	100.7	98.2	100.8
V	20	8	82	76	74
Cr		3	45	24	68
Ni	3	5	13	13	31
Zn	446	100	70	75	114
Sc	2	2	10	14	18
Cu		3			
As	58	12	8	7	6
Rb		168	66	61	38
Sr	33	33	369	470	302
Y	73.4	91.0	20.2	23.6	37.0
Zr	447	454	211	174	154
Nb	47.5	37.4	12.9	12.1	24.4
Ba	7	182	602	772	247
La	73.3	63.4	20.2	30.0	21.7
Ce	155.1	137.4	55.9	62.9	68.8
Pr	18.5	16.6	5.8	7.4	7.1
Nd	70.4	68.8	22.6	28.2	29.6
Sm	13.6	14.5	5.00	5.63	7.04
Eu	1.06	1.32	0.84	1.27	0.97
Gd	10.9	13.3	4.07	4.63	6.05
Dy	9.94	14.2	3.68	4.15	6.06
Tb	1.63	2.21	0.61	0.70	0.95
Ho	2.02	2.86	0.73	0.81	1.27
Er	5.70	8.24	2.09	2.38	3.76
Tm	0.85	1.20	0.33	0.37	0.60
Yb	5.50	7.92	2.36	2.65	4.22
Lu	0.84	1.12	0.35	0.41	0.71
Hf	10.2	9.50	5.39	3.84	4.71
Ta	1.48	1.60	0.84	0.65	1.42
Pb	20	30	17	4	19
Th	14.9	12.6	11.3	8.28	14.1

Sample No.	08CL269A-02	08CL322A-02	08CL150B-02	08CL167A-02	08CL175A-02
Lithology	MHG	MHG	diorite dyke	diorite dyke	diorite dyke
SiO_2	75.21	73.84	67.79	54.31	51.09
Al_2O_3	13.51	13.92	15.51	13.80	17.06
FeO	0.60	0.65	1.75	7.60	6.20
Fe2O3	0.55	0.63	1.90	4.60	3.14
MgO	0.14	0.20	0.50	2.87	5.61
CaO	0.47	0.85	1.59	5.44	7.68
Na_2O	4.24	4.56	4.81	4.00	2.77
K_2O	4.49	4.83	5.98	2.31	2.20
TiO_2	0.12	0.14	0.58	2.32	0.86
MnO	0.05	0.05	0.07	0.19	0.15
P_2O_5	0.02	0.03	0.14	0.22	0.17
LOI	0.65	0.66	0.36	0.52	1.82
Total	100.0	100.3	101.0	98.2	98.8
V			2	177	232
Cr	2	2	3	3	32
Ni		2	6	15	19
Zn	33	35	67	134	93
Sc	1	1	8	29	39
Cu			2		3
As		3	6		
Rb	206	194	141	180	109
Sr	147	191	163	306	519
Y	17.5	25.6	46.8	37.5	12.9
Zr	121	139	507	238	90
Nb	16.4	20.9	29.2	16.9	4.8
Ba	475	534	1210	932	1030
La	17.5	21.1	69.2	34.6	20.6
Ce	34.0	41.7	136.3	73.6	40.1
Pr	3.6	4.9	16.2	9.5	5.3
Nd	13.4	18.3	59.8	37.2	21.8
Sm	2.63	3.68	10.37	8.27	4.57
Eu	0.31	0.47	1.57	1.94	1.46
Gd	2.14	3.40	8.95	7.35	3.77
Dy	2.68	3.62	8.20	2.98	1.47
Tb	0.37	0.55	1.35	1.08	0.50
Ho	0.57	0.75	1.58	1.45	0.60
Er	1.87	2.42	4.67	4.14	1.64
Tm	0.34	0.40	0.72	0.56	0.25
Yb	2.49	3.07	4.80	3.97	1.43
Lu	0.40	0.49	0.73	0.61	0.22
Hf	3.48	3.79	11.6	5.69	2.30
Ta	1.26	1.36	1.23	0.23	0.07
Pb	29	27	25	17	3
Th	17.1	14.8	12.5	6.85	3.05

Note: Analyses are below detection limit where no data is given for element

Sample No.	08CL204A-02	08CL465A-02	08CL399A-02	08CL374A-02	08CL370A-02
Lithology	pegmitite	conglomerate	OHG	OHG	felsic dyke
SiO_2	72.83	53.89	72.52	72.77	71.66
Al_2O_3	17.58	15.00	12.91	12.66	14.65
FeO	0.19	8.28	3.29	2.19	2.16
Fe2O3	0.10	5.56	1.74	1.08	1.07
MgO	0.10	2.72	1.55	1.11	1.09
CaO	0.04	4.20	0.30	0.51	0.26
Na_2O	0.09	10.63	0.98	0.60	0.52
K_2O	9.76	3.33	3.45	3.63	4.17
TiO_2	0.06	1.19	5.27	6.36	5.84
MnO	0.03	0.80	0.35	0.18	0.43
P_2O_5		0.29	0.07	0.01	0.05
LOI	0.39	0.71	0.62	0.45	0.46
Total	101.0	98.5	99.8	99.4	100.3
V		165		2	
Cr	2	1	2	1	2
Ni		2	3		2
Zn		23	90	128	62
Sc	1	30	5	2	6
Cu	2	1811			
As		9	8	18	4
Rb	194	27	214	170	143
Sr	191	554	90	93	70
Y	25.6	16.8	77.8	54.1	25.5
Zr	139	84	378	266	270
Nb	20.9	3.7	29.9	26.6	17.6
Ba	534	1368	606	110	1101
La	21.1	16.5	146.3	88.0	50.1
Ce	41.7	37.8	271.6	170.4	100.7
Pr	4.9	5.2	29.1	19.9	11.5
Nd	18.3	23.9	95.9	72.7	43.1
Sm	3.68	5.45	16.8	12.3	7.21
Eu		1.58	1.12	0.26	1.03
Gd	3.40	5.17	11.7	9.04	5.31
Dy	3.62	3.31	11.4	8.46	5.10
Tb	0.55	0.60	1.87	1.37	0.83
Ho	0.75	0.63	2.15	1.69	1.01
Er	2.42	1.69	6.39	5.07	3.09
Tm	0.21	0.21	0.99	0.80	0.48
Yb	3.07	1.38	6.64	5.48	3.32
Lu	0.49	0.23	1.09	0.83	0.53
Hf	3.79	2.05	11.2	7.01	6.03
Ta	1.36	0.04	1.72	1.36	0.94
Pb		28	32	24	23
Th	14.8	1.49	23.3	17.2	10.8

Note: Analyses are below detection limit where no data is given for element

Sample No.	08CL456A-02	08CL384B-02
Lithology	felsic dyke	gabbro sill
SiO_2	72.24	56.57
Al_2O_3	14.17	15.83
FeO	1.94	8.08
Fe2O3	0.98	5.09
MgO	0.96	2.99
CaO	0.21	4.77
Na_2O	0.60	6.40
K_2O	4.02	3.78
TiO_2	5.65	2.13
MnO	0.31	0.69
P_2O_5	0.03	0.17
LOI	0.46	1.20
Total	99.7	99.8
V		145
Cr	1	28
Ni	2	32
Zn	59	75
Sc	6	23
Cu	25	46
As	4	2
Rb	158	42
Sr	36	520
Y	39.6	17.0
Zr	355	103
Nb	19.2	6.4
Ba	623	875
La	60.6	23.3
Ce	120.9	45.1
Pr	14.3	5.5
Nd	51.8	21.3
Sm	8.88	4.68
Eu	0.81	1.21
Gd	6.81	3.94
Dy	6.34	3.30
Tb	0.99	0.58
Ho	1.30	0.61
Er	3.85	1.75
Tm	0.62	0.37
Yb	4.21	1.62
Lu	0.64	0.30
Hf	8.07	3.06
Ta	1.06	0.37
Pb	27	7
Th	12.1	3.28

Note: Analyses are below detection limit where no data is given for element

Appendix C.2: Whole rock Nd isotopic data for diorite dyke not directly relevant to this study

Sample Number	Lithology	Age (Ma)	Sm (ppm)	Nd (ppm)	$^{147}Sm/^{144}Nd$ (measured)	$^{143}Nd/^{144}Nd$ (measured)	$^{143}Nd/^{144}Nd$ (initial)	eNd CHUR (T)[c]	T_{DM}^{*} (Ma)
08CL167A-02	Diorite dyke	1800 (?)	8.03	38.58	0.1300	0.511623	0.510084	-4.42	2788

* T_{DM} = Nd depleted mantle model age - calculated using $^{143}Nd/^{144}Nd$ 0.513163; and $^{147}Sm/^{144}Nd$ of 0.2137 (Goldstein et al., 1984)

[c]calulated using present day chondritic uniform reservoir with $^{143}Nd/^{144}Nd = 0.512638$ & $^{147}Sm/^{144}Nd = 0.1967$ (DePaolo, 1981) and ^{147}Sm decay constant (λ) of $6.54 * 10^{-12}$ (Lugmair and Marti, 1978)